Chaperone-mediated autophagy in neuronal dendrites recruits cargo for local activity-dependent lysosomal release

Zur Erlangung des Grades der Doktorin der Naturwissenschaften

Doctor rerum naturalium (Dr. rer. nat.)

am Fachbereich für Biologie der Fakultät für Mathematik, Informatik und Naturwissenschaften der Universität Hamburg

im Juni 2022

eingereichte Dissertation,

vorgelegt von

Marit Sperveslage

Gutachter

1. Dr. Michael R. Kreutz

RG Dendritic Organelles and Synaptic Function, Center for Molecular Neurobiology Hamburg, Hamburg, Germany

2. Prof. Dr. Tim Gilberger

RG Cell Biology of Human Parasites, Centre for Structural Systems Biology, Hamburg, Germany

Datum der Disputation: 06.10.2022

Abstract

Neurons are complex, polarized cells that exhibit a specialized morphology adapted to their key function in synaptic transmission. The synaptic activity results in a tremendous protein turnover at the neuronal contact sites, which can be localized at great distances from the cell body. For a long time, the existence of the degradation machinery was thought to be restricted to the soma of neurons, in particular the presence of lysosomes. Lysosomes are highly acidified organelles responsible for the digestion of numerous molecules to maintain proteostasis, reflecting the catabolic center of the autophagic, as well as endolysosomal pathways. The abundance of lysosomes in the axonal and dendritic compartment has been a matter of debate and local catabolic processes, especially in connection to synaptic function, have not been studied in much detail. More recently, intriguing evidence was provided for the abundance of mature lysosomes in dendrites. It was thereby demonstrated that lysosomal trafficking was regulated by neuronal activity and activity-dependent lysosomal fusion with the plasma membrane resulted in dendritic spine growth, implicating their potential contribution to synaptic plasticity. Despite these findings, the molecular identity of dendritic lysosomes and their functional connection to neuronal function is barely understood.

The present work aimed to gain a better understanding of lysosomal populations in the dendritic compartment of neurons. To this end, the two most commonly used lysosomal markers of the family of lysosome-associated membrane proteins (LAMPs), LAMP1 and LAMP2, were utilized to study lysosomal distribution, motility and maturity, including the presence of hydrolases. To further investigate the link between neuronal activity and lysosomal function, the activity of GluN2B-containing N-methyl-D-aspartate receptors (NMDARs), which are important glutamate receptors involved in synaptic plasticity, were studied in regard to lysosomal trafficking and potential fusion.

The obtained results highlight the presence of highly heterogeneous lysosomal populations with distinct trafficking patterns, with LAMP1 and LAMP2 serving as markers for different lysosomal pools. Interestingly, it could be demonstrated that the activation of NMDARs led to the stalling, as well as exocytosis, of LAMP2-, but not LAMP1-positive lysosomes in the proximity of the GluN2B subunit. Furthermore, conducted biochemical assays revealed that the cytoplasmic tail of LAMP2 directly binds to the SH3-GK module of SAP102, a GluN2B scaffold protein. SAP102 and GluN2B are located not only at synapses but also at extrasynaptic sites and the involvement of the extrasynaptically located pool of GluN2B-containing NMDARs in the stalling and fusion of LAMP2-positive lysosomes was suggested.

Moreover, evidence was provided for the presence of chaperone-mediated autophagy (CMA) processes in dendrites. In CMA, a wide range of intracellular proteins that contain a KFERQ-like motif are recognized by the chaperone protein Hsc70 and subsequently translocated to the lysosomal lumen by the obligatory receptor LAMP2A. The studied lysosomal pool was not only shown to be associated with CMA machinery but also a known CMA target, TAR DNA-binding protein 43 (TDP-43), was found to be localized to the acidified LAMP2-positive lysosomes in dendrites. Further, the activation of NMDARs resulted in a release of TDP-43 from neuronal cells.

In summary, the data provide evidence for the existence of heterogeneous dendritic lysosomal pools as well as the presence of a novel mechanism of CMA-substrate release upon the activity-dependent fusion of dendritic LAMP2-containing lysosomes with the plasma membrane. The release of lysosomal content, including active hydrolases, could,

in consequence, allow for synaptic remodeling, unveiling a new function of lysosomes in dendrites and their connection to neuronal plasticity.

Zusammenfassung

Neuronen sind komplexe, polarisierte Zellen, die eine spezialisierte Morphologie aufweisen, angepasst an ihre Hauptfunktion der synaptischen Transmission. Die synaptische Aktivität resultiert in einem enormen Umsatz an Proteinen an den neuronalen Kontaktstellen, welche sich in großer Entfernung vom Zellkörper befinden können. Es wurde lange Zeit angenommen, dass die Existenz der Abbaumaschinerie auf das Soma der Neuronen beschränkt ist, insbesondere das Vorkommen von Lysosomen. Lysosomen sind stark angesäuerte Organellen, die für die Verdauung zahlreicher Moleküle zur Aufrechterhaltung der Proteostase verantwortlich sind und das katabolische Zentrum des autophagischen sowie des endolysosomalen Weges darstellen. Die Existenz von Lysosomen im axonalen und dendritischen Kompartiment war hingegen umstritten, und die lokalen Abbauprozesse, insbesondere im Zusammenhang mit der synaptischen Funktion, nicht detailliert untersucht. Vor kurzer Zeit wurde allerdings die Abundanz von reifen Lysosomen in Dendriten gezeigt. Dabei wurde nachgewiesen, dass der lysosomale Transport durch neuronale Aktivität reguliert wird und dass die aktivitätsabhängige Fusion von Lysosomen mit der Plasmamembran zum Wachstum dendritischer Dornen führt. Dies deutet auf einen möglichen Zusammenhang zur synaptischen Plastizität hin. Trotz dieser Erkenntnisse ist weder die molekulare Identität der dendritischen Lysosomen noch ihre funktionelle Verbindung zur neuronalen Funktion hinreichend erforscht.

Ziel der vorliegenden Arbeit war es, ein fundiertes Verständnis über die lysosomalen Populationen im dendritischen Kompartiment von Neuronen zu erlangen. Zu diesem Zweck wurden die beiden am häufigsten verwendeten lysosomalen Marker aus der Familie der Lysosomen-assoziierten Membranproteine (LAMPs), LAMP1 und LAMP2, verwendet, um die lysosomale Verteilung, Motilität und Reife, einschließlich der Anwesenheit von Hydrolasen, zu untersuchen. Um den Zusammenhang zwischen neuronaler Aktivität und lysosomaler Funktion weiter zu beleuchten, wurde die Aktivität von GluN2B-haltigen N-Methyl-D-Aspartat-Rezeptoren (NMDARs) im Hinblick auf den lysosomalen Transport und die mögliche Fusion untersucht. Diese NMDARs sind wichtige Glutamatrezeptoren, die eine wichtige Rolle bei der synaptischen Plastizität spielen.

Die vorgelegten Ergebnisse veranschaulichen heterogene lysosomale Populationen mit unterschiedlichen Bewegungsmustern, wobei LAMP1 und LAMP2 als Marker für verschiedene lysosomale Pools dienen. Interessanterweise führte die Aktivierung von NMDARs zum Stoppen sowie zur Exozytose von LAMP2-, aber nicht von LAMP1-positiven Lysosomen in unmittelbarer Umgebung der GluN2B-Untereinheit. Darüber hinaus zeigten biochemische Untersuchungen, dass die zytoplasmatische Sequenz von LAMP2 direkt an das SH3-GK-Modul von SAP102, einem GluN2B-Gerüstprotein, bindet. Da SAP102 und GluN2B nicht nur an Synapsen, sondern auch an extrasynaptischen Stellen zu finden sind, wurde die Beteiligung des extrasynaptisch gelegenen Pools von GluN2B-haltigen NMDARs am Stoppen und der Fusion von LAMP2-positiven Lysosomen vermutet.

Darüber hinaus wurde das Vorkommen von Prozessen der „chaperone-mediated autophagy" (CMA) in Dendriten gezeigt. Bei der CMA wird ein breites Spektrum intrazellulärer Proteine, die ein KFERQ-ähnliches Motiv enthalten, durch das Chaperonprotein Hsc70 erkannt und anschließend durch den obligatorischen Rezeptor LAMP2A in das lysosomale Lumen transloziert. Die Ergebnisse belegen nicht nur eine Assoziation des untersuchten lysosomalen Pools mit der CMA-Maschinerie, sondern auch, dass ein bekanntes Zielprotein der CMA, das TAR-DNA-bindende Protein 43 (TDP-43), in den angesäuerten LAMP2-positiven Lysosomen in Dendriten lokalisiert ist. Darüber

hinaus führte eine Aktivierung von NMDARs zu einer Freisetzung von TDP-43 aus neuronalen Zellen.

Zusammengenommen stellt die vorliegende Arbeit die Existenz heterogener dendritischer lysosomaler Pools dar und beschreibt einen neuartigen Mechanismus zur Entsorgung von Zielproteinen der CMA durch die aktivitätsabhängige Fusion von dendritischen LAMP2-haltigen Lysosomen mit der Plasmamembran. Die Freisetzung lysosomaler Inhalte, einschließlich aktiver Hydrolasen, könnte folglich den synaptischen Umbau ermöglichen, was eine neue Funktion von Lysosomen in Dendriten und ihre Verbindung zur neuronalen Plastizität enthüllt.

Dieser Dissertation sind keine Veröffentlichungen vorangegangen.

Table of content

Abbreviations

4AP	4-aminopyridine
AAV	Adeno-associated virus
AIS	Axonal initial segment
AMPAR	α-amino-3-hydroxy-5-methyl-4-isoxasolepropionic acid receptor
ANOVA	Analysis of Variance
AP	Action potential
AV	Autophagic vacuoles
Bic	Bicuculline
BSA	Bovine serum albumin
Bsn	Bassoon
CaM	Calmodulin
CaMKII	Calcium/calmodulin-dependent protein kinase II
cAMP	Cyclic adenosine monophosphate
Cas9	CRISPR associated protein 9
CatB/D	Cathepsin B/D
Cbln1	Cerebellin 1
CNS	Central nervous system
Co-IP	Co-immunoprecipitation
CPP	Cell penetrating peptide
CREB	cAMP response element-binding protein
CRISPR	Regularly interspaced short palindromic repeat
CSF	Cerebrospinal fluid
DIV	Day(s) *in vitro*
DMEM	Dulbecco's Modified Eagle's Medium
DMSO	Dimethylsulfoxide
dNTPs	Deoxynucleosidtriphosphate
EE	Early endosome
ELISA	Enzyme-linked immunosorbent assay
ER	Endoplasmic reticulum
ERGIC	Endoplasmic reticulum-Golgi intermediate compartment
EVPs	Extracellular vesicles and particles
F-actin	Filamentous actin
FCS	Fetal calf serum
GA	Golgi apparatus
GC	Genome copies
GFP	Green fluorescent protein
GK	Guanylate kinase
gRNA	Guide
GS	Golgi satellites
HEK293T	Human embryonic kidney cell line expressing SV40 antigen
ICC	Immunocytochemistry
ILV	Intraluminal vesicle
KD	Knockdown
KO	Knockout
LAMP	Lysosome-associated membrane protein
LE	Late endosome
LSD	Lysosomal storage disorder

LTD	Long-term depression
LTP	Long-term potentiation
MAP2	Microtubule-associated protein 2
MARCKS	Myristoylated alanine-rich C kinase substrate
MS	Mass spectrometry
mTORC	Mammalian target of rapamycin complex
MVB	Multivesicular body
NAADP	Nicotinic acid adenine dinucleotide phosphate
NMDAR	N-methyl-D-aspartate receptor
OD	Optical density
PAGE	Polyacrylamide gel electrophoresis
PBS	Phosphate buffered saline
PD	Pulldown
PEI	Polyethylenimine
PFA	Paraformaldehyde
PI	Propidium iodide
PLL	Poly-L-lysine
PSD	Postsynaptic density
RFP	Red fluorescent protein
ROI	Region of interest
RT	Room temperature
SD	Standard deviation
SDS	Sodium dodecyl sulfate
SEM	Standard error of the mean
SH3	Scr homology 3
SV	Synaptic vesicle
tdTomato	Tandem dimer Tomato
TFEB	Transcription Factor EB
TIRF	Total internal reflection
tRFP	Tag red fluorescent protein
TTX	Tetrodotoxin
WB	Western blot

1. Introduction

1.1 Morphology and function of neurons

1.1.1 Neurons are highly compartmentalized cells

The brain enables the processing and storage of received information and coordinates responses to the environment. Around 86 billion nerve cells, or neurons, are found in the human brain, forming complex neuronal networks that flexibly adjust to environmental inputs, hence allowing proper brain function (Herculano-Houzel, 2009).

Neurons show a great diversity including variations in their morphology depending on the cell type and brain area. They are highly polarized cells and consist of three main compartments: a cell body with an emerging long axon and multiple arborized dendrites (Figure 1; Donato et al., 2019). One neuron can harbor thousands of contact sites with other cells even far from the soma, where the axon connects with dendrites. At this intercellular connection site, the synapse, the axon transmits signals from the presynaptic site to the signal-receiving postsynaptic site of the dendrite.

Axons and dendrites are exemplary for the high degree of compartmentalization within one cell and, interestingly, differ in many aspects. Anatomically, axons are much more elongated and display a smaller and constant diameter compared to dendrites. While axons are devoid of protrusions, in dendrites the majority of excitatory synapses can be found at small protrusions, the dendritic spines (Gray, 1959). A special feature of axons is the axonal initial segment (AIS), a compartment at the proximal axon, which exhibits a distinct cytoskeleton composition to filter molecules and organelles entering the axon from the soma. Moreover, it is characterized by a high number of ion channels that are crucial for the initiation of action potentials (APs; Kole et al., 2008). The composition of organelles is distinct as well, with dendrites containing various somatic organelles while, on the contrary, relatively few organelles are present in axons (Goaillard et al., 2020). The movement of membrane-bound organelles is dependent on cytoskeleton components that are arranged differently in the neuronal compartments.

Figure 1: Neurons are polarized cells with a complex morphology. Neurons consist of different compartments including a cell body (soma), a long axon and branching dendrites. Dendritic spines emerge throughout the dendritic shaft in form of small protrusions and provide a platform for the formation of synaptic contacts.

Microtubules, as one major cytoskeletal component, display a mixed polarity in dendrites, whereas only plus-end-out oriented microtubules can be found in axons (Conde and Cáceres, 2009). These structural differences are accompanied by distinct microtubule dynamics and the association with certain Microtubule-associated proteins (MAPs), namely MAP2 solely in dendrites in contrast to the presence of Tau proteins in axons (Goaillard et al., 2020). Further, the dendritic and axonal compartments are functionally distinguishable. While the axon transmits neural signals, dendrites receive and process them. Apart from the soma, axon, and dendrites as neuronal compartments, smaller sub-compartments can be found, for instance, the presynaptic boutons, dendritic spines, as well as the AIS, which highlights the unique organization of neurons (Donato et al., 2019). The compartmentalization of neurons is thereby crucial for the ability of neurons to perform proper transmission of signals occurring at the synaptic contact sites, allowing brain function.

1.1.2 Synaptic transmission as the basis of neuronal communication

One of the neuronal cell types in the mammalian central nervous system (CNS) is the pyramidal neuron, which is mainly present in forebrain structures involved in complex cognitive functions, such as the cerebral cortex, hippocampus, or amygdala (Spruston, 2008). Pyramidal neurons are a major type of excitatory neurons and form glutamatergic synapses with their axons and dendrites. The chemical signal transduction at these synapses is achieved by the generation of an action potential (AP) upon depolarization of the cell membrane potential. In the AIS, voltage-gated sodium (Na^+) channels open when the neuronal membrane potential is above a certain activation threshold, leading to an AP. The AP travels along the axon and reaches the presynaptic terminal, resulting in an influx of calcium (Ca^{2+}) by voltage-gated calcium channels. In response to this, synaptic vesicles (SVs) fuse with the membrane and neurotransmitters are released from the presynaptic terminal into the synaptic cleft that consequently bind to receptors on the postsynaptic site (Dolphin and Lee, 2020). The activation of postsynaptic receptors by binding of neurotransmitters enables Na^+ and Ca^{2+} ion influx that regulate downstream processes. The influx of Na^+ accompanied by efflux of K^+ ions can lead to a change of the membrane electrical potential, consequently depolarization and, therefore, potentially generates another AP (Kennedy, 2016). In the case of excitatory synapses, the major neurotransmitter is glutamate. The release of glutamate thereby has to be tightly regulated to achieve the controlled activation of the postsynaptic glutamate receptors and to avoid toxic overstimulation (Zhou and Danbolt, 2014).

Changes in the efficacy of neuronal transmission at the synaptic compartments are crucial for brain function and form the cellular basis of memory and learning. One key area within the brain associated with memory and learning is the hippocampus, where the

strengthening of synaptic connections between neurons enables the formation and storage of memories (Kennedy, 2016). The neuron therefore physically modifies the synapse and adapts in an activity-dependent manner, a phenomenon called synaptic plasticity (Citri and Malenka, 2007).

1.1.3 Synaptic plasticity and the role of postsynaptic receptors

The content of receptors at the postsynaptic site is a determining factor for the strength or weakness of a synapse. One group of receptors is the class of α-amino-3-hydroxy-5-methyl-4-isoxasolepropionic acid receptors (AMPARs), which are ionotropic glutamate receptors assembled as a tetrameric complex by the subunits GluA1-A4 and key players during synaptic communication as mediators of fast excitatory transmission (Chater and Goda, 2014; Kennedy, 2016). The localization and number of AMPARs is tightly regulated by their exo- and endocytosis, processes that have been shown to be dependent on the phosphorylation status of the receptors (Collingridge et al., 2004; Lee et al., 2003).

The AMPAR amount and the phosphorylation state is tightly coupled to the presence and activity of another group of glutamate receptors, the N-methyl-D-aspartate receptors (NMDARs). NMDARs are ligand-gated cation channels that exhibit a crucial role in the context of synaptic plasticity. These glutamatergic receptors are located at excitatory synapses and show unique properties, such as the requirement of glutamate binding together with one co-agonist, either glycine or D-serine, for activation, high Ca^{2+}, as well as Na^+, permeability, and voltage-dependent channel blockage by extracellular magnesium (Mg^{2+}; Johnson and Ascher, 1987; Kleckner and Dingledine, 1988; Lerma et al., 1990; Schell et al., 1995).

In contrast to NMDARs, AMPARs depolarize the postsynaptic membrane rapidly after activation by glutamate through the resulting influx of Na^+ ions and K^+ efflux (Figure 2A). Due to a pore blockage by Mg^{2+}, the ion flow caused by NMDAR activation is minimized under basal conditions. Repeated membrane depolarization upon AMPAR activation releases the Mg^{2+} blockage, leading to a prominent influx of Ca^{2+} (Li et al., 2021; Mayer et al., 1984; Nowak et al., 1984). The Ca^{2+} influx by NMDARs is a requirement for long-term potentiation (LTP), as well as long-term depression (LTD), which modify the synaptic strength and hence underlie plasticity. During LTP, high Ca^{2+} influx by high-frequency stimulation results in activation of numerous kinases and downstream insertion of AMPARs (Hayashi et al., 2000). One key kinase in this process localized to a complex multiprotein web underneath postsynaptic membranes, the postsynaptic density (PSD), is the Ca^{2+}/calmodulin-dependent protein kinase II (CaMKII; Kelly et al., 1984). CaMKII binds calmodulin (CaM) in complex with Ca^{2+} (Ca^{2+}/CaM) and regulates the further activity of the NMDAR and phosphorylation state of the AMPAR subunit GluA1 (Leonard et al., 1999). The direct binding of Ca^{2+}/CaM to NMDARs results in inactivation of the channel and

consequently a lower rise in Ca^{2+} concentrations. In contrast, the binding of Ca^{2+}/CaM-bound CaMKII preserves the activity of the channel by the inhibition of direct binding of Ca^{2+}/CaM, one crucial step in the phase of early LTP (Sumi and Harada, 2020). LTD, on the other hand, requires a more gradual increase of Ca^{2+} which consequently activates phosphatases such as calcineurin (CaN) and initiates endocytosis of AMPARs (Carroll et al., 2001). Apart from the molecular reorganization, spines undergo structural changes with enlargements observed in response to LTP and shrinkage after induction of LTD (Bosch and Hayashi, 2012).

NMDARs are tetrameric transmembrane proteins composed of four subunits with two obligatory glycine-binding GluN1 subunits and two glutamate-binding GluN2 subunits (A-D), resulting in a diverse pool of NMDARs (Figure 2B-C; Sheng et al., 1994). The arrangement of the subunits thereby determines the properties of the receptor. GluN2A- and GluN2B-containing receptors, for instance, have comparable pore conductance and Ca^{2+} permeability properties, however, show a different temporal synaptic response due to the kinetics of their activation mechanism (Borschel et al., 2012; Glasgow et al., 2015; Monyer et al., 1994). During development, the expression patterns of the NMDAR subunits change. For instance, GluN2A expression starts shortly after birth and increases constantly until it is abundantly found in the adult brain. On the contrary, GluN2B is the more abundant subunit during development prior to synaptogenesis, however, is found in lower levels in the adult brain (Monyer et al., 1994; Paoletti et al., 2013; Sheng et al., 1994). Nevertheless, in the hippocampus and cortex, GluN2A and GluN2B are the predominant subunits, pointing to their importance for synaptic function and plasticity (Akazawa et al., 1994; Monyer et al., 1994).
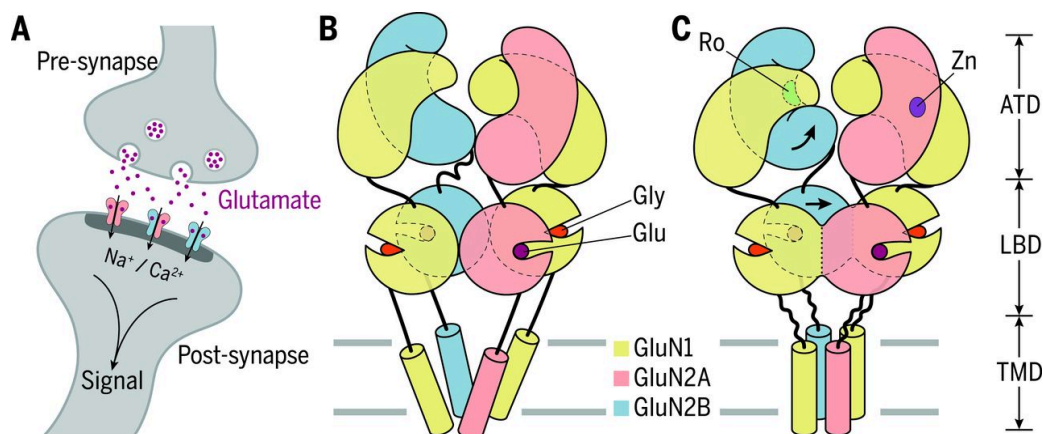
Figure 2: Di- and triheteromeric NMDARs are found in the postsynapse. (A) NMDARs are located at the postsynaptic site of a synapse. The binding of glutamate released from the pre-synapse activates the receptors and enables the influx of Na^+ and Ca^{2+} ions involved in downstream signaling. **(B)** Glycine binds to the GluN1 subunits whereas glutamate binds to the GluN2 subunits. **(C)** Structure of the NMDAR with its amino-terminal domain (ATD), ligand-binding domain (LBD), and transmembrane domain (TMD). The closure of the channel can be achieved by binding of the allosteric antagonists zinc and Ro to GluN2A and GluN2B, respectively (Lü et al., 2017).

NMDARs are anchored in the PSD of glutamatergic synapses by members of the membrane-associated guanylate kinases (MAGUKs), which display crucial constituents of the PSD structure and play an important role in the regulation of synaptic receptor contents, as well as in synaptic plasticity (Frank and Grant, 2017; Vieira et al., 2020; Won et al., 2017). The family of MAGUKs is composed of several members, namely PSD-95, PSD-93, SAP102, and SAP97. PSD-95 is the most prominent and well-studied member, whereas lesser is known about other MAGUK proteins. NMDARs interact with the different members of the MAGUKs and it was proposed that the activation of distinct downstream signaling pathways results from differential interactions of the receptors with the scaffold proteins (Frank et al., 2016). Contrary to PSD-95, SAP102 was shown to exhibit a higher binding affinity to the GluN2B over other subunits of the NMDAR and displays higher mobility (Elias et al., 2008; Sans et al., 2000; Zheng et al., 2010). NMDARs are not only found at synaptic but also at peri- and extrasynaptic sites, where the GluN2B subunit is more prevalently localized, although, extrasynaptic presence of GluN2A was also shown (Zhou et al., 2013a). In line with this, SAP102 is preferably localized at peri- and extrasynaptic sites (Chen et al., 2012; Hardingham and Bading, 2010; Zheng et al., 2011).

Extrasynaptic NMDARs can be activated by released glutamate from adjacent cells, such as astrocytes, or high-frequency stimulation of neurons that can result in glutamate spillover from the synaptic cleft (Figure 3; Asztely et al., 1997; Fellin et al., 2004; Rusakov and Kullmann, 1998). The activation of extrasynaptically localized NMDARs has been mainly associated with excitotoxicity and neuronal cell death, nonetheless, positive effects have been reported as well, such as neuroprotective signaling and enhanced synaptic strength (Hardingham and Bading, 2010; Harris and Pettit, 2008; Petralia, 2012). The content of NMDARs in the synapse is regulated by lateral diffusion and,
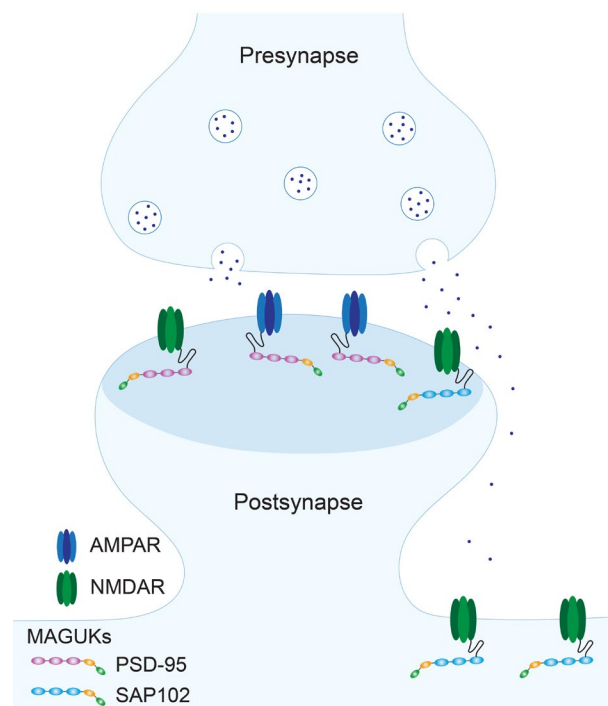
Figure 3: AMPARs and NMDARs are located at dendritic spines and are anchored by different MAGUK proteins. NMDARs can be localized at synaptic contact sites at the dendritic spines but are also extrasynaptically localized. In the dendritic spine, NMDARs and AMPARs are mainly anchored by PSD-95 whereas SAP102 is the preferential binding partner of GluN2B-containing extrasynaptic NMDARs. High stimulation can result in glutamate spillover, activating NMDARs that are located extrasynaptically.

5

interestingly, it was proposed that there is a potential exchange between synaptic and extrasynaptic pools of GluN2B-containing NMDARs by lateral movement of the receptors (McQuate and Barria, 2020). This could reflect a fast mechanism for regulation of activated downstream signaling pathways and therefore susceptibility to plasticity.

1.2 Protein homeostasis ensures cellular function

1.2.1 Protein synthesis and the secretory pathway

Neuronal transmission relies on a constant supply of various proteins of the synaptic membrane and is thereby dependent on proper transmembrane protein synthesis, sorting, and trafficking. Although the main translation capacity is found in the cell body, ribosomes and mRNA were shown to be present in dendrites, as well as in axons (Rangaraju et al., 2017). Dendritic mRNAs exhibit a surprisingly huge diversity and are essential for synaptic development and plasticity, encoding, among other proteins, neurotransmitter receptors, ion channels as well as adhesion molecules (Cajigas et al., 2012; Holt et al., 2019; Zhong et al., 2006). For a long time, there was controversy about the occurrence of local translation in axons, however, with more recent technological advances the presence of mRNA translation, as well as its functional implications have become clear (Dalla Costa et al., 2021). The transcription of mRNAs and protein synthesis were demonstrated to be activity-dependent, highly dynamic processes (Dieterich et al., 2010; Takei et al., 2004). These findings support the view of local synthesis that provides an efficient mechanism to maintain the local proteome and to meet the demands of the synapse directly at the site of transmission.

Newly synthesized transmembrane proteins can reach the synapse by different routes. In the canonical secretory pathway, transmembrane proteins are passing through numerous organelles to reach their destination. The endoplasmic reticulum (ER) is the starting point of the secretory pathway as it serves as a site for protein synthesis after the recruitment of ribosome-mRNA complexes to its membrane and is responsible for the proper folding of synthesized proteins as well as their first modifications (Schwarz and Blower, 2016). Following the release from the ER, proteins reach the Golgi apparatus (GA) through the ER-to-Golgi intermediate compartment (ERGIC), a sorting hub. In the GA, different modifications of the incoming proteins occur, such as the addition of sugar moieties as essential modifications for various cellular processes (Zhang and Wang, 2016). The cargo progresses through the *trans*-Golgi network (TGN) and is next delivered as modified version to the plasma membrane (Bard and Malhotra, 2006). Due to their intricate morphology, secretory organelles have adapted to neurons and are arranged differently in this cell type (Grochowska et al., 2022; Kennedy and Hanus, 2019). The ER, for instance, is found in the soma as a cisternal structure mainly with a ribosome-containing rough ER, whereas dendrites contain tubules of smooth ER with fewer ribosomes present (Krijnse-

Locker et al., 1995). The presence of Golgi-related compartments in dendrites, however, has been a matter of debate. The GA in dendrites is found not as Golgi stacks as normally observed in the soma but in form of small independent Golgi outposts (GOs) that are present in a subset of neurons and are generally constrained to the proximal primary dendrite and dendritic branching points (Hanus and Ehlers, 2008; Hanus and Schuman, 2013; Horton and Ehlers, 2003; Pierce et al., 2001). More recently, there has been evidence for a microsecretory system comprised of Golgi-related organelles, named Golgi satellites (GS), in the proximity of ERGIC and retromer which allow the passage of transmembrane proteins to the plasma membrane throughout the dendritic stretch (Mikhaylova et al., 2016). The retromer thereby mediates retrograde transport and therefore recycling of transmembrane proteins from the endosome back to the TGN or the plasma membrane (Burd and Cullen, 2014). This has been observed in the dendritic shaft and serves as a mechanism for fast receptor insertion at extrasynaptic and synaptic sites by retaining proteins instead of degrading them (Choy et al., 2014). Recently, there has been evidence that the formation of GS is activity-dependent, leading to increased glycosylation and consequently reshaping of the dendritic surface (Govind et al., 2021). The ER-ERGIC-GS-retromer microsecretory system reflects a highly adapted secretory pathway for local control of transmembrane protein processing and allows the local synthesis and post-translational modifications of synaptic proteins (Grochowska et al., 2022; Mikhaylova et al., 2016).

Synaptic neurotransmission imposes a tremendous metabolic demand and requires tight coordination of not only continuous protein synthesis but also degradation to ensure neuronal function (Grochowska et al., 2022).

1.2.2 Degradation pathways

1.2.2.1 Ubiquitin proteasome system (UPS)

Proteostasis includes the degradation of proteins, a process that can be achieved by different pathways. The ubiquitin-proteasome system (UPS) being one of them, is an efficient and fast way for numerous short-lived soluble proteins to be removed. The 26S proteasome, a large multicatalytic protease complex, recognizes ubiquitin-tagged proteins destined for degradation (Tai and Schuman, 2008). Target proteins get ubiquitinated by a three-step process involving the addition of small ubiquitin to a lysine residue (Kocaturk and Gozuacik, 2018). The UPS has been widely studied and was shown to degrade 80-90 % of eukaryotic cell proteins (Voges et al., 2003). It is, among others, involved in the regulation of cellular quality control, cell cycle, and DNA repair (Lilienbaum, 2013).

In neurons, the UPS was first described in the context of neurodegenerative diseases in which ubiquitin was found to be a component of protein deposits. Over time, the UPS was shown to be important for neuronal development and synaptogenesis, synaptic plasticity

as well as neuronal survival (Yi and Ehlers, 2007). Due to the complex morphology and compartmentalization of neuronal cells, proteasomal degradation faces certain challenges, though. Interestingly, the proteasome itself can be regulated by synaptic activity. It was shown that the proteasome is present in dendrites where it can translocate from dendritic shafts to the dendritic spines upon depolarization with KCl in an NMDAR-dependent manner. There, it could possibly degrade synaptic substrates such as PSD-95 to drive local remodeling of spines (Bingol and Schuman, 2006; Colledge et al., 2003). In axons, the proteasome activity is a requirement for axonal degeneration during development and post nerve injury as well as activity-dependent presynaptic silencing (Jiang et al., 2010; Watts et al., 2003).

In the case of a non-functional or overloaded UPS, other degradation pathways are upregulated and compensate for this loss, changing the view of independently acting systems to a rather possible cross-talk and adaption between them (Korolchuk et al., 2010; Mebratu et al., 2020).

1.2.2.2 Macro- and microautophagy

Autophagic processes reflect other highly conserved degradation pathways consisting of three major types: macroautophagy, microautophagy, and chaperone-mediated autophagy (CMA). Autophagy targets cellular material such as defective organelles and misfolded proteins for lysosomal digestion (Aman et al., 2021). In macroautophagy, cargo is engulfed by a cup-shaped double membrane phagophore which then closes to form a vesicle called autophagosome. The autophagosome eventually fuses with the acidified, catabolic active lysosome, forming a hybrid-organelle named autolysosome (Andres-Alonso et al., 2021). Autophagosomes can additionally fuse with late endosomes (LEs) or multivesicular bodies (MVBs), resulting in the hybrid organelle amphisome, that eventually finds its way to the lysosome as well (Figure 5; Andres-Alonso et al., 2021). During the formation of the phagophore and autophagosome, membrane sources including the plasma membrane, the Golgi apparatus, the ER, and mitochondria are essential, whereas autophagy-related genes (ATGs) are the key mediators (Ariosa and Klionsky, 2016; Hamasaki et al., 2013).

For a long time, autophagy was thought to be a nonselective degradation pathway, however, more recently it was shown to be crucial for selective degradation of not only specific proteins but also organelles. The clearance of organelles is essential for organelle integrity and number depending on the environment. Selective degradation of organelles was observed for various organelles such as mitochondria ("mitophagy"), peroxisomes ("pexophagy"), lysosomes ("lysophagy"), ER ("ERphagy") and the nucleus ("nucleophagy"; Anding and Baehrecke, 2017).

Another autophagic pathway, called microautophagy, is a non-selective autophagic pathway that relies on endosomal membrane invaginations and thereby sequesters cytosolic target proteins to form MVBs (Figure 5; Sahu et al., 2011). It has been mainly studied in yeast cells but was more recently observed in mammalian cells as well (Seki and Katsuki, 2022).

Although macroautophagy is well studied in non-neuronal cells, less is known about its characteristics in neurons. The organization of the autophagic machinery is adjusted to the high compartmentalization, which is already reflected by the different molecular composition of autophagosome populations found in the soma as compared to axonal ones (Maday and Holzbaur, 2016). Autophagosome biogenesis can be observed especially in distal axons where it is, as well as autophagosome motility, regulated in an activity-dependent manner (Hill and Colón-Ramos, 2020; Kallergi et al., 2020; Wang et al., 2015). Surprisingly, in contrast to non-neuronal cells, starvation signals such as amino acid deprivation do not have a detectable impact on autophagy levels in axons of hippocampal neurons (Maday and Holzbaur, 2016; Mizushima et al., 2004). This could indicate the existence of a protective mechanism to make the axon less susceptible to stress signals in the post-mitotic neuron. Interestingly, neuronal amphisomes were found to exhibit also a non-degradative signaling function at presynaptic boutons during retrograde movement to promote transmitter release upon presynaptic signaling (Andres-Alonso et al., 2019).

In contrast to axons, lesser is known about autophagy in dendrites. Recently, it has been shown that in dendrites, but not in axons, synaptic activity leads to changes in autophagic vacuoles (AVs) motility and increases the number of degradative autolysosomes (Kulkarni et al., 2021). Additionally, evidence was provided that autophagy is important in dendrites to degrade postsynaptic proteins, hence being indispensable for LTD (Kallergi et al., 2022).

Taken together, autophagy in neurons is thought to play a less important role for amino acid mobilization and a more critical role for development and homeostasis, especially in connection to synaptic activity (Maday and Holzbaur, 2014; Shehata et al., 2012; Shen and Ganetzky, 2009).

1.2.2.3 Chaperone-mediated autophagy (CMA)

Another autophagic process is chaperone-mediated autophagy (CMA), in which soluble cytoplasmic cargo that contains a specific CMA-recognition motif (KFERQ-like sequence) is recognized by heat shock-cognate chaperone 70 kDa (Hsc70), and its co-chaperones. After binding, the complex is directly delivered to the lysosome, where dimerization of LAMP2A, a lysosomal membrane protein, enables subsequent translocation of the unfolded target client into the lysosomal lumen (Figure 4; Kaushik and Cuervo, 2018).

Hsc70 is a member of the heat shock protein (HSP70) family of chaperones which is involved in ATP-dependent binding of unfolded or aggregated peptides to protect them from unwanted interactions with other molecules or target them for degradation, in the latter case, especially in response to heat or other cellular stress stimuli (Fernández-Fernández et al., 2017; Ryu et al., 2020). The activity of chaperones of the HSP70 family is dependent on their co-chaperones. Hsc70, for instance, is regulated, among others, by DnaJ/Hsp40 proteins which stimulate ATPase activity and present target proteins to Hsc70 as observed in CMA (Meimaridou et al., 2009). Hsc70 is mainly present in the cytoplasm but is additionally found in the lysosomal lumen (lys-Hsc70) where it proceeds to facilitate protein import in an ATP-independent manner (Agarraberes et al., 1997; Meimaridou et al., 2009). The intraluminal localization is in line with the presence of two KFERQ motifs in its sequence that may mediate its own translocation (Cuervo et al., 1997). Until now, Hsc70 is the only chaperone that is known to exhibit direct binding to the required pentapeptide sequence and therefore to mediate CMA (Kaushik and Cuervo, 2018). The rate-limiting factor for the degradation of CMA targets, however, is the lysosomal membrane protein LAMP2A levels and dynamics. LAMP2A levels thereby change by regulation of its degradation or transcription in response to different stimuli (Kaushik and Cuervo, 2018).
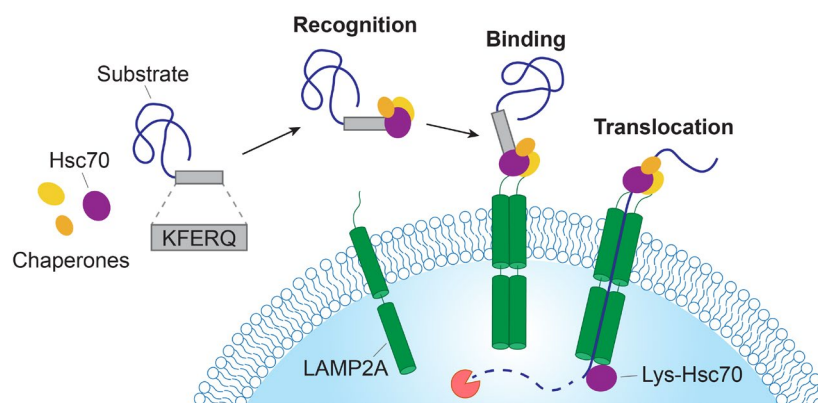
Figure 4: Chaperone-mediated autophagy (CMA) mediates the degradation of cytoplasmic proteins carrying a specific pentapeptide sequence. Intracellular substrates with a KFERQ-like-motif are recognized by the chaperone Hsc70 and its co-chaperones. The chaperone-substrate complex binds to the cytoplasmic tail of LAMP2A at the lysosomal surface, resulting in the formation of a translocation complex. The lys-Hsc70, a lysosome resident form of Hsc70, mediates the internalization of the target protein, following its degradation by lysosomal enzymes. Lys-Hsc70 additionally induces the disassembly of multimerized LAMP2A after the substrate is translocated.

CMA is a major pathway involved in the degradation of up to 40 % of cytoplasmic proteins (Hosaka et al., 2021). Until now, CMA has only been observed in mammalian cells and birds and was shown to be upregulated by prolonged starvation and oxidative stress in non-neuronal cells (Cuervo et al., 1995; Kiffin et al., 2004). During age, CMA rates decline due to decreased stability of LAMP2A and could account for the increased protein damage, as well as aggregation (Zhang and Cuervo, 2008).

CMA is found in neurons as well, where it reflects an essential component in the maintenance of the neuronal proteome. For instance, it modulates the neuronal survival machinery by degradation of transcription factor myocyte enhancer factor 2D (MEF2D) to ensure the proper response to injury (Yang et al., 2009). Additionally, CMA is associated with numerous neurodegenerative diseases such as Parkinson's disease (PD), Alzheimer's disease (AD), and Huntington's disease (HD; Auzmendi-Iriarte and Matheu, 2021). Interestingly, CMA has not been well studied concerning the different neuronal compartments and it is not known if the process of CMA can be observed locally in dendrites or axons.

One known substrate of CMA is the TAR DNA binding protein 43 kDa (TDP-43), a protein linked to amyotrophic lateral sclerosis (ALS) and frontotemporal lobar degeneration (FTLD), diseases in which the presence of TDP-43 aggregates in protein inclusions in neuronal cells of affected patients is a characteristic hallmark (Ormeño et al., 2020). TDP-43 was originally described as a transcription factor and splicing regulator, but over time, additional functions in the regulation of RNA metabolism such as mRNA stability, mRNA transport, and stress granules formation, were shown (Ratti and Buratti, 2016). Although it exhibits a prominent nuclear localization, TDP-43 shuttles to the cytoplasm aggregation can occur, leading either to gain-of-toxic-function or a loss-of-function (Ayala et al., 2008; Ling et al., 2013; van den Broeck et al., 2015). While CMA is involved in the turnover of TDP-43 to control a proteostatic equilibrium prior to its aggregation, TDP-43 aggregates themselves affect CMA performance by upregulation of both Hsc70 and LAMP2A, a mechanism that has been observed for other aggregate-prone proteins as well (Koga et al., 2011; Mak et al., 2010; Ormeño et al., 2020). Interestingly, DnaJ/Hsc70 chaperone complexes regulate the release of different proteins associated with neurodegenerative diseases to the extracellular space, including TDP-43 (Fontaine et al., 2016).

1.2.2.4 Endolysosomal pathway

In the endolysosomal pathway, endocytosed material is delivered to the lysosome through a process that involves various fusion and fission events, including the delivery of internalized material to the early endosome (EE) as a first step. In the EE, cargo is directed to recycling endosomes (REs) for its reuse back to the plasma membrane or, alternatively, processed further by the endosomal sorting complex required for transport (ESCRT) machinery (Henne et al., 2011; Katzmann et al., 2001; Li and DiFiglia, 2012). Ubiquitination of cargo thereby serves as a sorting signal for the ESCRT for the subsequent packing into intraluminal vesicles (ILVs), leading to the generation of MVBs (Katzmann et al., 2001). During the maturation process of the EE, the lumen acidifies and late endosomes (LEs) arise that eventually fuse with the lysosome (Figure 5). The fusion processes are thereby regulated by Rab proteins, small GTPases of the Ras superfamily.

Rab proteins go through cycles of GTP binding and GDP hydrolysis, leading to conformational changes (Homma et al., 2021). In the early endocytic pathway, Rab5, Rab4, and Rab11 facilitate vesicle fusion whereas Rab7 and Rab9 are involved in fusion events of EEs/LEs and lysosomes (Wandinger-Ness and Zerial, 2014). Rabs are frequently used markers for the different intermediate organelles within the endolysosomal and autophagic pathways.

Central to all autophagic pathways as well as the endolysosomal route is the lysosome, the main catabolic organelle in the cell where final degradation takes place, a process critical for neuronal survival.
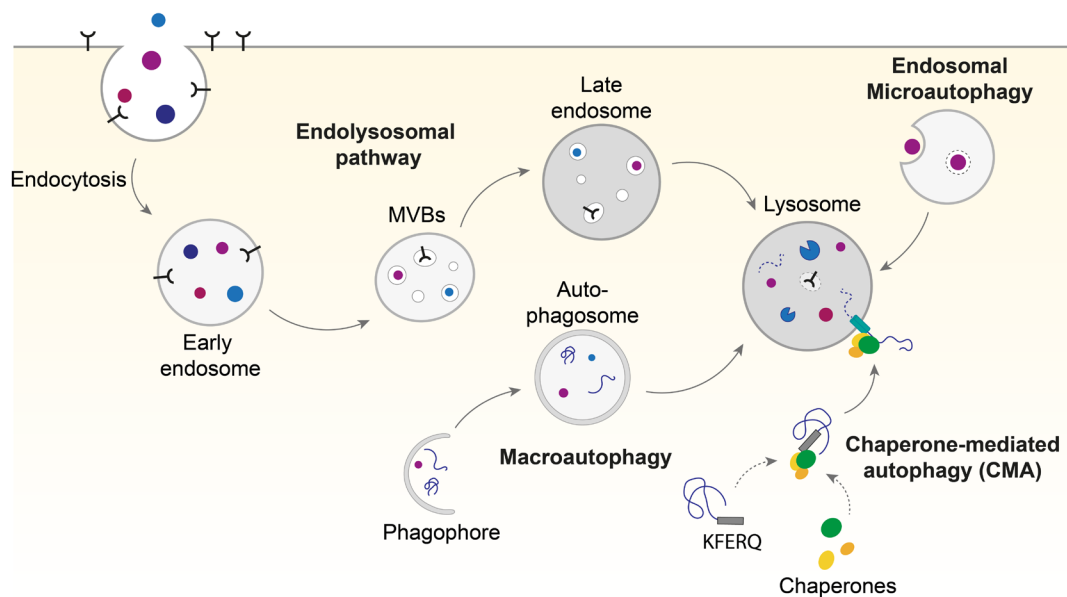
Figure 5: Various degradation pathways end in the central degradative organelle, the lysosome. Endocytosed cargo is sorted to the early endosome (EE) following sorting to multivesicular bodies (MVBs) for further transport via the late endosome (LE) to the lysosome for final degradation. Autophagic pathways target intracellular cargo either by invaginations, as seen for (endosomal) microautophagy, or by the formation of a double-membrane phagophore becoming an autophagosome, observed in macroautophagy. Cargo containing a KFERQ-like motif can be recognized by chaperones which bind to LAMP2A at the lysosomal surface for translocation of target proteins, a process called chaperone-mediated autophagy (CMA). The lysosome is an acidified organelle containing numerous hydrolases and is therefore the catabolic center of various degradation pathways.

1.3   The lysosome

The lysosome is considered the endpoint of long-lived proteins, mainly membrane, and endocytosed proteins, as well as cargo targeted by autophagy (Luzio et al., 2007). The lysosome was discovered in the 1950s by Christian de Duve, who observed an electron-dense organelle in electron micrographs of fractionated cells and concluded that this was an acidified vesicle packed with hydrolytic enzymes for digestion of macromolecules (de Duve et al., 1955). Nowadays, the lysosome has been extensively studied and described in different cell types. It is characterized by the low pH (4.5-5.0) within its lumen that is

maintained by a proton-pumping vacuolar ATPase, hence providing a suitable environment for the activity of more than 60 acid hydrolases required for its catabolic function (Figure 6A; Ballabio and Bonifacino, 2020; Mindell, 2012). To reach the lysosome, these enzymes acquire a mannose-6-phosphate (M6P) tag in the Golgi and are recognized in the *trans*-Golgi network (TGN) by the mannose-6-phosphate receptor (M6PR; Repnik et al., 2013). They travel as a complex through EEs to then dissociate from each other in the acidic lumen of LEs. The M6PR recycles back for reuse to the TGN, whereas the hydrolases reach the lysosome (Hunziker and Geuze, 1996). Several studies have described M6P-independent routes for hydrolases as well as the involvement of alternative receptors, for instance, β-glucocerebrosidase which is delivered by the lysosomal integral membrane protein-2 (LIMP2; Blanz et al., 2015; Dittmer et al., 1999; Reczek et al., 2007).

A large proportion of lysosomal proteases are members of the family of cathepsins. Cathepsins can be classified into cysteine, serine, or aspartic proteases, depending on the amino acid residue required for their catalytic activity (Turk et al., 2012). At present, 15 human cathepsin classes have been described (Patel et al., 2018). Of these, cathepsin B, D, and L represent the most abundant proteases of the lysosome with cathepsin B being present with a high concentration equivalent to 1 mM in the lysosomal lumen (Yadati et al., 2020). Apart from protein degradation, cathepsins are essential for numerous physiological functions and have been implicated, among others, in MHC-II-mediated antigen presentation, bone remodeling, and prohormones activation (Brix et al., 2001; Honey and Rudensky, 2003; Saftig et al., 2002; Turk et al., 2002). Therefore, cathepsins and their dysregulations are connected to a wide range of diseases such as cancer, cardiovascular diseases, and metabolic disorders (Reiser et al., 2010).

Although most cathepsins require an acidic pH to be active, some were described to exhibit activity even at neutral pH (Kirschke et al., 1986; Sapolsky et al., 1974). Also, their localization is not limited to the endolysosomal system but they can be found additionally in the cytoplasm, cell nucleus, or extracellular space (Brix et al., 2008; Goulet et al., 2004). In the extracellular space, cathepsin B and D, in particular, play a role in extracellular matrix (ECM) remodeling by degrading structural components, a process that could be essential for axon migration during development and dendritic spine growth, hence synaptic plasticity (Tran and Silver, 2021; Vidak et al., 2019). Abnormal activity of cathepsins in the CNS has been reported in traumatic brain injury as well as neurodegenerative diseases, highlighting their broad range of function (Hook et al., 2020). In the case of neurodegenerative disorders such as Alzheimer's, Parkinson's, and Huntington's disease but also lysosomal storage disorders (LSDs) a common feature is the accumulation of storage material (Parenti et al., 2021). The majority of LSDs are

caused by deficiencies in soluble hydrolases involved in the degradation of substrates or their impaired sorting to the lysosome (Platt et al., 2018). However, it is not clear yet if the observed pathology in these diseases is due to the storage and accumulation of non-degraded material or rather secondary events such as secondary storage of unrelated material, abnormal membrane composition and fusion events, defective Ca^{2+} signaling, and activation of inflammatory processes (Parenti et al., 2021; Platt et al., 2018).

1.3.1 Lysosomal membrane composition

The lysosomal membrane consists of a variety of integral lysosomal membrane proteins (LMPs) of which the lysosome-associated proteins (LAMPs), particularly LAMP1 and LAMP2, represent the majority (Saftig and Klumperman, 2009). LAMP1 and LAMP2 are transmembrane proteins with a sequence homology of 37 % characterized by a heavily glycosylated luminal domain and a short cytoplasmic tail (Saftig and Klumperman, 2009). Due to the high degree of glycosylation, LAMP1 and LAMP2 are considered to form a "glycocalyx" layer on the luminal site of the lysosome as protection from the acidic environment and hydrolases (Neiss, 1984).

Despite their similarity, LAMP1 and LAMP2 are proposed to serve different functions. This became apparent in knockout (KO) mice where deletion of LAMP1 led to a rather mild phenotype with upregulated LAMP2 expression, reflecting a potential compensation mechanism. However, LAMP2 deletion resulted in a much more severe phenotype with increased postnatal mortality and the accumulation of autophagic vacuoles in various tissues (Tanaka et al., 2000). Indeed, it was shown that mutations in the LAMP2 gene are the underlying cause of Danon disease, an X chromosome-linked disorder characterized by impaired glycogen degradation and abnormal autophagic vacuoles resulting in cardiomyopathy and mental retardation (Endo et al., 2015). In a study investigating LAMP-deficient cells, the lysosomal morphology, as well as the degradative ability and acidification of lysosomes, was demonstrated to not be impaired, further pointing to other lysosomal membrane proteins potentially compensating for the loss (Eskelinen et al., 2004).

Following alternative splicing, three different isoforms of LAMP2 (A, B, and C) are expressed that differ in their amino acid sequence identity, especially in the cytosolic region (Figure 6B; Eskelinen et al., 2005; Gough et al., 1995). The isoforms exhibit distinct tissue distribution patterns and are each implicated in different cellular functions. LAMP2A is, with its unique cytosolic tail, the required receptor for protein translocation in the process of CMA as described above (Cuervo and Dice, 2000). LAMP2B, on the other hand, is connected to lysosomal fusion and maturation as well as macro-autophagy, whereas LAMP2C is involved in the uptake of RNA/DNA molecules and inhibition of CMA (Fujiwara et al., 2013a, 2013b; Pérez et al., 2016).
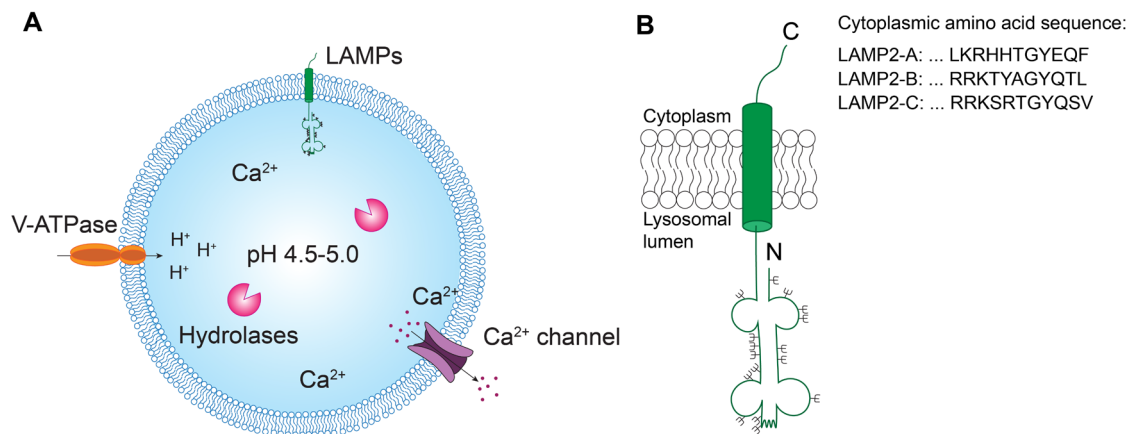
Figure 6: The lysosome as the central acidic organelle and the lysosomal membrane protein LAMP2. (A) The lysosome is a single membrane organelle exhibiting a low pH (4.5-5.0) environment, required for the proper activity of multiple hydrolases and thereby maintained by a V-ATPase. High levels of Ca^{2+} in the lumen of the lysosome can be released by Ca^{2+} channels. **(B)** Structure of LAMP2 and the amino acid sequence of the isoforms LAMP2A-C according to the nomenclature proposed by Eskelinen et al. (2005). Forks represent *N*-glycosylation, disulfide bonds form the loops and the zigzag shows the hinge region rich of proline where additional *O*-glycosylation sites can be found (Eskelinen et al., 2005).

1.3.2 Lysosomal calcium

The lysosome is filled with various enzymes for its canonical function of degradation. Beyond this, the lysosomal organelle emerged as an essential intracellular Ca^{2+} store with surprisingly high levels of around 0.5 mM Ca^{2+}, an amount comparable to the Ca^{2+} present in the ER which reflects one of the largest Ca^{2+} stores within the cell (Christensen et al., 2002; Parenti et al., 2021). Ca^{2+} is required for various lysosomal functions and impaired Ca^{2+} homeostasis causes lysosome dysfunction. Ca^{2+} release thereby mediates lysosomal acidification, membrane trafficking, as well as fusion of the lysosome with other structures, such as endosomes or the plasma membrane (Lloyd-Evans and Waller-Evans, 2020). Additionally, contacts with the ER are formed in a Ca^{2+}-dependent manner which is essential for the refilling of lysosomal Ca^{2+} stores (Garrity et al., 2016; Wang et al., 2017). One important Ca^{2+} channel in the lysosomal membrane is the transient receptor potential cation channels of the mucolipin 1 (TRPML1) that regulates the release of Ca^{2+} from the lumen of the lysosome upon different stimuli, for instance starvation (Parenti et al., 2021; Wang et al., 2014). In addition, the endolysosome-specific membrane phosphoinositide phosphatidylinositol 3,5-biphosphate ($PI(3,5)P_2$), can serve as an activator of TRPML1, highlighting its involvement in intracellular processes such as membrane trafficking (Dong et al., 2010). Apart from TRPML1, Ca^{2+} efflux can be mediated by other channels, and in response to other stimuli such as pH changes or even by molecules like ATP or nicotinic acid adenine dinucleotide phosphate (NAADP; Ballabio and Bonifacino, 2020).

1.3.3 Lysosome as a signaling hub

The presence of catabolic hydrolases ensures the degradative function of lysosomes, however, the lysosome is additionally implicated in various other processes. One example is its, more recently, emerged role as a major signaling hub. In connection to this, different protein complexes can be formed at the lysosomal membrane in response to stimuli (Heitman et al., 1991). In response to nutrients, the multicomponent kinase mammalian target of rapamycin complex 1 (mTORC1) is recruited to the lysosomal surface and binds to a Rag GTPase-Ragulator complex (Lawrence and Zoncu, 2019; Sancak et al., 2010). This activation initiates downstream signaling pathways, supporting anabolic processes and growth in presence of amino acids, and negatively regulates autophagy. The activation of mTORC1 additionally leads to phosphorylation of transcription factor EB (TFEB), one master regulator of lysosomal biogenesis and function, and thus regulates its localization predominantly to the cytosol as an inactive form (Martina et al., 2012; Napolitano et al., 2018). During starvation, mTORC1 is inactivated and allows the translocation of TFEB to the nucleus to promote transcription of genes involved in the expression of lysosomal proteins and enzymes and regulates acidification, positioning, and exocytosis of lysosomes, as well as autophagosome biogenesis and autophagy (Ballabio and Bonifacino, 2020; Palmieri et al., 2011; Sardiello et al., 2009). Interestingly, LAMTOR1, as part of the Ragulator, inhibits TRPML1 activity and thereby regulates lysosomal trafficking in a Ca^{2+}-dependent manner (Sun et al., 2022). This inhibition is accompanied by GluA1 dephosphorylation, reflecting the importance of Ca^{2+} as a signaling molecule in connection to synaptic strength and plasticity. mTORC2 is another protein complex that can be formed in response to growth factors, though it does not show involvement in TFEB phosphorylation (Settembre et al., 2012). However, mTORC2 is involved in GFAP phosphorylation through AKT signaling, an important signaling cascade for CMA (Arias et al., 2015). Both mTORC1 and mTORC2 are thereby composed of a unique set of proteins, hence signal to distinct downstream effectors.

1.3.4 Trafficking of lysosomes

The response to various stimuli is coupled with regulated mobility and localization of lysosomes. Lysosomes are highly mobile and can move bi-directionally on microtubule tracks throughout the cell (Pu et al., 2016). In non-neuronal cells as well as in axons of neurons, long-range retrograde movement is mediated by minus-end-directed dynein-dynactin motor complexes whereas anterograde movement is carried out by plus-end-directed kinesin motors (Lawrence and Zoncu, 2019). While microtubules display a uniform arrangement in axons with the growing plus-end facing the axon tip, they show a mixed polarity in dendrites (Conde and Cáceres, 2009). Therefore, the trafficking has to be organized differently in dendritic compartments, with either kinesin or dynein being

responsible for retrograde trafficking (Winckler et al., 2018). Dynein-dependent movement is regulated through the small GTPase Rab7 that interacts with its effector RILP leading to the recruitment of dynein-dynactin motor complexes (Jordens et al., 2001). RILP was proven to be essential for neuronal autophagosome transport and biogenesis, regulating autophagic turnover in response to mTOR activity (Khobrekar et al., 2020). The trafficking of lysosomes by a kinesin-dependent mechanism, on the other hand, is mediated by the multi-subunit complex BLOC1-related complex (BORC) at the lysosomal membrane where it interacts with the small GTPase ADP-ribosylation factor-like protein 8 (Arl8) and its effector SKIP to couple lysosomes to kinesin-1, one member of the kinesin superfamily. This lysosomal transport mechanism was shown in non-neuronal cells as well as axons, but not dendrites, of neurons (Farías et al., 2017; Pu et al., 2015; Rosa-Ferreira and Munro, 2011). Interestingly, a study showed that lysosomes in HeLa cells can be coupled to kinesin-1 by the ER-localized protrudin, Rab7, and its effector FYCO1 upon ER-endolysosome contact as an alternative mechanism (Raiborg et al., 2015). In dendrites, another protein from the kinesin family, kinesin-3, was recently identified to mediate anterograde lysosomal transport via Arl8A (Hummel and Hoogenraad, 2021).

One of the subunits of the Ragulator complex, LAMTOR1, was shown to interact with BORC as a regulatory mechanism for lysosomal positioning depending on nutrient availability in non-neuronal cells (Pu et al., 2017). Depletion of amino acids strengthens the interaction between Ragulator and BORC and as consequence leads to a perinuclear distribution of lysosomes whereas epidermal growth factor stimulation negatively regulates the association and results in more outward lysosomal movement (Filipek et al., 2017; Pu et al., 2017). The trafficking and position of lysosomes in the cell are coupled to their pH and it was shown that peripheral lysosomes are strikingly less acidic in mammalian cell culture (Johnson et al., 2016). In neurons, the degree of acidification was also proposed to be dependent on the distance to the cell body, for both axonal as well as dendritic lysosomes, with distal parts containing mainly non-acidified organelles (Cheng et al., 2018, 2015; Gowrishankar et al., 2015; Maday et al., 2012; Yap et al., 2018).

1.3.5 Lysosomes in neurons: axons versus dendrites

Over time, it became apparent that lysosomes exhibit high heterogeneity in terms of their functions, morphology, motility, localization, and molecular characteristics such as membrane composition. In axons, the unidirectional transport of less acidic autophagosomes from the distal end towards the soma was shown, proposing that during this retrograde movement autophagosomes acquire hydrolases and undergo a maturation process resulting in acidified degradative organelles (Figure 7; Farfel-Becker et al., 2019; Maday and Holzbaur, 2016; Maday et al., 2012). These observations lead to a model of gradual lysosomal acidification and maturation upon retrograde trafficking of endosomes

not only in the axon but also in dendrites of neurons, suggesting the presence of mature lysosomes with active enzymes solely in the soma and its vicinity (Cheng et al., 2015, 2018; Gowrishankar et al., 2015; Maday et al., 2012; Yap et al., 2018).
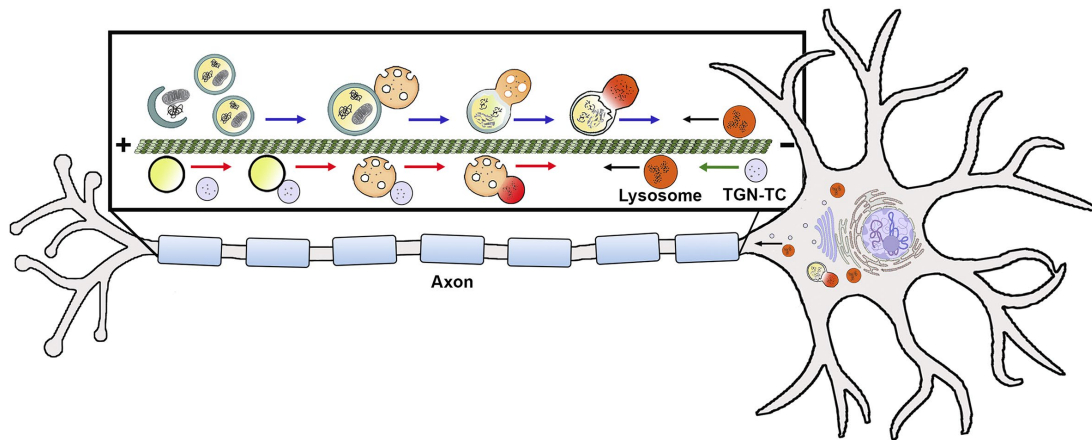
Figure 7: Maturation of endo- and autolysosomal organelles during retrograde movement in axons. The scheme at the top displays the formation of autophagosomes in distal axon tips and the fusion with LEs. On the bottom, the route of cargo is shown from EEs to LEs. Lysosomal contents, including enzymes, can be delivered by lysosomes or TGN-derived transport carriers (TCs; modified from Roney et al., 2022).

Nonetheless, some reports demonstrate a distribution of lysosomes that contain active hydrolases in axon bundles and distal axon tips (Farfel-Becker et al., 2019; Farías et al., 2017; Roney et al., 2021). Intriguingly enough, the presence of acidified lysosome was observed in dendrites and dendritic spines even in more peripheral regions (van Bommel et al., 2019; Goo et al., 2017; Padamsey et al., 2017).

The function of lysosomes in dendrites was thereby more recently linked to synaptic activity, reflected by the described enhancement of recruitment of LAMP1-positive organelles to dendritic spines and decreased spine density upon lysosomal inhibition (Goo et al., 2017). The localization of lysosomes correlated with internalized synaptic proteins, such as AMPARs, and was regulated by AMPAR- as well as NMDAR-activity (Goo et al., 2017). Evidence was provided that the positioning of lysosomes at dendritic spines is thereby an actin-mediated mechanism in which lysosomes stall at filamentous actin (F-actin) patches present in excitatory shaft synapses, as well as at the base of dendritic spines (van Bommel et al., 2019). Another study revealed activity-dependent lysosomal exocytosis, a process that leads to ECM remodeling and dendritic spine growth (Padamsey et al., 2017). The fusion event is mediated by lysosomal Ca^{2+}-release in response to back-propagating action potentials (bpAPs), therefore driving the exocytosis of LAMP2-positive lysosomes and disposal of their content to the extracellular space. It was proposed that cathepsin B activates matrix metalloproteinase 9 (MMP-9), an enzyme involved in the remodeling of ECM and consequently dendritic spine growth, therefore regulating plasticity (Padamsey et al., 2017). Apart from lysosomal hydrolases, such as

cathepsin B, the lysosomal content that is considered to be disposed by this mechanism, has not been further investigated.

1.3.6 Secretory lysosomes and exocytosis

The process of lysosomal fusion has been demonstrated for a distinct subset of lysosomes, the secretory lysosomes. Secretory lysosomes are specialized organelles that have been described in non-neuronal cell types, in which exocytosis is observed upon stimuli connected to plasma membrane injury, cellular stress, cancer, or signals from cytokines (Reddy et al., 2001; Samie and Xu, 2014). During the event of exocytosis, lysosomes are positioned close to the plasma membrane to subsequently release their content to the extracellular space in a Ca^{2+}-dependent manner. The fusion is thereby mediated by soluble N-ethylmaleimide-sensitive factor-attachment protein receptors (SNAREs) complexes that are additionally involved in autophagosome-late endosome fusion or the fusion of late endosomes with lysosomes (Buratta et al., 2020). SNAREs are classified into vesicle-associated SNAREs (v-SNAREs) and target-associated SNAREs (t-SNAREs), depending on their location. The v-SNARE vesicle-associated membrane protein 7 (VAMP7) on the lysosomal surface forms a complex together with syntaxin-4 and synaptosome-associated protein of 23 kDa (SNAP23) which are both located on the plasma membrane, collectively forming a *trans*-SNARE complex (Rao et al., 2004). The two membranes are consequently pulled closer together to allow the lysosome to dock at the plasma membrane (Figure 8). A local rise in Ca^{2+}-levels initiates the final fusion by promoting interaction between synaptotagmin VII (SytVII) and the formed *trans*-SNARE complex, in which the lysosome itself potentially serves as the required Ca^{2+} source by the release of Ca^{2+} through TRPML1 from its lumen (Buratta et al., 2020). This was further supported by the finding that TFEB overexpression and consequent TRPML1 activation increased exocytosis *in vitro* and *in vivo* (Medina et al., 2011). Interestingly, lysosomal exocytosis was more recently shown to further be involved in intercellular signaling by astrocytes that release ATP through fusion of lysosomes (Dou et al., 2012). Although exocytosis of lysosomal vesicles is a known phenomenon, it remains elusive which pool of lysosomes, including its required characteristics and molecular markers, can undergo this process.
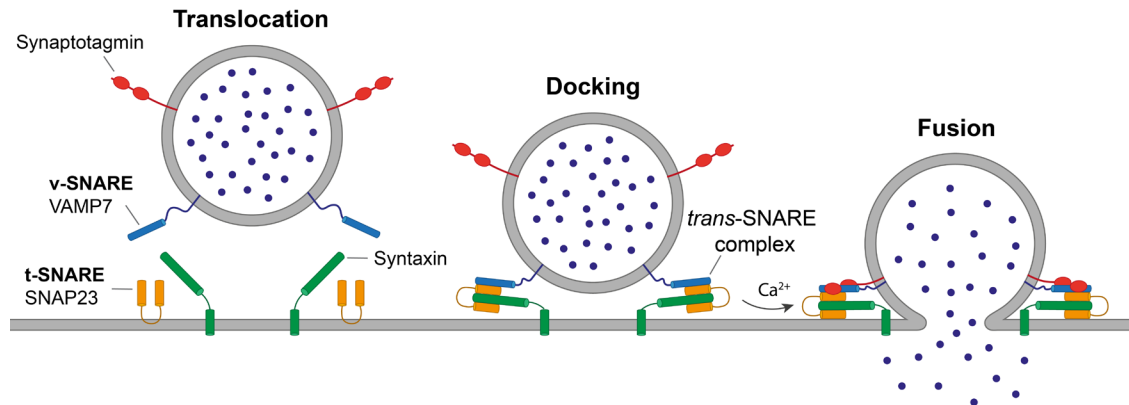
Figure 8: Exocytosis is mediated by SNARE proteins and their complex assembly. The fusion of vesicles with the cell membrane is mediated by SNARE proteins. A v-SNARE localized to an approaching vesicle, such as VAMP7 (blue), interacts with the t-SNARE SNAP23 (orange) at the plasma membrane as well as with syntaxin (green). Synaptotagmin (red) is a Ca^{2+}-sensing regulatory protein. The assembly of a *trans*-SNARE complex results in a docking of the vesicle. Upon Ca^{2+} influx, the ions bind to the Ca^{2+}-binding domains of synaptotagmin and therefore the membranes are pulled together. This leads to the opening of a fusion pore, allowing the release of vesicular content.

1.4   Aims and objectives of the thesis

The presence of lysosomes, as the central catabolic hub, has been described for the soma, as well as axons of neurons, and, more recently, mature lysosomes have been additionally observed in the dendritic compartment. Intriguingly, the motility of dendritic LAMP1-positive lysosomes was shown to be regulated by the activity of the excitatory glutamate receptors AMPARs and NMDARs (Goo et al., 2017), whereas LAMP2-positive lysosomes were observed to perform activity-dependent fusion with the plasma membrane (Padamsey et al., 2017), providing evidence for local control of lysosomes by neuronal activity. Nonetheless, still little is known about the dendritic pool of lysosomal organelles.

The purpose of this thesis is to further unravel the localization, molecular composition, as well as functional implications of lysosomes in dendrites of hippocampal neurons. Furthermore, the connection to neuronal activity and potential alternative functions, such as the exocytosis of content, are of interest. Taken together, this thesis aims to shed new light on local lysosomal processes potentially underlying synaptic plasticity, the basis of learning and memory. Moreover, despite their digestive function, lysosomes have various non-degradative tasks and an impaired lysosomal function is connected to numerous neurodegenerative pathologies, making them an interesting subject for further studies.

More specifically the aims of the thesis are:

1. to characterize the molecular identity of dendritic lysosomes and their association with GluN2B-containing NMDARs, as one of the key glutamate receptors involved in synaptic plasticity. Therefore, colocalization studies with the focus on LAMP1 and LAMP2, as commonly used lysosomal markers, were conducted, with or without co-labeling of synaptic proteins. Additionally, the association of LAMP2 with the GluN2B subunit was examined in live-cell imaging experiments.

2. to evaluate the influence of NMDAR activation on lysosomal mobility and potential exocytosis. To this end, live-cell imaging with cultured hippocampal neurons was performed.

3. to investigate the interplay between exocytic lysosomes and chaperone-mediated autophagy (CMA), a process that targets a wide range of cytoplasmic proteins and is dependent on LAMP2. Along with this, the localization and potential lysosomal release of a known CMA target protein, TDP-43, upon NMDAR activation was studied.

2. Materials and methods

2.1 Materials

2.1.1 Chemicals

Compound	Biological activity	Application	Supplier
Ifenprodil hemitartrate	Selective GluN2B-subunit inhibitor	5 µM for 30-45 min	Tocris Bioscience
(+)-MK-801 hydrogen maleate	Non-competitive NMDAR-pore blocker	100 µM for 1-2 h	Sigma-Aldrich
Bafilomycin A1	Inhibitor of V-ATPase	1 µM for 1 h	Sigma-Aldrich
Tetrodotoxin (TTX)	Selective inhibitor of sodium channel conductance	1 µM for 1-2 h	Alomone Labs
Bicuculline methiodide (Bic)	$GABA_A$ receptor antagonist	50 µM for 30 min	Tocris Bioscience
4-Aminopyridine (4AP)	Selective blocker of voltage-gated K^+ channels	2.5 mM for 30 min	Sigma Aldrich
N-Methyl-D-aspartic acid (NMDA)	NMDAR agonist	20 µM for 15 min	Sigma-Aldrich
Propidium iodide (PI)	DNA/RNA binding fluorescence probe for cell viability check	1.5 µM for 10 min	Sigma-Aldrich
Magic Red™ Cathepsin B Kit	Cathepsin B substrate	0.5 % for 30-60 min	Bio-Rad
BODIPY™ FL pepstatin A	Fluorescent (green) Cathepsin D probe	10 nM for >1 h	Invitrogen
Immobilon Crescendo Western HRP substrate	Chemiluminescent HRP detection reagent		Millipore

2.1.2 Enzymes and kits

All restriction enzymes and respective buffers as well as 1 kb DNA ladder and DNA loading dye were used from New England BioLabs.

Name	Supplier	Application
Hybrid DNA polymerase	Roboklon	Cloning

Deoxynucleoside triphosphate set (dNTPs)	Thermo Fisher Scientific	
T4 DNA Ligase	New England BioLabs	
NucleoSpin Gel and PCR Clean-up	Macherey-Nagel GmbH	
NucleoBond Xtra Midi EF	Macherey-Nagel GmbH	
DNase I	Roche	Preparation cortex culture
MultiMACS GFP Isolation Kit	Miltenyi Biotec GmbH	Co-immunoprecipitation
GFP ELISA Kit	Abcam (ab171581)	ELISA

2.1.3 Buffer and media

Name	Composition	Application
RIPA buffer	50 mM Tris-HCl (pH 8.0), 150 mM NaCl, 1 % Triton X-100, 0.5 % (w/v) deoxycholate	Cell lysis (Co-IP)
4x SDS sample buffer	250 mM Tris-HCl, pH 6.8, 1 % (w/v) SDS, 40 % (v/v) glycerol 20 % (v/v) β-mercaptoethanol, 0.004 % bromophenol blue (w/v)	SDS-PAGE
Electrophoresis buffer	192 mM glycine, 0.1 % (w/v) SDS, 25 mM Tris-base, pH 8.3	SDS-PAGE
Blotting buffer	192 mM glycine, 0.2 % (w/v) SDS, 20 % (v/v) methanol, 25 mM Tris-base, pH 8.3	Western blot
Ponceau Red	0.5 % (w/v) Ponceau S in 3 % (v/v) acetic acid solution	Transfer efficiency verification
TRIS buffered saline (TBS)	25 mM Tris-HCl, 150 mM NaCl, pH 7.4	Washing buffer
TBS-T	TBS + 0.1 % (v/v) Tween-20, pH 7.4	Washing buffer
TBS-A	TBS + 0.02 % (w/v) NaN_3, pH 7.4	Antibody dilution
Phosphate-buffered saline (PBS)	154 mM NaCl, 1 mM KH_2PO_4, 5.5 mM Na_2HPO_4 in H_2O, pH 7.4	Washing ICC
Permeabilization buffer	PBS, 0.25 % Triton-X-100, pH 7.4	Permeabilization ICC

ICC blocking solution	2 % (w/v) glycine, 2 % BSA (w/v), 0.2 % (w/v) gelatine and 50 mM NH_4Cl in PBS	Blocking ICC
50 x TAE buffer	2 M Tris-acetate, 0.05 M EDTA	DNA electrophoresis and agarose gels
Mowiol	10 % (w/v) Mowiol, 25 % (v/v) glycerol, 100 mM Tris-HCl, pH 8.5, 2.5 % (w/v) 1,4-Diazabicyclo[2.2.2]octane	Mounting ICC
P1 buffer	50 mM Tris-HCl, 10 mM EDTA, pH 8.0	DNA purification (mini)
P2 buffer	200 mM NaOH, 1 % (w/v) SDS	DNA purification (mini)
P3 buffer	3 M CH_3CO_2K, pH 5.5	DNA purification (mini)
Tyrode's buffer	128 mM NaCl, 5 mM KCl, 1 mM $MgCl_2$, 2 mM $CaCl_2$, 4.2 mM $NaHCO_3$, 20 mM glucose, 15 mM HEPES; pH 7.2-7.4	Live-cell imaging, surface staining and ELISA

2.1.4 Culture media and chemicals

Name	Composition	Application
Trypsin	0.25 % Trypsin-EDTA + phenol red (Gibco)	Tissue trypsinization for neuronal culture
Trypan Blue solution	0.4 % Trypan Blue (Gibco)	Cell counting
Hanks' Balanced Salt Solution (HBSS)	1 % glucose, 0.35 % $NaHCO_3$ + phenol red (Sigma-Aldrich)	Preparation rat/mouse neuronal culture
Neurobasal A (NB)	No phenol red (Gibco; #12349-015)	Preparation mouse hippocampal neurons
NB+	Neurobasal A (Gibco) + 1x B27 (Gibco), 4 mM GlutaMAX (Gibco), 1 mM sodium pyruvate (Gibco)	Culturing mouse hippocampal neurons
Full medium (DMEM+)	DMEM (Gibco) + 10 % fetal calf serum (FCS), 1 % penicillin/streptomycin, 2 mM L-glutamine	Preparation rat/mouse neurons
BrainPhys Neuronal Medium (BP)	Stemcell Technologies	Transfection rat neurons

Culture medium (BP+)	BrainPhys Neuronal Medium + 1x SM1 (Stemcell Technologies), 2 mM L-glutamine (Gibco)	Culturing rat hippocampal/cortex neurons
Poly-L-Lysine (PLL) coating solution	0.1 mg/ml PLL (Sigma-Aldrich) in 0.15 M boric acid (Carl Roth) solution, pH 8.4	Coating of glass coverslips
SOC-medium	20 % (w/v) peptone 140 (Gibco), 5 % (w/v) yeast extract (Gibco), 10 mM NaCl, 2.5 mM KCl, 10 mM $MgCl_2$, 10 mM $MgSO_4$, 20 mM glucose	Bacterial transformation
Lysogeny broth (LB)-medium	20 % (w/v) LB-Bouillon (Sigma-Aldrich) containing 5 % (w/v) NaCl, 10 % (w/v) tryptone, 5 % (w/v) yeast extract	Bacterial growth medium
LB-agar	15 % (w/v) LB agar (Carl Roth) containing 5 % (w/v) NaCl, 10 % (w/v) tryptone, 5 % (w/v) yeast extract, 15 % agar-agar	Agar plates for bacteria

2.1.5 Antibodies for immunocytochemistry (ICC) and western blot (WB)

Antibody	Source	Identifier/Dilution
Mouse anti-LAMP1	Thermo Fisher Scientific	MA1-164; ICC (1:500)
Rabbit anti-LAMP1	Abcam	Ab24170; ICC (1:500)
Mouse anti-LAMP1 (1D4B)	Developmental Studies Hybridoma Bank	AB_528127; ICC (1:50)
Rat anti-LAMP2	Thermo Fisher Scientific	MA1-165; ICC (1:500)
Mouse anti-LAMP2	Thermo Fisher Scientific	MA1-205; ICC (1:500)
Mouse anti-LAMP2 (ABL-93)	Developmental Studies Hybridoma Bank	AB_2134767; ICC (1:50)
Mouse anti-LAMP2 (H4B4)	Santa Cruz Biotechnology	#sc-18822; WB (1:1000)
Guinea pig anti-LAMP2A	Synaptic Systems	#437.005; ICC (1:500)
Rabbit anti-GluN2B	Alomone Labs	AGC-003; ICC (1:500; 1:200 for surface staining)
Rabbit anti-pCREB (Ser133)	Cell Signaling Technology	#9198; ICC (1:500)
Guinea pig anti-SAP102	Synaptic Systems	#124.214; ICC (1:500)

Rabbit anti-SAP102	Synaptic Systems	#124.202; ICC (1:500)
Guinea pig anti-Shank3	Synaptic Systems	#162.304; ICC (1:500)
Mouse anti-Bassoon (SAP7F407)	Enzo	ADI-VAM-PS003; (IF 1:500)
Mouse anti-Homer1	Synaptic Systems	#160.011; ICC (1:500)
Guinea pig anti-MAP2	Synaptic Systems	#188.004; ICC (1:500)
Mouse anti-GFP	BioLegend	#MMS-118P; WB (1:1000)
Rabbit anti-tRFP	Evrogen	#AB233; WB (1:1000)
Rabbit anti-RFP	Rockland	#600-401-379; ICC (1:500)
Anti-mouse AlexaFluor 568	Thermo Fisher Scientific	ICC (1:750)
Anti-mouse AlexaFluor 647	Thermo Fisher Scientific	
Anti-rabbit AlexaFluor 488	Thermo Fisher Scientific	
Anti-rabbit AlexaFluor 568	Thermo Fisher Scientific	
Anti-rabbit AlexaFluor 647	Thermo Fisher Scientific	
Anti-guinea pig AlexaFluor 405	Thermo Fisher Scientific	
Anti-guinea pig AlexaFluor 568	Thermo Fisher Scientific	
Anti-guinea pig AlexaFluor 647	Thermo Fisher Scientific	
Anti-mouse-Abberior STAR 635P	Abberior	
Anti-rabbit-IgG-HRP	Dianova	WB (1:10.000)
Anti-mouse-IgG-HRP	Dianova	
4',6-diamidino-2-phenylindole (DAPI)	Biozol	ICC (1:1000)

2.1.6 Constructs and viruses

Oligonucleotides for cloning of constructs were supplied by Integrated DNA Technologies, Thermo Fisher Scientific or Sigma Aldrich.

Construct	Backbone and promoter	Source
AAV_GFP	pAAV; synapsin	This study
AAV_TDP-43-GFP	pAAV; synapsin	This study
EBFP2-N1	EBFP2-N1; CMV	Addgene #54595
FUGW-MARCKS-GFP	CMV	Sebastian Samer
GFP-HSPA8 (Hsc70)	pcDNA3.1	Addgene #121161
GFP-SAP102	GFP-C1; CMV	This study
GFP-SAP102-PDZ1-3	GFP-C1; CMV	This study
GFP-SAP102-SH3-GK	GFP-C1; CMV	This study
GluN2B-840-1482-GFP	GFP-N1; CMV	Dr. Anna Karpova
GluN2B-840-1482-tRFP	tagRFP-N1; CMV	Melgarejo da Rosa et al., 2016
His-SUMO	pET28b; lacI	Dr. Rajeev Raman
His-SUMO-LAMP2-404-415	pET28b; lacI	Dr. Rajeev Raman
LAMP1-GFP	pCI-mKate2-N; synapsin	This study
LAMP1-mKate	pCI-mKate2-N; synapsin	This study
LAMP2-BFP	pCI-mKate2-N; synapsin	This study
LAMP2-GFP	pCI-mKate2-N; synapsin	This study
LAMP2-mKate	pCI-mKate2-N; synapsin	This study
LAMP2-tRFP	CMV	This study
mKate2	pCI-mKate2-N; synapsin	Dr. Thomas Oertner
PEX3-tRFP	pAAV; synapsin	Dr. Maria Andres-Alonso
pGolt-mCherry	pmCherryN1; CMV	Addgene #73297
pHuji-LAMP2	pCI-mKate2-N; synapsin	This study
pSuper	CMV	Dr. Anna Karpova
pTagRFP-N (tRFP)	CMV	Evrogen #FP142
SEP_NR2B	pCI; CMV	Addgene #23998

SEP-LAMP1	pCI-mKate2-N; synapsin	This study
SEP-LAMP2	pCI-mKate2-N; synapsin	Dr. Nigel Emptage
wtTDP43tdTOMATO-HA	pCAG-EGFP/RFP-int; CMV	Addgene #28205

2.1.7 shRNA and gRNA sequences

Name	Sequence (5' - 3')	Source
SAP102 shRNA1	GGTTAAGTGACGATTATTA	Murata and Constantine-Paton, 2013
SAP102 shRNA3	CCCTGGGTTAAGTGACGATTA	Bonnet et al., 2013
Scrambled shRNA	GGATGAGTCCTCCATGTTCT	Dr. Anna Karpova
GluN2B gRNA1	GTTGGCCGTCTTGGCCGTAT	Dr. Dawid Głów
GluN2B gRNA2	GTGTTCGGACAGCATGTCCG	Dr. Dawid Głów

2.1.8 Peptides

Peptide	Sequence	Source
TAT-LAMP2-404-415	YGRKKRRQRRRGRRKTYAGYQTL	Genosphere biotechnologies
TAT-Scrambled	YGRKKRRQRRRYKTAQYRLTGRG	Genosphere biotechnologies

2.2 Methods

2.2.1 Neuronal cultures, transfection, transduction and neuronal stimulation

All animal experiments were conducted in accordance with the Animal Welfare Law of the Federal Republic of Germany (Tierschutzgesetz der Bundesrepublik Deutschland, TierSchG) and the European Communities Council Directive (2010/63/EU). They were carried out with approval by the ethics committees of the city-state of Hamburg (Behörde für Gesundheit und Verbraucherschutz, Fachbereich Veterinärwesen) and the animal care committee of the University Medical Center Hamburg-Eppendorf.

Rat dissociated hippocampal neurons were prepared as described in Mikhaylova et al., 2018. Hippocampi were dissected from Wister rat E18 embryos, collected in HBSS and digested for 15 min in 0.025 % Trypsin-EDTA at 37°C. After multiple washing steps with DMEM+ and mechanical dissociation with needles (G 20/G 26), the density of cells was

counted in a Neubauer chamber with Trypan Blue solution. Neurons were plated with a density of 60.000 cells/ml on PLL-coated glass coverslips. The cells were maintained in the incubator at 37°C in full medium (DMEM+) for 1 h, afterward the medium was exchanged to BP+ and the neurons were kept at 37°C, with 5 % CO_2 and 95 % humidity until further experiments.

To obtain cortical cultures, cortex tissue from E18 rat embryos was collected in HBSS and further processed as for hippocampal neurons. During mechanical dissociation with needles, DNase A (1 mg/ml in DMEM-; final concentration 200 µg/ml) was added to the tissue. The cortical neurons were plated PLL-coated glass coverslips with a density of 150.000 cells/ml.

Cultured mouse neurons were obtained from the line LSL-Cas9-Cre. This line was created by crossing B6;129-*Gt(ROSA)26Sor*[tm1(CAG-cas9*,-EGFP)Fezh]/J (Jackson laboratory strain #024857; Platt et al., 2014) with CMV-Cre-deleter mice (Schwenk et al., 1995).

For the preparation of mouse dissociated hippocampal neurons, mice were decapitated and the hippocampi were dissected from the brains to be collected in HBSS. The tissue was treated with 0.025 % of Trypsin-EDTA for 15 min at 37°C. After washing the hippocampi in prewarmed HBSS, the hippocampi were mechanically triturated with needles. The cell suspension was plated onto PLL-coated glass coverslips at a density of 85.000 cells/ml. After 1 h, the medium was exchanged to NB+ and the cells were left, until further usage, in the incubator at 37°C, with 5 % CO_2 and 95 % humidity.

All neuronal cultures were fed with either BP+ for rat cells or NB+ for mouse neuronal cultures on DIV7. Experiments were conducted on DIV14-17 neurons unless otherwise stated.

Primary hippocampal neurons were transfected by dilution of each DNA and Lipofectamine 2000 in BP (rat neurons) or NB (mouse neurons) medium, mixed (DNA/Lipofectamine ratio 1:2) and incubated for 20 min. The neuronal culture medium was collected and replaced in the well with either prewarmed BP or NB. After addition of the DNA:Lipofectamine mixture to the cells, the medium was replaced after 45 min incubation at 37°C to the previously collected conditioned medium. Expression periods varied from 16-48 h.

For SAP102 knockdown (KD) experiments, neurons were transfected at DIV7 with plasmids encoding for scrambled or shRNA1/shRNA3 sequence and kept for 7 days. For KO experiments, GluN2B gRNA1 and gRNA3 encoding constructs were transfected together at DIV7 and kept for 6 days of expression.

For viral infections of cortical cultures, adeno-associated virus of serotype 9 (AAV9) diluted in sterile PBS was added to the cells on DIV7 to the respective culture medium in a

concentration of $2*10^{10}$ GC/well for AAV_GFP (2 µl of 10^{13} genome copies (GC)/ml) and AAV_TDP-43-GFP (20 µl of 10^{12} GC/ml).

Neuronal stimulation, corresponding to the experiments assessing the degree of GluN2B/LAMP colocalization and localization (Figure 10), was conducted as previously described (Karpova et al., 2013). In brief, cultured hippocampal neurons were silenced prior to the experiment with 1 µM TTX for 1 h in culture medium to block sodium channels. After wash out of TTX, 2.5 mM 4AP, an inhibitor of voltage-gated K^+ channels, as well as 50 µM bicuculline (bic), for blockage of GABAergic inhibition, were applied for 30 min. All stimulations with NMDA, to activate the NMDARs, were carried out with a concentration of 20 µM for 15 min.

2.2.2 Immunocytochemistry (ICC)

The cells were fixed in 4 % paraformaldehyde (PFA) + 4 % (w/v) sucrose for 15 min at RT, washed with PBS and permeabilized with 0.2 % Triton-X100 in PBS for 10 min. After blocking in blocking solution (2 % glycine, 2 % BSA, 0.2 % gelatine and 50 mM NH_4Cl in PBS), the primary antibody was incubated overnight at 4°C diluted in blocking solution. After three washing steps with PBS, the cells were incubated for 1 h in secondary antibody diluted in blocking solution at RT and, following another three washes with PBS, mounted in Mowiol.

Surface staining of GluN2B was performed for 10 min at RT in primary antibody diluted Tyrode's buffer (128 mM NaCl, 5 mM KCl, 1 mM $MgCl_2$, 2 mM $CaCl_2$, 4.2 mM $NaHCO_3$, 20 mM glucose, and 15 mM HEPES; pH = 7.2–7.4), washed with Tyrode's buffer and fixed as described above.

2.2.3 Image acquisition

Images were acquired in a Leica TCS SP5 system controlled by Leica LAS AF software using HCX PL APO 63× 1.40. Areas of 82 × 82 µM were scanned with 405, 488, 568 and 635 nm laser lanes (12-bits, 80 × 80 nm pixel size, 700 Hz, Z-step 0.3 µm). Fluorescent signal was collected using three HyD detectors and with scans between frames.

Live-cell imaging experiments were performed using a Nikon Eclipse Ti-E controlled by VisiView software (Visitron Systems). The built-in Nikon perfect focus system kept the region of interest in a fixed focal plane. 405, 488, 561 and 640 nm excitation lasers were used. Cells were imaged with a 100× (Nikon, CFI Plan Apochromat Lambda 100×/1.45) objective. TIRF microscopy images were obtained with an iLAS2 (Gattaca systems) spinning-TIRF system. The frequency of acquisition varied depending on the experiment between 1-0.5 Hz. At all systems, in live-cell experiments hippocampal neurons were imaged in Tyrode's buffer and were maintained at 37°C and 5 % CO_2 during acquisition.

During fusion imaging experiments, 1 μM of bafilomycin A1 was present throughout the imaging.

2.2.4 Image analysis and statistics

For colocalization analysis of endogenous LAMP1 and LAMP2, spots were created in Imaris (Imaris, Bitplane) for each channel and their colocalization was calculated using the "Colocalize spots" plugin. The colocalization for surface GluN2B with Shank3, and Bassoon, was conducted in the same way. For the quantification of spine and shaft localization, the spots were created and counted manually according to the dendritic morphology visualized by MARCKS-GFP.

Other colocalization analysis was performed in Fiji (NIH) software (Schindelin et al., 2012) by the creation of regions of interest (ROIs) in the channel of interest by point selection of maxima and enlargement of those by 3 pixels, resulting in ROIs of 7 pixels diameter. The signal in the respective other channel was determined either by measurement of mean intensity and counting "positive" above a set threshold or by manual counting. Only for the creation of ROIs for TDP-43 signal, the lasso tool from Fiji was used.

Kymographs were created using Fiji (NIH) software with the "KymographClear" plugin (Mangeol et al., 2016) or the Multi Kymograph function. Dendritic stretches were traced using the segmented line tool. Line thickness was chosen between 3-5 depending on the thickness of the dendrite. Trajectories seen in the kymographs were traced by line. In experiments with multiple channels imaged simultaneously, overlapping traces were counted as co-trafficking.

KD and KO efficiency of proteins was verified by analysis of the mean intensity of fluorescence staining normalized to the mean intensity of the control group in dendritic stretches for GluN2B and SAP102.

To quantify the relation between LAMP2-mKate and SEP-GluN2B, positive puncta were determined by creation of ROIs on the merged first 5 frames in the SEP-GluN2B channel based on the intensity with the "Find maxima" function following an enlargement of maxima to a diameter of 0.77 μm in Fiji. Stopping puncta of LAMP2/Magic Red within these ROIs for more than 5 frames (5 s) were counted as positive/visiting puncta. Overlapping or opposing puncta were counted on merged first 5 frames based on the ROIs created in SEP-GluN2B and LAMP2-mKate channel as described above. Association of LAMP2-GFP and SEP-GluN2B signal was analyzed by creation of ROIs based on the signal in each channel and manually counting of overlapping and opposing signal.

In experiments measuring the movement and velocity of vesicles, NMDA was applied after 20-40 frames of baseline acquisition. Cells were imaged with an acquisition

frequency of 0.5 Hz. Kymograph were created as described above and the velocity was measured with the help of the "Velocity Measurement Tool" (Volker Baecker, INSERM, Montpellier, RIO Imaging; J. Rietdorf, FMI Basel; A. Seitz, EMBL Heidelberg; http://dev.mri.cnrs.fr/projects/imagej-macros/wiki/Velocity_Measurement_Tool). For LAMP2-mKate and Magic Red lines were traced at the beginning and the end of the stream, for PEX3-tRFP and LAMP1-mKate the velocity throughout the stream was calculated.

In fusion experiments, the average fluorescence intensity of the first 5 frames was defined as baseline (pre-stimulation; $F_{baseline}$) and the difference in fluorescence intensity compared to the end of the acquired stream (F) in percentage was calculated by $\Delta F = (F - F_{baseline})/F_{baseline} * 100$. In the experiments including GluN2B KO cells, the last 3 min of each stream were used for the calculation. In general, a fusion event was determined in a ROI created based on the find maxima function of Fiji and the enlargement to 0.77 µm when the average fluorescence intensity of the last 20 frames was higher than 1.5 x standard deviation (SD) of baseline fluorescence intensity.

Data are shown as mean ± standard error of the mean (SEM) and n-numbers are described in each panel or figure. Graphs and statistical analysis were created using GraphPad Prism (GraphPad Software). First, D'Agostino and Pearson normality test was performed to assess the data distribution. Significance was assessed by parametric or non-parametric tests, accordingly. For parametric data, two-tailed unpaired Student's *t*-test or one-way ANOVA with Bonferroni's posthoc test for multiple comparisons was used. For data not passing the normality test, Mann-Whitney *U* test was used to compare two groups or Kruskal-Wallis test for multiple comparisons. Two-way ANOVA with Tukey posthoc test for multiple comparisons. P-values were considered as following: P > 0.05 = ns; ≤ 0.05 = *; ≤ 0.01 = **; ≤ 0.001 = ***; ≤ 0.0001 = ****.

2.2.5 Cloning

DNA was amplified by the polymerase chain reaction (PCR) using Hybrid DNA polymerase. The reaction contained 10 ng of DNA, 1 unit of Hybrid DNA polymerase, 1x Hybrid buffer including 1.5 mM $MgCl_2$, 0.5 mM of each forward and reverse primer and 0.2 mM of each dNTP in a total volume of 50 µl. The annealing temperature (T_m) was calculated with the roboklon calculator and the program was run according to the manufacturer's instructions with the following program:

Process	Time and temperature		Cycles
	3- step protocol	**2-step protocol**	
Initial denaturation	98°C for 30s	98°C for 30s	1

Denaturation	98°C for 10s	98°C for 10s	
Annealing	T_m°C for 30s	-	25-30
Elongation	72°C for 15s/kb	72°C for 15s/kb	
Final elongation	72°C for 7 min	72°C for 7 min	1
Cooling and storage	∞ at 8°C	∞ at 8°C	1

For separation and visualization of DNA fragments with different lengths, agarose gel electrophoresis was performed with gels containing 0.5-1.5 % agarose in TAE buffer. The samples were run and DNA was visualized using a UV transilluminator. Desired DNA was cut out, eluted with NucleoSpin Gel and PCR Clean-up kit (Macherey-Nagel) and, if needed, digested with restriction enzymes. After another purification step with the kit, the respective amount of the restricted insert and 50 ng of vector were ligated (ratio 3:1) with T4 DNA Ligase according to the manufacturer's protocol. The ligation reaction was further used for DNA transformation into chemically competent *E. coli* bacteria (XL10-Gold), which were plated after transformation onto LB-plates containing the respective antibiotic for selection and incubated overnight at 37°C. Single colonies were used for inoculation of LB medium with added antibiotic for small- (mini) or large-scale (midi) DNA purification.

The LAMP1 rat sequence was amplified from mEos4b-Lysosomes-20 (Addgene #57512, kindly provided by Dr. Marina Mikhaylova) and subcloned into mKate2. SAP102 was amplified for further cloning from pBlueScript vector containing the rat SAP102 sequence (kind gift from Dr. Craig Garner). All KD shRNA sequences were inserted with oligos in the pSuper vector (kind gift from Dr. Anna Karpova). Constructs encoding for guide RNA (gRNA) used for the KO experiments conducted with the clustered regularly interspaced palindromic repeat (CRISPR) and CRISPR-associated protein 9 (CRISPR/Cas9) system were cloned and kindly provided by Dr. Dawid Głów.

2.2.6 Plasmid DNA purification

Mini DNA purification was carried out by the alkaline lysis method. Overnight cultured bacteria were centrifuged for 5 min at 1000 x g and the pellet was resuspended in P1 buffer by vortexing. After the addition of P2 buffer, the tubes were incubated for 5 min at RT. P3 buffer was then added and after another 10 min incubation step at RT, the tubes were centrifuged at 16000 x g for 5 min at 4°C. 500 µl of the supernatant were transferred to isopropanol, incubated at RT for 10 min and centrifuged again as before. The pellet was washed with 70 % ethanol, centrifuged and then air-dried before solving the DNA in 30 µl Tris-HCl (pH 8.0). For large-scale DNA extraction, the NucleoBond Xtra Midi EF kit was used according to the manufacturer's instructions.

2.2.7 HEK293T cells and polyethylenimine (PEI) transfection

HEK293T cells were cultured in DMEM+ in the incubator at 37°C, 5 % CO_2 and 95 % humidity. The cells were transfected with PEI when confluency was 50-60 %. The DNA was mixed together with PEI in a ratio of 1:3 (DNA:PEI) in DMEM medium without supplements (DMEM-) and incubated for 20 min at RT. The culture medium of the HEK293T cells was exchanged for DMEM-. The DNA-PEI-mixture was added to the cells and the medium was changed to the previously collected DMEM+ after 4 h of incubation.

2.2.8 Heterologous co-immunoprecipitation (Co-IP)

HEK293T cells were transfected, harvested and lysed in RIPA buffer (50 mM Tris-HCl pH 8.0, 150 mM NaCl, 1 % Triton X-100, 0.5 % sodium deoxycholate, 0.1 % sodium dodecyl sulfate (SDS), EDTA-free protease inhibitor and PhosSTOP (Roche)) for 1.5 h rotating at 4°C. The lysate was cleared by centrifugation and incubated with anti-GFP-coated magnetic beads (MultiMACS GFP Isolation Kit). The Co-IP was carried out according to the manufacturer's protocol.

2.2.9 Sodium dodecyl sulfate (SDS)-PAGE and Western blot

Proteins were separated via SDS-polyacrylamide gel electrophoresis. Samples were boiled prior to loading at 98°C for 10 min and separated on a 10 % polyacrylamide gel at 100-120 V. Afterwards, the proteins were transferred on a nitrocellulose membrane by semi-dry blotting for 45 min at 200 mA in blotting buffer. If wanted, the transfer efficiency was checked by incubation of the membrane in Ponceau Red solution. The membrane was then blocked for 1 h in 5 % (w/v) in milk in TBS-T and subsequently incubated in primary antibody diluted in TBS-A overnight at 4°C with gentle agitation. The next day, the membrane was washed with TBS and TBS-T and incubated with the corresponding HRP-linked secondary antibody in 5 % milk for 1 h at RT. After additional washing steps, HRP substrate solution was added to the membrane and chemiluminescence was detected.

2.2.10 Protein immobilization, purification and pulldown (PD) assay

Protein immobilization, purification and PD assays were carried out in collaboration with Dr. Rajeev Raman.

His-SUMO and His-SUMO-LAMP2-404-415 were expressed in *E. coli* BL21 (DE3), induced with 400 µM IPTG followed by incubation at 25°C for 4 h. After lysis with lysis buffer (50 mM NaH_2PO_4, 300 mM NaCl, 10 mM imidazole, pH 8.0, EDTA-free protease inhibitor and PhosSTOP), the lysate was centrifuged at 20000 x g for 15 min, the supernatant was loaded on Ni-NTA resin and washed with wash buffer (50 mM NaH_2PO_4, 300 mM NaCl, 20 mM imidazole, pH 8.0) thus both proteins were immobilized on beads. To check the purity and to quantify the protein amount immobilized on beads, both His-SUMO and His-SUMO-LAMP2-404-415 were resolved using 15-18 % SDS-PAGE gels.

GFP-SAP102-PDZ1-3, GFP-SAP102 SH3-GK as well as GFP-Hsc70 were expressed in COS-7 cells and lysed using lysis buffer (50 mM HEPES pH 7.0, 100 mM NaCl, 1% Triton X-100, EDTA-free protease inhibitor and PhosSTOP). The lysate was incubated at 4°C for 1 h rotating followed by brief sonication and centrifugation for 10 min at 12000 × g and the supernatant was collected.

PD assays were used to assess the direct interaction between LAMP2-404-415 with GFP-SAP102-PDZ1-3, GFP-SAP102 SH3-GK or GFP-Hsc70. Briefly, 5 μg of His-SUMO-LAMP2-404-415 along with the equivalent amount of the control protein His-SUMO bound on the beads was incubated with COS-7 cell lysate, obtained as described above, overnight at 4°C on a rotatory shaker. After three washing steps with wash buffer (50 mM NaH$_2$PO$_4$, 300 mM NaCl, 20 mM imidazole, pH 8.0, 1 % Triton X-100, EDTA-free protease inhibitor and PhosSTOP) the complex was eluted in 2x SDS sample buffer and subjected to western blot. In a competitive PD, 10 μg of TAT-Scrambled or TAT-LAMP2-404-415 peptide was incubated along with COS-7 cell lysate expressing the requisite protein.

2.2.11 Enzyme-linked immunosorbent assays (ELISA)

To determine the release of GFP-tagged proteins, rat cortical neurons were infected with either AAV9-GFP or AAV9-TDP-43-GFP on DIV7. After 7-9 days of expression, the cells were incubated with propidium iodide (PI) to verify cell viability. Prior to the experiment, the neurons were silenced with 1 μM TTX for 2 h in the culture medium. After one quick washing step with Tyrode's buffer, the coverslips with neurons were flipped on 150 μl of Tyrode's buffer with respective chemicals for stimulation. After 15 min incubation at RT, the medium was collected and centrifuged at 1500 rpm for 10 min at 4°C. For the detection of GFP proteins, the GFP ELISA kit was used according to the manufacturer's instructions and the optical density (OD) was measured at 450 nm.

3. Results

The presented data were collected in part with the help of Dr. Katarzyna Grochowska (ZMNH Hamburg; Figure 16-19 and Figure 22E). Pulldown experiments were conducted in collaboration with Dr. Rajeev Raman (LIN Magdeburg; Figure 23 and Figure 24).

3.1 Synaptic contact sites and their association with lysosomal proteins in dendrites

Previous work described lysosomes entering the dendritic spine (Goo et al., 2017), where the majority of excitatory synapses are located. Still, it is unclear whether lysosomes are also associated with another type of synaptic contact, the shaft synapses. In contrast to spine synapses, shaft synapses are formed directly on the shaft of the dendrite and are thought to represent only a smaller fraction of excitatory synaptic contact sites in mature neurons (Reilly et al., 2011). These shaft synapses are composed of PSD proteins, as well as glutamate receptors, such as NMDARs (Jang et al., 2015).

To investigate the linkage between lysosomes and synaptic activity, the spatial relation between lysosomal and synaptic proteins was assessed. To get an insight into the distribution of synapses in cultured hippocampal neurons, dendrites were characterized in regard to the presence of spine and shaft synapses. To this end, hippocampal neurons were immunostained against PSD proteins, as the basis for synaptic contact sites, to investigate shaft synapses in cultured neurons. The cell outline was visualized by neuronal transfection with a construct encoding for GFP-tagged myristoylated alanine-rich C kinase substrate (MARCKS), a protein that is localized to the inner leaflet of the plasma membrane (Brudvig and Weimer, 2015). Homer1 is a commonly used marker for the PSD, as well as the abundant, widely utilized PSD protein Shank3. To test if both proteins reliably label the same compartment, colocalization between endogenous Homer1 and Shank3 was analyzed (Figure 9A, B). The analysis revealed an overlap of ~90 % of Shank3 with Homer1, highlighting the presence of both proteins in the majority of PSDs (Figure 9B). No significant difference in the colocalization between the proteins from either site could be detected, however, a slight trend for decreased colocalization of Homer1 with Shank3 was seen. Due to its high prominence, Shank3 was chosen to be used in further experiments to label the postsynaptic part of a synapse. Also, the density of spines of the cultures was counted and quantified in primary, as well as secondary, dendrites. The quantification revealed the presence of 0.6 spines per µm dendritic stretch, irrespective in regard to primary or secondary dendrites (Figure 9C).

Since glutamate receptors are located at excitatory shaft synapses, the question arose if Shank3-labeled PSDs contain NMDARs, which are key receptors for synaptic function. The NMDAR subunit GluN2B is here of particular interest since it exhibits a high affinity for the binding with CaMKII by its distinct C-terminal tail, in contrast to the subunit

GluN2A, and this association is crucial for LTP (Barria and Malinow, 2005; Zhou et al., 2007). Also, GluN2B was shown to be present not only in dendritic spines but also at extrasynaptic sites adjacent to dendritic spines (Parsons and Raymond, 2014). Therefore, GluN2B was chosen as a suitable candidate to investigate NMDARs in regard to their localization and interplay with lysosomal organelles in connection with synaptic activity.

As the first step, the pool of surface GluN2B was labeled by immunostaining and its localization was quantified in primary, as well as secondary, dendrites with respect to immunosignal detected in the dendritic spine or shaft (Figure 9D, E). The surface staining was performed to avoid the labeling of the intracellular pool of GluN2B, including newly synthesized proteins, as well as proteins undergoing recycling via REs. The analysis showed the localization of over 61 % of GluN2B at dendritic spines, whereas around 39 % was present in the dendritic shaft independent of primary or secondary dendrites analyzed (Figure 9E). Next, to investigate if GluN2B was localized to potential synapses including a PSD, Shank3 staining was included. Less than 20 % of total surface GluN2B was positive for Shank3 (Figure 9F). Also, the amount of surface GluN2B that was Shank3 positive or negative was quantified as the fraction of the dendritic shaft surface GluN2B signal (Figure 9G). In primary dendrites, more than one third (~37 %) of surface GluN2B localized to the dendritic shaft was positive for Shank3, whereas ~63 % showed no co-signal. In secondary dendrites, the distribution was slightly different with around ~45 % counted as positive and ~55 % as negative for Shank3. This highlights the co-presence of GluN2B-containing NMDARs and PSD proteins, likely visualizing the relatively small portion of shaft synapses that increases in relation to the distance to the cell body.

To assess the degree of formed synapses including a pre- and postsynaptic part, hippocampal neurons were immunostained against Shank3, as a PSD marker, and Bassoon (Bsn), a widely used marker protein localized in the active zone of the presynapse (Tom Dieck et al., 1998). Also, in this set of experiments, to exclude labeling of intracellular pools, surface staining of GluN2B was performed. A high amount of signal positive for Shank3, Bsn as well as surface GluN2B (~77 %) was hereby found in dendritic spines and only a smaller portion in the dendritic shaft (~23 %; Figure 9H-I).

Taken together, the conducted analysis highlights the presence of the GluN2B subunit to a higher degree in dendritic spines, however also in dendritic shafts where more than one third of GluN2B subunits colocalize with PSD proteins. More than 20 % of synapses formed by a pre- and postsynaptic site are localized to dendritic shafts and, therefore, reflect the pool of shaft synapses.
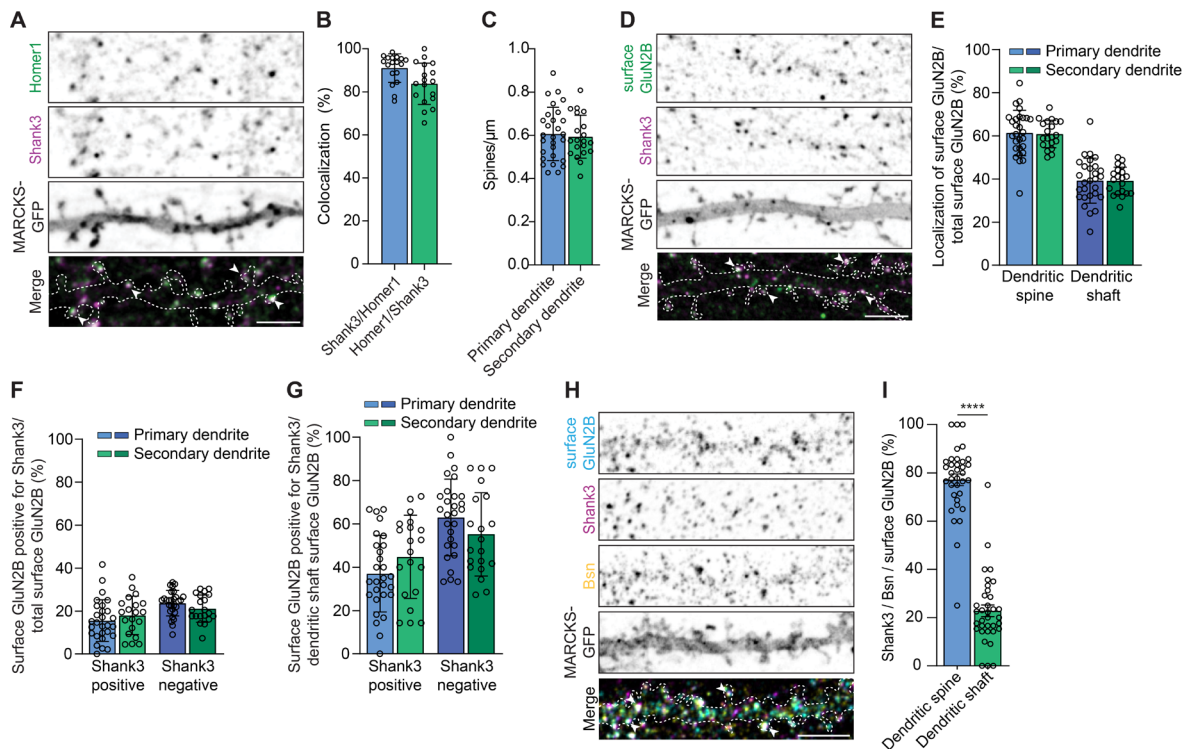
Figure 9: Spine and shaft synapse exhibit different GluN2B and Shank3 compositions irrespective of primary or secondary dendrites. (A) Representative confocal images of hippocampal neurons transfected with MARCKS-GFP and stained against endogenous Homer1 (green) and Shank3 (magenta) as markers for PSD proteins. White dashed lines indicate the dendritic outline visualized by MARCKS-GFP. **(B)** Scatter bar plots represent the quantified colocalization between Shank3 and Homer1, revealing a high degree of overlap between both proteins. N-number = 18 dendritic segments of 14 cells from 2 independent cultures. **(C)** The density of spines in cultured hippocampal neurons (DIV15) was calculated and plotted for both primary and secondary dendrites. **(D)** Confocal images of DIV15 primary hippocampal rat neurons expressing MARCKS-GFP (white dashed lines) immunostained for surface GluN2B (green) and Shank3 (magenta). **(E)** GluN2B surface signal was quantified in primary and secondary dendrites and showed a higher localization to spine synapses rather than dendritic shafts. **(F)** Colocalization of surface GluN2B and Shank3 was analyzed in primary and secondary dendrites normalized to the total GluN2B surface signal. No changes in the degree of colocalization between primary and secondary dendrites are detected. **(G)** Surface-stained GluN2B positive or negative for Shank3 of dendritic shaft GluN2B signal in primary and secondary dendrites was quantified. The majority of shaft GluN2B signal does not colocalize with Shank3. **(C-G)** N-number = 28 dendritic segments of 19 cells from 3 independent cultures for primary dendrites; 20 dendritic segments of 18 cells from 3 independent cultures for secondary dendrites. All scale bars represent 5 µm. White arrows indicate colocalizing signal. **(H)** Dendrites of cultured hippocampal neurons stained with antibodies targeted against GluN2B (cyan), Shank3 (magenta) and Bsn (yellow) in MARCKS-GFP transfected hippocampal neurons (DIV15-16). The dendritic outline is visualized by white dashed lines. **(I)** The percentage of triple-positive signal including Shank3, Bsn and surface GluN2B was quantified regarding their localization either in dendritic spines or dendritic shaft. ~77 % of signal was found in spines and around 23 % was in the dendritic shaft. Mann-Whitney *U* test. N-number = 12 cells from 3 independent cultures. All scale bars represent 5 µm.

To characterize the amount of GluN2B that potentially colocalizes with the most prominent, highly abundant, lysosomal membrane proteins LAMP1 or LAMP2, hippocampal neurons expressing MARCKS-GFP were immunostained against GluN2B, Shank3 and LAMP1 or LAMP2, respectively (Figure 10A-B). Neuronal activity was

induced by an established protocol utilizing 4AP and bic (Karpova et al., 2013) to check if a change in colocalization could be observed upon stimulation of the neurons. It has been shown that neuronal stimulation with 4AP/bic results in phosphorylation of the nuclear transcription factor cAMP response element-binding protein (CREB) at Serine 133 (Ser133; Lee et al., 2005; Wu et al., 2001). As a control for successful stimulation, neurons were therefore stained with an antibody specific for phosphorylated CREB at Ser133 to visualize the increase in fluorescence intensity of the immunostaining upon stimulation (Figure 10C).

First, the amount of GluN2B positive for LAMP1 and LAMP2 was quantified. This revealed colocalization of GluN2B with LAMP1 of ~20 % and with LAMP2 of ~35 % in neurons silenced with tetrodotoxin (TTX; Figure 10D). Interestingly, the amount of colocalization did not change detectably upon neuronal stimulation. Additionally, the localization of GluN2B that is positive for LAMP1 or LAMP2 was quantified. The analysis showed localization of GluN2B/LAMP1 signal, as well as GluN2B/LAMP2, to the highest degree in spine synapses (both above 50 %), whereas spine synapses were defined as additionally Shank3 positive signal localized to dendritic spines (Figure 10E-F). LAMP2 was more localized to shaft synapses (dendritic shaft signal positive for Shank3) together with GluN2B with ~26 % compared to LAMP1 (~20 %) while ~25 % of LAMP1 and ~20 % of LAMP2 positive for GluN2B were localized to the dendritic shaft and are negative for Shank3. In line with the previous analysis, 4AP/bic stimulation did not influence the colocalization or the localization of the GluN2B signal together with LAMP1 or LAMP2.

These results reveal a higher colocalization between the NMDAR subunit GluN2B and the lysosomal membrane protein LAMP2, in comparison to LAMP1. Also, LAMP2 localized slightly more to GluN2B in shaft synapses. One has to note that this experiment was performed on permeabilized neurons, hence labeling not only the GluN2B subunits on the surface but also the intracellular pool including proteins in the secretory, as well as the recycling, pathway.
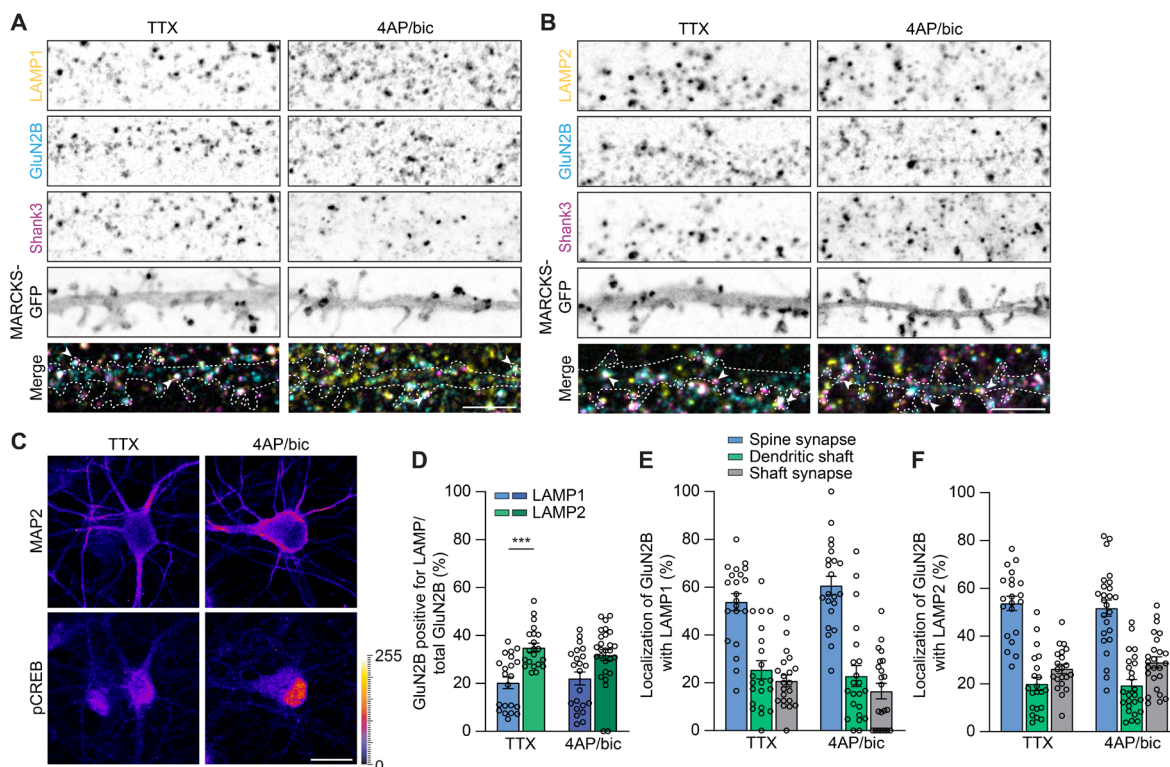
Figure 10: LAMP2 colocalizes more with GluN2B in dendrites of DIV17 hippocampal neurons. (A) Representative confocal images of rat hippocampal neurons transfected with MARCKS-GFP and immunostained against GluN2B (cyan), Shank3 (magenta) and LAMP1 or LAMP2 **(B)** are shown in yellow. The dendritic outline is indicated by white dashed lines and arrows indicate co-signal. Scale bar 5 µm. **(C)** Confocal images of DIV17 hippocampal neurons immunostained against pCREB and MAP2. Neuronal activation by 4AP/bic results in an increase in pCREB signal, as seen by the pixel intensities from 0 to 255 shown in the heat map. Scale bar 20 µm. **(D)** Quantification of dendritic GluN2B signal colocalizing with LAMP1 or LAMP2 normalized to the total detected GluN2B signal. Neurons were either silenced with TTX or stimulated by 4AP/bic. GluN2B exhibits more co-signal with LAMP2 compared to LAMP1. Kruskal-Wallis test. **(E)** Scatter bar plots of analyzed GluN2B signal that is positive for LAMP1 in dendritic stretches normalized to the total amount of double-positive signal. The signal was distributed in spine synapses (Shank3 positive), dendritic shaft (Shank3 negative) or shaft synapse (Shank3 positive). The same quantification was conducted for LAMP2 **(F)**. The legend accounts for **(E-F)**. N-number = 21 dendritic segments from 11 cells for TTX and 22 dendritic stretches of 11 cells for 4AP/bic for LAMP1-stained neurons; 22 dendritic segments from 10 cells for TTX and 27 dendritic stretches from 12 cells for 4AP/bic for LAMP2-stained cells; all from 2 independent cultures.

3.2   Lysosomes exhibit high heterogeneity in dendritic compartments

Lysosomes are formed by dynamic fusion and fission events and are therefore considered heterogeneous organelles regarding their molecular membrane and content composition, as well as their motility. The distribution of lysosomes in dendrites has been a matter of debate and only recently the presence of acidified lysosomes has been shown in dendritic compartments (Goo et al., 2017; Padamsey et al., 2017). LAMP1 and LAMP2, as the most abundantly found lysosomal membrane proteins, are used interchangeably in published studies despite their different functional implications, hence possibly being present on different pools of lysosomes.

To shed more light on the distribution of LAMP1 and LAMP2 in dendrites, rat hippocampal neurons were immunostained with antibodies targeted against MAP2, as a dendritic marker, as well as LAMP1 and LAMP2 (Figure 11A). In various studies, it was proposed that lysosomal structures are enriched in the soma and proximal dendrites of neurons while distal dendrites display a lack of lysosomes. With this in mind, the colocalization analysis was conducted in proximal, as well as distal, regions of dendrites. The analysis revealed that around 33 % of LAMP1 colocalizes with LAMP2 and ~37 % of LAMP2 overlaps with LAMP1 in proximal segments (Figure 11B). Surprisingly, there was no significant difference observed in the spatial distribution, with ~30 % (LAMP1/LAMP2) and ~33 % (LAMP2/LAMP1) colocalizing in distal parts of dendrites.

To address the question of potential differences in trafficking, LAMP1 and LAMP2, fused to the fluorescent protein mKate, were overexpressed and the movement of vesicles was monitored in live-cell imaging experiments. LAMP1-mKate vesicles thereby showed significantly less mobile movement, with almost 50 % accounting for the stationary pool, compared to only around 20 % of non-mobile LAMP2-mKate vesicles (Figure 11C). A significant effect of the distance from the soma on the mobility could not be observed, as already seen for the colocalization analysis with endogenous stainings. The stationary pool of LAMP2-mKate displayed a trend of increase from ~18 % in proximal regions (0-25 µm) to ~29 % in distal parts (>25-50 µm). The mobile fraction distributed into anterograde, retrograde and bidirectional moving vesicles with was a slight observed preference towards retrograde trafficking, reflecting vesicle movement towards the cell body (Figure 11D), as visualized with created kymographs, showing the movement of vesicles over time in regard to distance and directionality (Figure 11E).
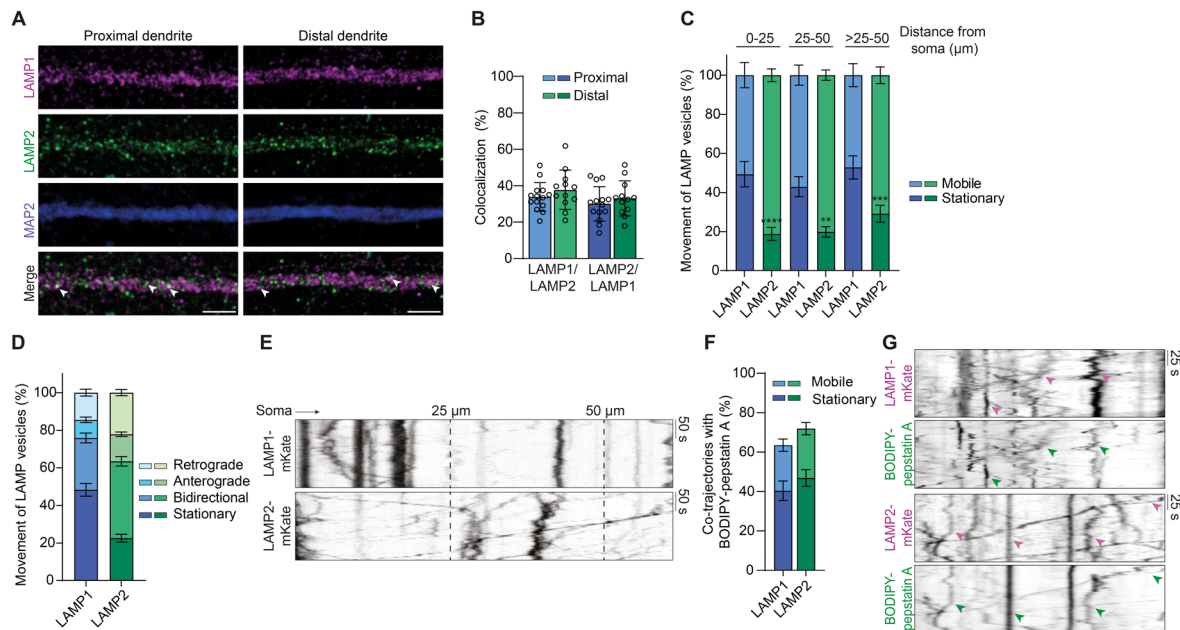
Figure 11: High heterogeneity of lysosomes is revealed by endogenous staining of hippocampal neurons, as well as in live-cell imaging experiments. (A) Representative confocal images of proximal and distal dendritic stretches of DIV16 hippocampal neurons stained against endogenous LAMP1 (magenta), LAMP2 (green), and MAP2 (blue). White arrows indicate colocalizing signal. Scale bar 5 μm. **(B)** Colocalization of LAMP1 with LAMP2 or LAMP2 with LAMP1 was quantified in proximal and distal dendrites. The analysis was conducted with Imaris software (Spots function). N-number = 14 cells from 2 independent cultures (14 proximal and 12 distal dendrites). **(C)** The movement of LAMP1-mKate or LAMP2-mKate vesicles was recorded in live-cell imaging experiments and quantified by kymographs. LAMP2 shows a more mobile movement compared to LAMP1. The overall movement pattern did not change depending on the distance from the cell body. Ns = p>0.999 for distance factor and **** = p<0.0001 for lysosomal marker factor by two-way ANOVA with posthoc Tukey. **(D)** Quantified movement from **(C)** merged in regard to distance from the soma and split into stationary, bidirectional, anterograde, and retrograde movement. LAMP1 and LAMP2 do not show a preference regarding retrograde or anterograde movement. **(C-D)** N-number = 31 dendritic segments of 14 cells from 5 independent cultures for LAMP1 and n-number = 43 dendritic segments of 27 cells from 4 independent cultures for LAMP2. **(E)** Kymographs from streams with a total acquisition time of 180 s (1 Hz acquisition frequency) visualize the more stationary pool for LAMP1-mKate in dendrites. The localization of the soma is indicated, the arrow reflects anterograde movement. **(F)** Majority of LAMP1-mKate and LAMP2-mKate display co-trafficking petterns with fluorescently labeled CatD by incubation of hippocampal neurons with BODIPY-pepstatin A. N-number = 19 cells from 3 independent cultures for LAMP1-mKate and 17 cells from 3 independent cultures for LAMP2-mKate. **(G)** Representative kymographs of LAMP1- and LAMP2-mKate (magenta) transfected neurons incubated with BODIPY-pepstatin A (green). Green arrows show BODIPY-pepstatin A traces, whereas magenta marks the LAMP1/2-mKate traces that overlap with BODIPY-pepstatin A signal.

LAMP1 is thought to associate more with LEs, implying the absence of active hydrolases (Yap et al., 2018). To evaluate if the observed vesicles are acidified lysosomes with active enzymes, the cells were incubated with BODIPY-pepstatin A. BODIPY-pepstatin A, a fluorescent probe, is transported to lysosomes where it binds to cathepsin D (CatD) and consequently exhibits fluorescence (Chen et al., 2000). The quantification of co-trajectories in dendrites of hippocampal neurons showed that ~64 % of LAMP1 and ~72 % of LAMP2 contained CatD (Figure 11F-G). Interestingly, both for LAMP1 and LAMP2, the

majority of co-signal with BODIPY-pepstatin A could be observed for the stationary vesicles.

Overall, the data reflect the high heterogeneity within lysosomes including different membrane compositions, as well as the distinct presence of active enzymes. Against the proposed model of gradual decrease of acidified lysosomes from the soma to the vicinity, the colocalization together with trafficking analysis revealed no changes between proximal and distal dendritic segments.

3.3 LAMP2-positive lysosomes and NMDAR activity

### 3.3.1 Trafficking of LAMP2-positive lysosomes is influenced by NMDAR activation

Recent studies showed that trafficking of LAMP1-positive lysosomes was regulated by activation of NMDARs and AMPARs (Goo et al., 2017), whereas LAMP2-positive lysosomes are able to undergo activity-dependent exocytosis (Padamsey et al., 2017). Previous experiments showed a higher association of LAMP2 with the GluN2B subunit of NMDARs compared to LAMP1 (Figure 10D) and therefore, the question arose if also LAMP2-positive vesicles could be regulated by NMDAR activity in terms of their localization and potential fusion.

To investigate this, the NMDA receptor subunit GluN2B was tagged with superecliptic pHluorin (SEP), a pH-sensitive fluorescent protein that exhibits fluorescence at neutral pH while the fluorescence is quenched at lower pH (pH < 6.0) milieus (Miesenböck et al., 1998). This consequently allows visualization of GluN2B-subunits located at the plasma membrane without detection of the intracellular pool localized to (mildly) acidified vesicles.

Hippocampal neurons transfected with SEP-GluN2B, as well as LAMP2-mKate, were monitored during live-cell imaging experiments to visualize the potential interplay between the NMDAR subunit and the lysosomal protein. The analysis revealed that ~34 % of SEP-GluN2B signal was colocalizing with LAMP2-mKate, temporarily or permanently (Figure 12A-B), seen as stopping ("visits") of LAMP2-mKate at SEP-GluN2B signal. Each GluN2B subunit at the plasma membrane that was detected to be visited by LAMP2 for more than 5 s during the time of acquisition, was considered as "positive SEP-GluN2B". The total time of LAMP2 pausing at GluN2B at the plasma membrane corresponded on average to ~43 % of the acquisition time, hence 128 s, thereby one subunit was visited often by multiple LAMP2-containing vesicles. This provided the first evidence for an interplay between LAMP2 and GluN2B.

In the following live-cell imaging experiments, two different inhibitors were applied: Ifenprodil as a noncompetitive GluN2B-specific inhibitor of NMDARs (Williams, 1993) and MK801 as a blocker of NMDAR-associated ion channel sites (Huettner and Bean, 1988). Upon treatment with the inhibitors, the visit time of LAMP2-mKate at SEP-GluN2B sites

was reduced significantly from ~43 % to ~20 % after MK801 application and to ~27 % after inhibition with ifenprodil (Figure 12C), although the fraction of positive SEP-GluN2B, with at least one visit by LAMP2-mKate, did not change (Figure 12A-B). This would reflect shorter stalling times of LAMP2 at the NMDAR subunits with unchanged total numbers of GluN2B that are visited by LAMP2. Additionally, the amount of SEP-GluN2B in the proximity (maximum 0.77 µm from the center of each signal) of LAMP2-mKate was quantified, as well as reversed (LAMP2-mKate in proximity of SEP-GluN2B) with around 40 % in both cases (Figure 12D-E). The treatments with inhibitors did not alter these numbers as seen for the amount of SEP-GluN2B positive for LAMP2 (Figure 12B).
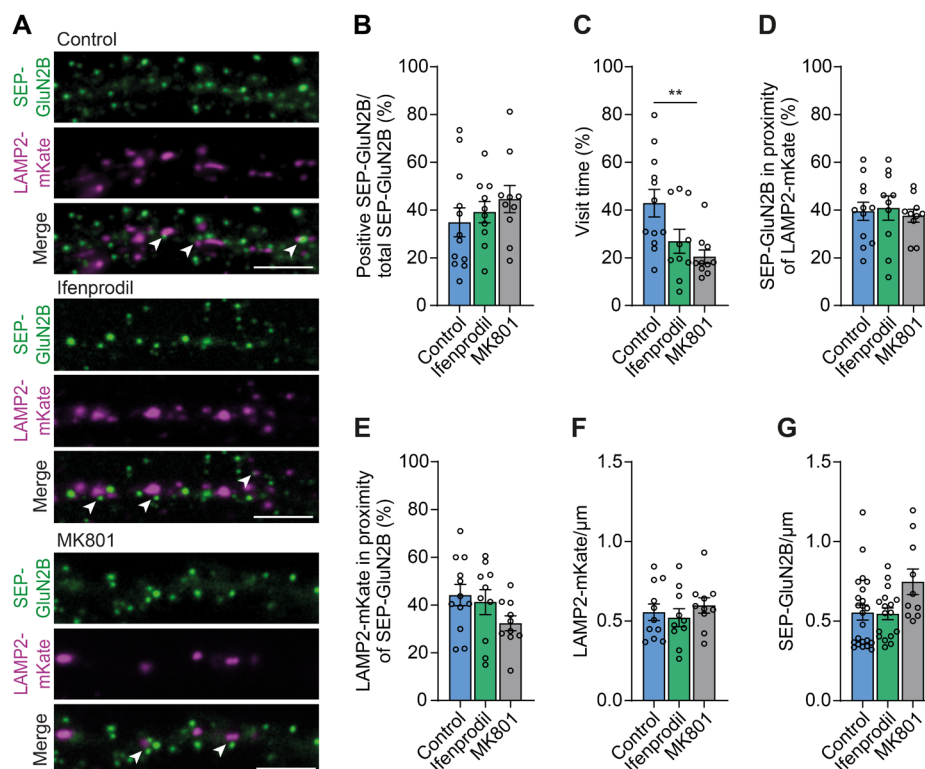
Figure 12: The NMDAR subunit GluN2B is associated with LAMP2 in an NMDAR-dependent manner. (A) Representative images from hippocampal neurons transfected with SEP-GluN2B (green) and LAMP2-mKate (magenta) either untreated (control) or treated with NMDAR inhibitors ifenprodil (5 µM for 30-45 min) or MK801 (100 µM for 1-2h). White arrows indicate signal that is directly in proximity. Scale bar 5 µm. **(B)** Quantification of SEP-GluN2B that is positive for LAMP2-mKate for more than 5 s during the acquisition time. Inhibition of NMDARs did not have a significant effect on the fraction of positive GluN2B. **(C)** The visit time of LAMP2-mKate at SEP-GluN2B was quantified. Application of either MK801 or ifenprodil leads to a decreased visit time. One-way ANOVA with Bonferroni's multiple comparisons test. **(D)** SEP-GluN2B in proximity of LAMP2-mKate or **(E)** LAMP2-mKate in proximity of SEP-GluN2B. **(F)** Quantification of LAMP2-mKate and **(G)** SEP-GluN2B signal per µm of the dendritic segment. **(B-G)** N-number = 8 cells from 6 cultures for control; 10 cells from 5 cultures for ifenprodil and 10 cells from 2 cultures for MK801.

To exclude the possible influence of the application of inhibitors on the density of signal, the detected signal per µm dendritic stretch was additionally assessed, revealing no differences between control and treatment conditions (Figure 12F-G).

The observed association during live-cell imaging experiments of LAMP2 with the NMDAR subunit GluN2B at the plasma membrane was verified by another experimental approach conducted in fixed cells. To this end, hippocampal neurons were transfected with LAMP2-GFP, fixed, and stained for surface GluN2B (Figure 13A). A fraction of almost 60 % of LAMP2-GFP could be detected in proximity of surface GluN2B, which could be also observed for ifenprodil-treated cells (Figure 13B). The density of GluN2B surface signal, however, did not show significant differences between the control and ifenprodil group (Figure 13C).
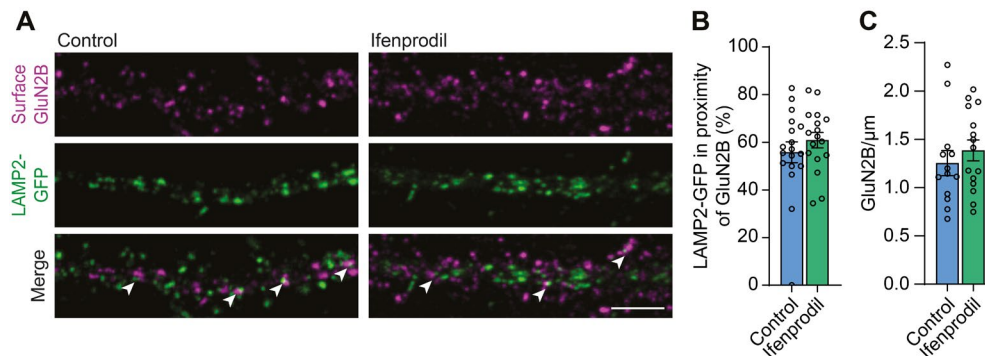
Figure 13: LAMP2-GFP signal in proximity of surface GluN2B. (A) Confocal images of hippocampal rat neurons transfected with LAMP2-GFP (green) and immunostained against surface GluN2B (magenta) treated with ifenprodil or without (control). Scale bar represents 5 µm. **(B)** LAMP2-GFP signal in proximity of GluN2B was quantified in DIV14-16 hippocampal neurons, revealing a high association in untreated, as well as ifenprodil-treated groups. **(C)** Quantification of GluN2B signal per µm of dendritic stretch. The application of ifenprodil did not alter the density of signal. N-number = 13 cells from 2 independent cultures for both control and ifenprodil.

Although LAMP2 is an abundantly found lysosomal protein, the conducted live-cell imaging experiments with BODIPY-pepstatin A revealed that not all LAMP2-containing vesicles contain active lysosomal hydrolases (Figure 11F). To further investigate the molecular characteristics of the stopping vesicles in regard to the presence of active enzymes, hippocampal neurons were incubated with Magic Red. Magic Red is a cell-permeable CatB substrate coupled to a fluorophore that exhibits fluorescence upon cleavage by the active enzyme (Boonacker et al., 2003). As before, live-cell imaging experiments were performed with rat hippocampal neurons transfected with SEP-GluN2B. Similar to the data obtained with LAMP2-mKate transfected neurons, Magic Red vesicles were observed to stop and pause at the NMDAR subunit (Figure 14A-B). In line with the previous experiments, the time of visits of Magic Red signal at SEP-GluN2B decreased upon inhibition of the NMDAR by ifenprodil (Figure 14B). The fraction of SEP-GluN2B and Magic Red being in proximity of each other was, with around 40 %, comparable to the results obtained for LAMP2-mKate (Figure 14C-D). The density of the Magic Red signal was, however, lower compared to LAMP2-mKate but did not change upon application of ifenprodil (Figure 14E).
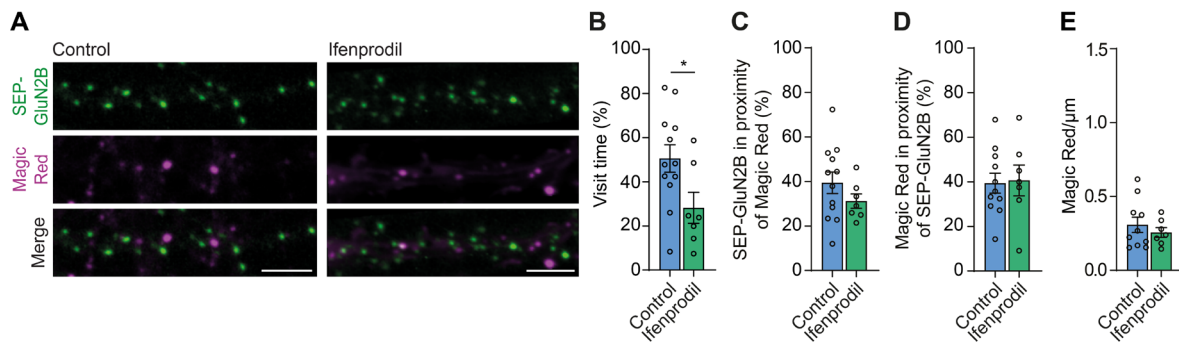
Figure 14: Vesicles containing active CatB reside at SEP-GluN2B. (A) Representation of dendritic stretches from hippocampal neurons transfected with SEP-GluN2B incubated with Magic Red (0.5 % for 30-60 min). Ifenprodil was applied to inhibit the GluN2B subunit and therefore NMDAR activity. Scale bar 5 μm. **(B)** Scatter bar plots represent the quantified visit time of Magic Red vesicles at SEP-GluN2B in percentages of the total time of the stream. Unpaired Student's *t*-test. **(C)** SEP-GluN2B in proximity to Magic Red was analyzed and as well as the other way around **(D)**. **(E)** The density of Magic Red signal per μm of dendritic stretch was quantified showing no effect of ifenprodil on the density of signal. N-numbers = 12 dendrites from 6 cells and 5 independent cultures for control; 7 dendrites from 5 cells and 2 cultures for ifenprodil treated cells.

In conclusion, the experiments showed that LAMP2-positive vesicles stop and reside at a fraction of SEP-labelled GluN2B in dendrites and thereby the residing time is NMDAR-activity-dependent. Since Magic Red showed similar behavior, one can conclude that at least a portion of the stopping LAMP2-mKate vesicles contains active enzymes, reflecting catabolic active lysosomes that associate with GluN2B-containing NMDARs.

3.3.2 GluN2B activation by NMDA leads to stalling of LAMP2-positive lysosomes

The preceding experiment demonstrated the stalling of LAMP2-positive lysosomes at SEP-GluN2B and the decreased residing time by inhibition of NMDARs. The next step was to investigate if direct activation of the NMDARs has an influence on the mobility of LAMP2-positive lysosomes, similar to the previously reported activity-dependent altered mobility of LAMP1-containing lysosomes by Goo et al. (2017). Previous observations in this thesis showed that neuronal stimulation with 4AP/bic did not have an effect on the GluN2B colocalization with LAMP2 or the localization of the co-signal of both proteins within the dendrite. The 4AP/bic protocol is thereby utilized for general synaptic activation, mainly targeting NMDARs at synaptic sites (Hardingham et al., 2002). However, the aim for the following experiments was to activate all NMDARs, hence bath application of moderate doses of NMDA was chosen to activate synaptic, as well as extrasynaptic, NMDARs (Zhou et al., 2013b). By utilization of total internal reflection fluorescence (TIRF) microscopy, only signal close to the plasma membrane was collected, excluding signal from other focal planes. Hippocampal neurons transfected with LAMP2-mKate and SEP-GluN2B were imaged for a total time of 15 min and 20 μM NMDA was applied during acquisition (application 40 s after start of acquisition). As seen in kymographs, 6-7 min

post NMDA application, LAMP2-mKate showed heavily reduced motility with most vesicles eventually becoming immobile (Figure 15A-C). In line with previous observations of stopping vesicles at the GluN2B subunits, the same effect was observed for neurons incubated with Magic Red (Figure 15D-F). The quantification of the velocity of moving vesicles in the beginning, as well as at the end of the stream, showed a significant and dramatic reduction of velocity close to 0 µm/s for LAMP2-mKate (Figure 15C) and Magic Red (Figure 15F).
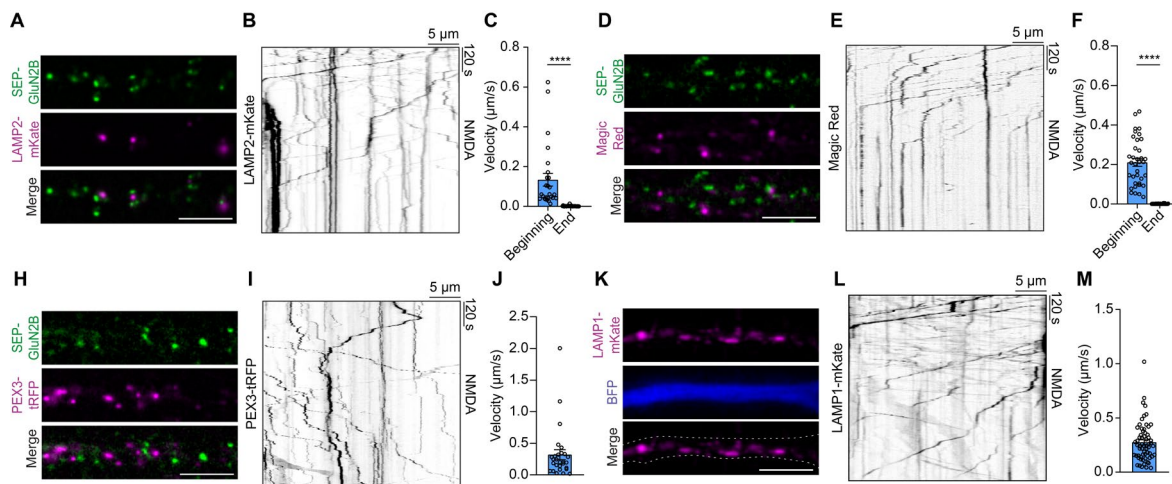
Figure 15: NMDAR activation leads to stalling of LAMP2- and Magic Red-positive vesicles in dendrites. (A) Representative images of SEP-GluN2B and LAMP2-mKate transfected neurons. Scale bar 5 µm. **(B)** Kymographs of dendrites from LAMP2-mKate transfected hippocampal neurons. The mobility is highly reduced after application of NMDA. **(C)** Quantification of vesicle velocity at the beginning as well as the end of the acquired stream. Mann-Whitney *U* test. N-number = 14 cells from 4 independent cultures. **(D)** TIRF microscopy images of SEP-GluN2B transfected hippocampal neurons incubated with Magic Red. Scale bar 5 µm. **(E)** Kymographs showing the movement of Magic Red labeled vesicles over time. Again, NMDA lead to an abolished movement of vesicles. **(F)** Velocity of Magic Red vesicles was measured and quantified at the beginning and end of the stream. Unpaired *t*-test. N-number = 8 cells from 5 independent cultures. **(I)** Kymographs of PEX3-tRFP and quantification of velocity **(J)** during the time of acquisition. N-number = 6 cells from 4 independent cultures. **(K)** Images from dendrites of LAMP1-mKate and BFP transfected neuronal cells. White dashed lines display the outline of the dendrite obtained by BFP signal. Scale bar 5 µm. **(H)** Representative images of SEP-GluN2B and PEX3-tRFP transfected hippocampal neurons. Scale bar 5 µm. **(L)** LAMP1-mKate mobility seen in kymographs and its quantified velocity **(M)** over time. There was no reduced mobility after application of NMDA. N-number = 4 cells from 2 independent cultures for LAMP1-mKate.

To check if the observed stalling of vesicles is specific for LAMP2-positive and catabolic active lysosomes, the same experiment was carried out with hippocampal neurons transfected with SEP-GluN2B and PEX3-tRFP (Figure 15H). PEX3, peroxisomal biogenesis factor 3, labels oxidative organelles named peroxisomes (Schrader and Pellegrini, 2017). Strikingly, the application of NMDA did not have an effect on the mobility of PEX3-tRFP vesicles (Figure 15I). The velocity was thereby quantified throughout the stream, involving vesicles traced at the beginning as well as the end of the stream (Figure 15J). Kymographs from dendrites of LAMP1-mKate and BFP expressing neurons also did

not show an effect of NMDA application on the mobility of vesicles (Figure 15K-L) and the quantification revealed high velocity throughout the stream (Figure 15M).

These findings reveal an impact of NMDAR activity on the mobility of LAMP2- and Magic Red-positive vesicles localized close to the plasma membrane in the dendritic compartment. Surprisingly, neither LAMP1-mKate nor PEX3-tRFP showed any differences in mobility after activation of NMDARs by NMDA application, therefore reflecting a phenomenon specific for LAMP2-positive mature lysosomes.

3.3.3 LAMP2-positive lysosomes undergo fusion with the plasma membrane upon neuronal stimulation

As demonstrated by previous studies, LAMP2-positive lysosomes are able to undergo activity-dependent fusion with the plasma membrane in dendrites of hippocampal neurons (Padamsey et al., 2017). To first investigate further if the LAMP2-positive pool that was observed to stop in proximity to the SEP-GluN2B had the ability to fuse with the plasma membrane as well, live-cell imaging experiments were carried out with mKate and SEP-LAMP2 transfected hippocampal neurons at DIV16. LAMP2 was tagged with SEP on its luminal part, therefore allowing visualization of LAMP2-positive vesicles that undergo exocytosis due to quenching of intracellular signal (Figure 16A). To mimic neuronal activity, two electrodes were attached to the imaging chamber to apply electrical field stimulation with 900 APs at 20 Hz frequency. In live-cell imaging experiments, an increase in fluorescent signal of SEP-LAMP2 upon stimulation was detected using TIRF microscopy, reflecting fusion events of SEP-LAMP2-containing vesicles with the plasma membrane (Figure 16B-D). The fusion was abolished upon inhibition of NMDAR activity by pre-incubation of ifenprodil. Interestingly, not only the increasing fluorescence but also the density of fusion per µm of dendritic stretch was reduced upon ifenprodil application (Figure 16E). As seen for the stopping of vesicles, the fusion of SEP-LAMP1 could not be observed in this set of experiments (Figure 16F-G).
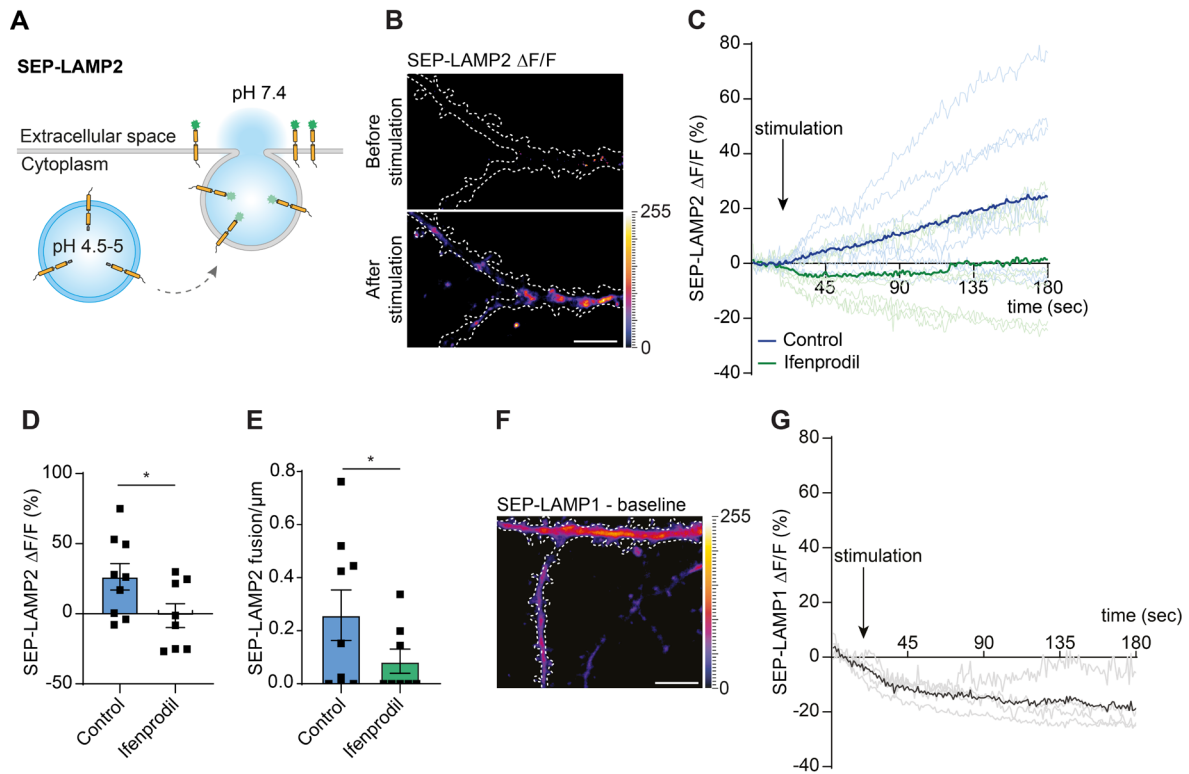
Figure 16: LAMP2-positive lysosomes fuse with the plasma membrane upon field stimulation. (A) Schematic representation of luminal SEP-tagged LAMP2. In acidic vesicles, such as lysosomes, the fluorescent signal is quenched. Upon fusion and exposure to a neutral pH environment, fluorescence can be detected. **(B)** Images of dendrites from hippocampal neurons expressing mKate and SEP-LAMP2 prior and past field stimulation. The intensity of fluorescent SEP-LAMP2 signal increases after field stimulation. White dashed lines show the dendritic outline. Pixel intensities from 0 to 255 are color coded as indicated. Scale bar 10 μm. **(C)** The difference of fluorescence of SEP-LAMP2 was plotted over time. During acquisition of the stream, field stimulation was conducted (start of stimulation indicated by the arrow) to drive neuronal activity. Treatment with 5 μM ifenprodil prior to the experiment resulted in abolished increase of fluorescence, hence fusion of SEP-LAMP2. Bafilomycin A1 was present (1 μM) throughout the experiment to avoid reacidification of vesicles. Averages of the traces are displayed in dark blue (control) and dark green (ifenprodil) whereas light colors display the respective single traces. N-number = 9 cells for control from 4 independent cultures and 8 cells for ifenprodil from 3 independent cultures. **(D)** Quantification of peak difference in fluorescence intensity of SEP-LAMP2. Two-tailed unpaired Student's *t*-test. **(E)** The detected fusion per μm of dendritic stretch was reduced in ifenprodil-treated cells. Poisson probability distribution. **(F)** Representative images from TIRF microscopy of hippocampal neurons transfected with mKate (white dashed line) and SEP-LAMP1. The heat map visualizes pixel intensities from 0 to 255. Scale bar 10 μm. **(G)** The fluorescence of SEP-LAMP1 after field stimulation did not increase as seen for SEP-LAMP2, therefore showing no fusion of SEP-LAMP1 vesicles. Shown are single traces (light grey) and the average (dark grey). N-number = 4 cells from 2 independent cultures.

The stopping and fusion events of LAMP2-positive lysosomes in an NMDAR-dependent manner raised the question about the localization of the observed events in regard to the GluN2B subunit. The quantification of the distance of either stopping of LAMP2-mKate or fusion of pHuji-LAMP2 to the next SEP-GluN2B signal showed a close proximity (Figure 17A). The stopping, as well as the fusion, were detected around 0.5 μm in ~50 % of the cases (Figure 17B). Taken together, the data support the findings from Padamsey et al.

(2017), describing fusion of LAMP2-containing vesicles in an activity-dependent manner. Moreover, the quantification revealed a spatial association of the fusion, as well as the stopping, events to the NMDAR subunit GluN2B.
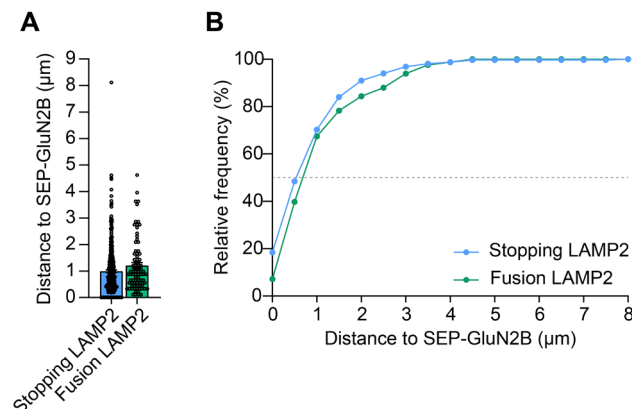
Figure 17: The stopping and fusion of LAMP2 vesicles in proximity of SEP-GluN2B. (A) The distance in µm between stopping LAMP2-mKate or fusing pHuji-LAMP2 was quantified in regards to SEP-GluN2B, revealing the majority of events in close proximity of the GluN2B subunit. **(B)** Relative frequency distribution of the measured distance of LAMP2-mKate that stop and pHuji-LAMP2 undergoing fusion in an activity-dependent manner. The dotted line indicates 50 %, hence half of the fusion and stopping was observed around 0.5 µm to the next detected GluN2B subunit. N-number = for stopping LAMP2-mKate 320 ROIs from 14 cells from 4 independent cultures, for fusion of pHuji-LAMP2 83 ROIs from 8 cells from 4 independent cultures.

3.3.4 Deletion of GluN2B leads to impaired fusion of LAMP2 vesicles

The findings of previously described experiments provide evidence for an association between the NMDAR subunit GluN2B and LAMP2. To corroborate these findings, the effect of an absence of GluN2B on LAMP2-containing vesicle fusion provided an elegant approach to verify the functional link between the two proteins. To this end, KO of GluN2B was established using hippocampal neurons obtained from CRISPR/Cas9 knockin mice. For the initial characterization, immunostaining of surface GluN2B was performed in cells transfected with tRFP or tRFP together with plasmids encoding for gRNA targeted against GluN2B (Figure 18A). The quantification of the mean fluorescence intensity of GluN2B surface staining revealed a vast reduction to ~45 % in mouse neurons carrying gRNA against GluN2B compared to control cells (Figure 18B).
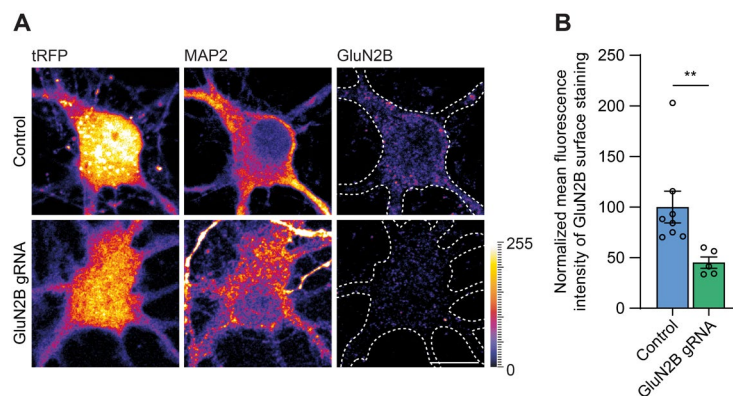
Figure 18: KO of GluN2B in hippocampal neurons of CRISPR/Cas9 knockin mice. (A) Representative confocal images of DIV14 hippocampal mouse neurons transfected with tRFP only or together with plasmids encoding for GluN2B-targeting gRNA. White dashed lines reflect the cell outline. Pixel intensities from 0 to 255 are shown in the heat map. Scale bar 10 µm. **(B)** Quantification of the mean fluorescence intensity of GluN2B surface staining in fixed hippocampal mouse neurons reveals a significant decrease of signal in gRNA expressing cells targeting GluN2B compared to the control group. Mann-Whitney *U* test. N-number = 8 cells for control and 5 cells for GluN2B gRNA from 1 culture.

To address the question of GluN2B-dependency in regard to the observed LAMP2-positive vesicle fusion, the fusion experiment was carried out with hippocampal neurons expressing gRNA targeted against GluN2B together with pHuji-LAMP2. pHuji is a pH-sensitive fluorescent protein, similar to SEP, however, exhibits red fluorescence (Shen et al., 2014). In contrast to the previously conducted field stimulation, the activation of NMDARs was induced by NMDA bath application. In the GluN2B KO cells, the increase of pHuji-LAMP2 fluorescent signal was reduced compared to Cas9 only cells (control) after stimulation with NMDA (Figure 19A-C). This could be seen in average traces of the change of fluorescence during the acquisition (Figure 19B) as well as in the quantification visualized by scatter bar plots (Figure 19C). Not only the fluorescence change of pHuji-LAMP2 was reduced in GluN2B KO cells but also density of fusion events was decreased (Figure 19D).
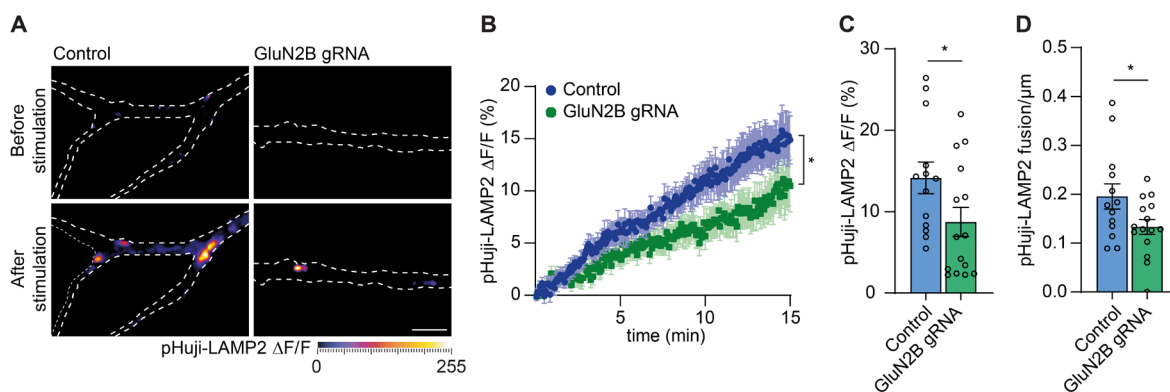
Figure 19: Fusion of pHuji-LAMP2 is impaired in GluN2B KO neurons. (A) Images obtained by TIRF microscopy represent dendrites transfected with plasmids encoding for BFP and pHuji-LAMP2 before and after stimulation. KO cells (Cas9+GluN2B gRNA) are additionally transfected with gRNA targeted against GluN2B. White dashed lines reflect the dendritic outline traced by BFP

fluorescence signal. The changes in fluorescence intensity is visualized as indicated in the heat map with pixel intensities from 0 to 255. Scale bar 5 µm. **(B)** The difference of pHuji-LAMP2 fluorescence during the acquisition is decreased in GluN2B KO cells. Average traces are shown in blue for control cells (Cas9 expressing cells) and in green for Cas9 expressing cells carrying gRNA against GluN2B. Mixed-effect analysis. **(C)** Scatter bar plots representing the analysis of differences in fluorescence intensity from **(B)**. Mann-Whitney U test. **(D)** Fusion density (fusion/µm of dendritic stretch) is reduced in dendrites of neurons transfected with GluN2B gRNA. Unpaired t-test. N-number = 13 cells for control and 15 cells for GluN2B gRNA from each 9 independent cultures.

The KO of GluN2B therefore supports the observations of a NMDAR-activity-dependent fusion of LAMP2-positive lysosomes. However, the effect of the GluN2B KO was rather modest, suggesting that the presence of GluN2B is not the only determinant for successful fusion.

3.3.5 LAMP2 interacts with the scaffold protein SAP102, but not with the NMDAR subunit GluN2B

The observed stalling and fusion of LAMP2-positive lysosomes was spatially, as well as functionally, connected to the GluN2B subunit of NMDARs, which could possibly reflect a "stopping hub" for subsequent fusion. This would imply a physical interaction between GluN2B and LAMP2. To test this, heterologous co-immunoprecipitation (Co-IP) experiments were conducted with lysates from transfected HEK293T cells. Super paramagnetic MicroBeads coated with a monoclonal GFP antibody were used to bind GFP-tagged proteins and their potential interaction partners. After separation of the samples by SDS-PAGE following Western Blot, membranes were incubated with antibodies targeted against GFP or LAMP2.

No interaction was observed in Co-IP experiments neither between GFP and tRFP-tagged LAMP2, nor between the GluN2B C-terminal domain fused to GFP (GluN2B-840-1482-GFP) and LAMP2-tRFP (Figure 20A). The C-terminus of GluN2B was thereby used since it is faced to the intracellular side of the cell, hence could serve as the required binding sequence for LAMP2. The inputs, as well as the IP (anti-GFP), show the expected bands and served as control for proper protein expression and Co-IP procedure (Figure 20A). WT-Jacob, a synapto-nuclear protein messenger and previously shown binding partner of the C-terminus of GluN2B (Melgarejo da Rosa et al., 2016), showed the expected interaction in Co-IP experiments (Figure 20B). GluN2B is anchored in the PSD by different proteins of the MAGUK family and the scaffold protein SAP102 was thereby shown to preferentially bind to GluN2B over other NMDAR subunits. Indeed, when HEK293T cells were transfected with GluN2B-840-1482-tRFP and GFP-tagged SAP102, an interaction was detected (Figure 20C).

Since SAP102 is localized to the PSD, the question arose if this could act as a potential linkage and binding partner of GluN2B and LAMP2. To first characterize the distribution of

GluN2B and SAP102 in cultured hippocampal neurons, cells were immunostained against endogenous GluN2B and SAP102 (Figure 20D). The colocalization analysis revealed a high degree of colocalization (~62 %) between the proteins (Figure 20E) which could be also observed in the confocal images (Figure 20D). Since this experiment was performed in permeabilized neurons, also the intracellular pool of GluN2B was labeled including subunits endocytosed for subsequent recycling or degradation as well as newly synthesized proteins. The same experiment was performed with GluN2B surface staining (Figure 20F). SAP102 colocalized to a higher degree (~70 %) with the GluN2B subunit when visualized on the surface (Figure 20G). The surface GluN2B, however, showed less colocalization with SAP102 with almost 55 % (Figure 20H).
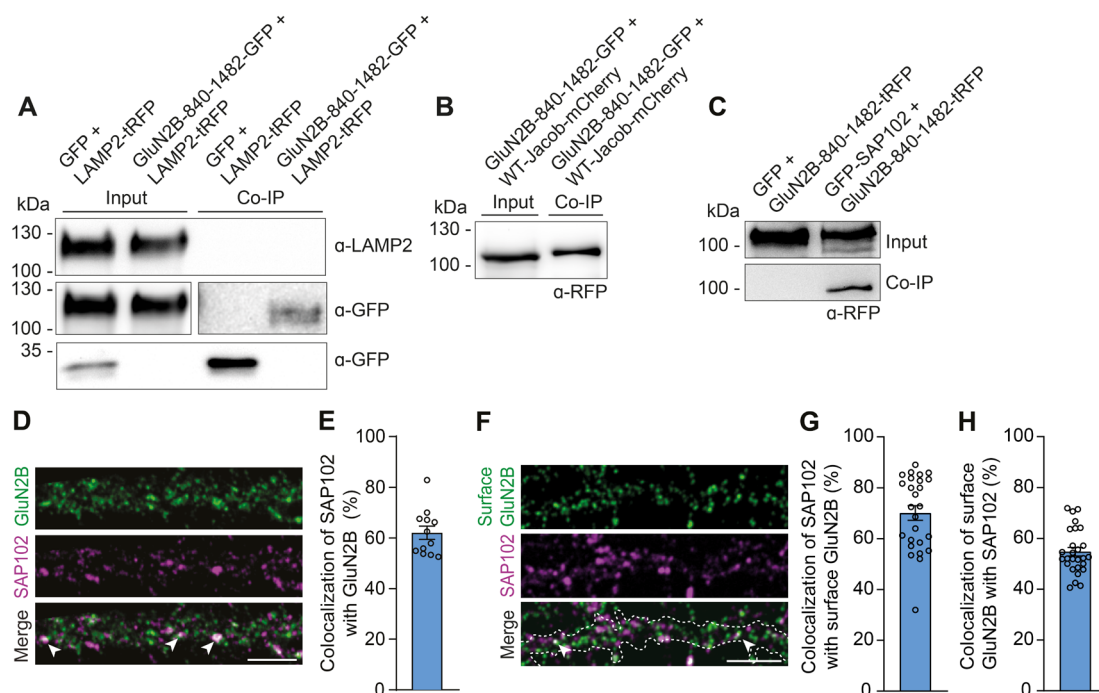
Figure 20: GluN2B does not show an interaction with LAMP2 but associates with the scaffold SAP102. (A) LAMP2-tRFP does not interact with GFP nor with GluN2B-840-1482-GFP in Co-IP experiments from HEK293T cells. **(B)** GluN2B-840-1482-GFP and WT-Jacob-mCherry show the expected co-immunoprecipitation. **(C)** Co-IP experiments reveal the interaction of the scaffold protein SAP102 with the C-terminal amino acid sequence of GluN2B. **(D)** Representative confocal images of dendrites from hippocampal neurons stained against endogenous proteins. Arrows indicate clear overlap of signal between both GluN2B (green) and SAP102 (magenta). Scale bar 5 μm. **(E)** Quantification of endogenous SAP102 colocalizing with GluN2B in primary hippocampal rat neurons demonstrates a high overlap. N-number = 12 cells from 3 independent cultures. **(F)** Confocal images of hippocampal neurons transfected with BFP (white dashed lines indicate dendrite outline) stained against surface GluN2B (green) and SAP102 (magenta). The overlap of signal is shown by white arrows. Scale bar 5 μm. **(G)** Quantification of SAP102 staining colocalizing with surface GluN2B, as well as surface GluN2B with SAP102 **(H)**. SAP102 colocalizes more with surface GluN2B then the other way around. N-number = 25 cells from 3 independent cultures.

To verify the specificity of the antibody, a shRNA KD approach for SAP102 was established. Hippocampal neurons expressing SAP102-targeting shRNA for 7 days were immunostained against endogenous SAP102 (Figure 21A). The analysis of the mean

fluorescence intensity of staining signal in the dendrite showed a significant decrease in fluorescence in cells expressing one of the shRNAs compared to cells transfected with scrambled shRNA (Figure 21B).
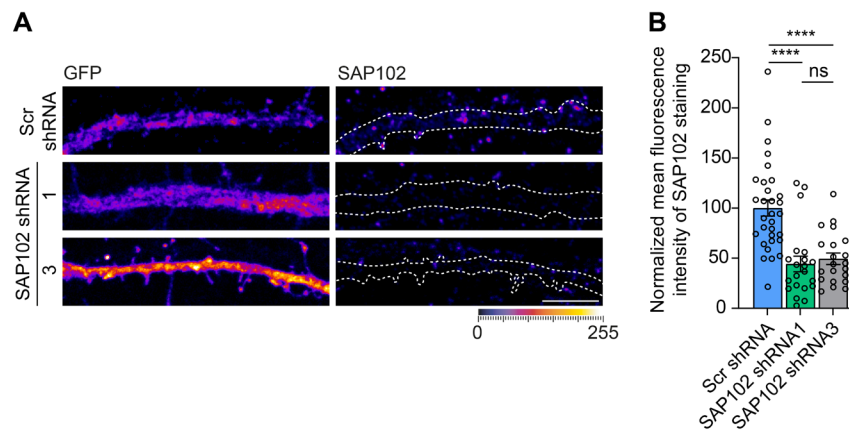
Figure 21: KD of SAP102 leads to a reduction of SAP102 staining intensity. (A) Confocal images from dendrites of hippocampal rat neurons expressing different shRNA encoding plasmids stained against endogenous SAP102. As part of the transfected plasmid, GFP indicates cells expressing the construct with the respective shRNA. Pixel intensities from 0 to 255 are color coded as indicated. Scale bar 7 µm. **(B)** Quantified normalized mean fluorescence intensity of SAP102 staining in dendrites of transfected cells shows a decrease of staining intensity. N-number = 22 cells from 4 independent cultures for scrambled shRNA, 18 cells for shRNA1 and 14 cells for shRNA3 from each 3 independent cultures. One-way ANOVA with Bonferroni posthoc test.

Since no interaction between LAMP2-tRFP and the C-terminus of GluN2B-GFP could be detected in heterologous Co-IP, a more indirect binding between the two proteins through another binding partner is conceivable. SAP102 consists of different domains, including PDZ domain 1-3, an SRC Homology 3 Domain (SH3) and a guanylate kinase-like domain (GK) at its C-terminus. To investigate if LAMP2 could potentially bind to one of the different modules, the domains of SAP102 were split to obtain GFP-fused PDZ1-3 or SH3-GK for further experiments (Figure 22A). The rather short cytoplasmic tail of LAMP2, corresponding to amino acids 404-415, was additionally fused to pGolt-mCherry. pGolt-mCherry contains the transmembrane domain of calneuron-2, a TGN-accumulated protein, together with an ER export signal and is therefore targeted to Golgi structures (Mikhaylova et al., 2016). HEK293T cells were transfected with the GFP-SAP102 constructs containing the different domains and either pGolt-mCherry, LAMP2-404-415-pGolt-mCherry or GluN2B-840-1482-pGolt-mCherry. Interestingly, this assay revealed the recruitment of GFP-SAP102-SH3-GK to the LAMP2-404-415-pGolt-mCherry signal which could not be observed for pGolt-mCherry expressing cells (Figure 22B). However, GFP-SAP102-PDZ1-3 was not targeted to the LAMP2-404-415-pGolt-mCherry signal. The GluN2B C-terminal part (840-1482) is known to bind to the PDZ domains of SAP102 which could be nicely seen in HEK293T cells transfected with GluN2B-840-1482-pGolt-

mCherry and GFP-SAP102-PDZ1-3, leading to clear recruitment and overlap of signal (Figure 22C).
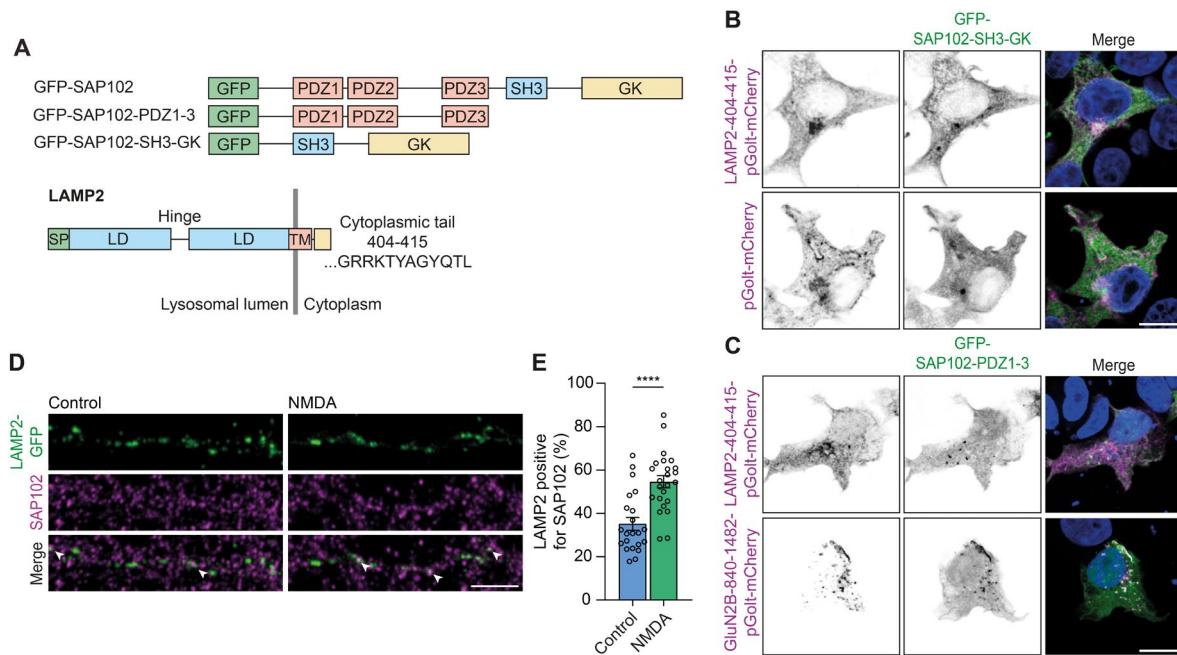

Figure 22: LAMP2 is associated with the MAGUK SAP102. (A) Scheme showing the different domains of GFP-SAP102 constructs used for the recruitment assay. Shown are PDZ domains 1-3 (rose), the SH3 domain (blue) and the GK domain (yellow). Different constructs were cloned encoding for either only PDZ1-3 or SH3-GK. LAMP2 consists of a signal peptide (SP; green), two luminal domains (LD; blue) connected by a hinge region, a transmembrane domain (TM; rose) and a short tail (AA 404-415; yellow). The C-terminus contains the sequence for potential cytosolic binding partners. **(B)** Recruitment assay with HEK293T cells transfected with the SH3-GK domain of SAP102 tagged with GFP (green) and LAMP2-404-415-pGolt-mCherry or pGolt-mCherry (magenta) alone stained with DAPI (blue). A recruitment of GFP-SAP102-SH3-GK can be observed for LAMP2-404-415-pGolt-mCherry. Scale 10 µm. **(C)** GFP-SAP102-PDZ1-3 was expressed together with either the cytoplasmic tail of LAMP2 or the C-terminal domain of GluN2B fused to pGolt-mCherry. GluN2B-840-1482 nicely recruited GFP-SAP102-PDZ1-3 which could not be seen for LAMP2-404-415 targeted to the Golgi. Scale 10 µm. **(D)** Images of LAMP2-GFP (green) transfected neurons immunostained against endogenous SAP102 (magenta) either non-treated (control) or treated with 20 µM NMDA for 15 min pre-fixation. Colocalization is indicated by white arrows. Scale bar 5 µm. **(E)** NMDA activation by application of NMDA increases the colocalization of LAMP2-GFP with endogenous SAP102 in comparison to control neurons as seen in the quantification. N-number = 22 cells for control and 24 cells for NMDA group from each 4 independent cultures.

To get a better insight into the relation between the two proteins in dendrites of hippocampal neurons, the colocalization between endogenous SAP102 and overexpressed LAMP2-GFP was assessed. The degree of co-signal was around 37 % and, surprisingly, increased to almost 60 % after 15 min application of 20 µM NMDA to the culture medium (Figure 22D-E). This provided evidence for an NMDAR-dependent recruitment of LAMP2 to SAP102.

Since the previous experiment demonstrated the recruitment of SAP102 to the cytoplasmic tail of LAMP2 in HEK293T cells, the next step was the conformation of

interaction by biochemical assays. To this end, pulldown (PD) experiments were carried out with lysate of COS-7 cells expressing the desired fusion proteins (Figure 23A). By the usage of immobilized His-SUMO-LAMP2-404-415 as bait, the GFP-tagged prey could be identified. The input revealed expression of all proteins by anti-GFP antibody incubation. In the PD, the cytoplasmic tail of LAMP2 together with GFP-fused Hsc70 and SAP102 SH3-GK domains (Figure 23B). No interaction could be seen for the PDZ1-3 domains of SAP102 as well as for His-SUMO only.

The TAT peptide is one of the known cell penetrating peptides (CPPs) which are able to translocate across cellular membranes, hence being used as vehicles for different cargo (Hällbrink et al., 2001). The TAT peptide sequence (GRKKRRQRRRPQ) was coupled to the cytoplasmic amino acid sequence of LAMP2 (TAT-LAMP2-404-415) for the purpose of designing a dominant negative peptide, possibly disrupting the binding of LAMP2 to SAP102. The PD was carried out with His-SUMO-LAMP2-404-415 and GFP-SAP102-SH3-GK in presence of TAT-LAMP2-404-415, leading to a disrupted binding between the proteins, however, this effect was not observed by incubation with TAT-Scrambled as control (Figure 23C). To confirm that no degradation of the purified proteins occurred, a coomassie gel stain was performed (Figure 23D).
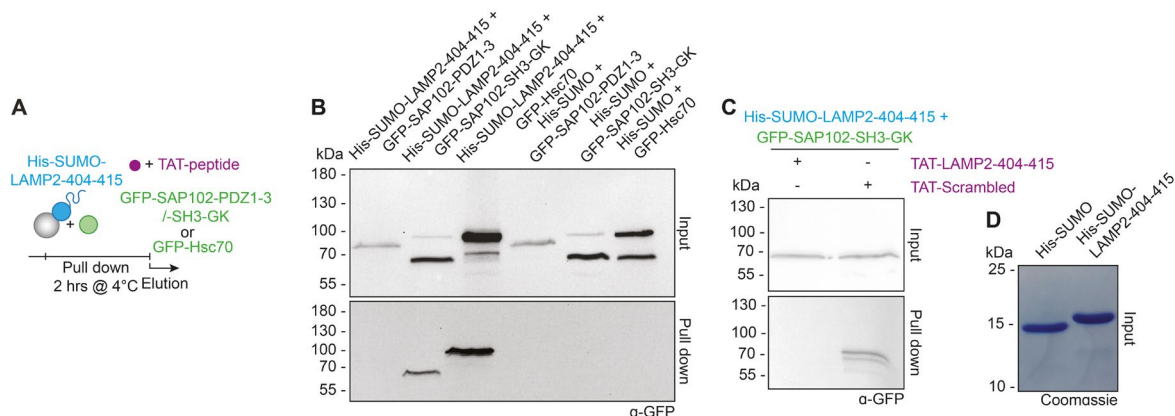
Figure 23: PD experiments reveal an interaction between the C-terminus of LAMP2 and SAP102-SH3-GK. (A) Scheme of PD experiments performed showing immobilized His-SUMO-LAMP2-404-415 on beads used for PD and the GFP-tagged constructs of SAP102 or Hsc70. In indicated experiments, the cell penetrating TAT-peptide was additionally added. **(B)** GFP-SAP102 transfected COS-7 cell lysate was used for PD with His-SUMO or His-SUMO-LAMP2-404-415. The input shows the presence of the respective proteins. The PD shows an interaction between His-SUMO-LAMP2-404-415 with the known binding partner Hsc70 as well as with SAP102-SH3-GK, each fused to GFP and visualized with an anti-GFP antibody. **(C)** The PD assay was performed with lysates of COS-7 cells transfected with GFP-SAP102-SH3-GK in presence of the CPPs TAT-LAMP2-404-415 or TAT-Scrambled. The interaction between LAMP2-404-415 and SAP102-SH3-GK was impaired upon TAT-LAMP2-404-415 application. **(D)** Coomassie stained gel showing non-degraded His-SUMO and His-SUMO-LAMP2-404-415 purified proteins.

3.4 Chaperone-mediated autophagy (CMA) in dendrites

3.4.1 The CMA machinery is associated with LAMP2-positive lysosomes

LAMP2 is implicated in CMA in which process LAMP2A serves as the receptor for subsequent translocation of target proteins that are delivered to the lysosomal membrane by the chaperone Hsc70. Until now, this was shown only for the LAMP2A isoform. To investigate if the LAMP2 isoform used in this thesis, LAMP2B, could be connected to CMA processes as well, LAMP2 tagged with mKate was overexpressed in hippocampal neurons and immunostained with an antibody specific for the isoform LAMP2A. The analysis of associated signal showed that around 70 % of LAMP2 is either overlapping or directly opposing to LAMP2A fluorescence signal, quantified as degree of association (Figure 24A-B). It is well known that Hsc70 is the required chaperone for the process of CMA and a binding partner of LAMP2A (Kaushik and Cuervo, 2018). To get a better insight into the potential binding to other LAMP2 isoforms, Co-IP experiments were performed with HEK293T cell lysates containing overexpressed LAMP2-tRFP and either GFP or GFP-Hsc70 (Figure 24C). A clear signal was detected for the immunoprecipitation of LAMP2-tRFP with GFP-Hsc70 but not with GFP, indicating binding between the proteins. In the previously performed PD assays, GFP-Hsc70 was already observed to bind to the cytoplasmic tail of LAMP2 (LAMP2-404-415; Figure 23B). The TAT-LAMP2-404-415 peptide was present in different ratios during the PD experiment, resulting in a clear reduction of the signal (Figure 24D). By incubation with the TAT-Scrambled peptide, there was no decrease in signal detected in the PD experiment (Figure 24E).
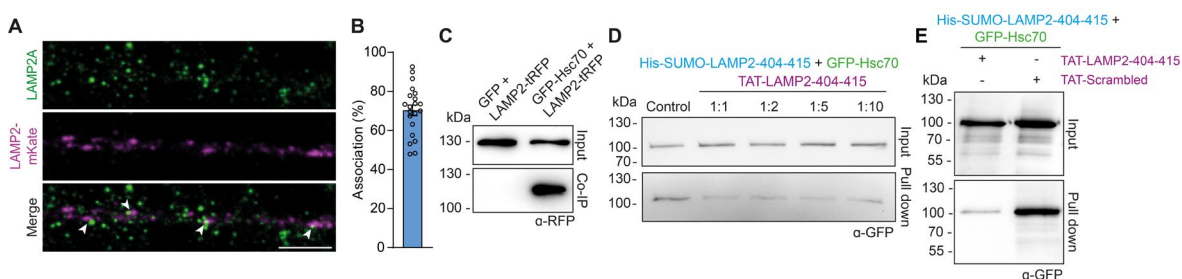
Figure 24: LAMP2 colocalizes with LAMP2A and is associated with CMA machinery. (A) Confocal images of LAMP2-mKate transfected hippocampal neurons stained against the endogenous LAMP2A isoform. Scale bar 5 µm. **(B)** The degree of association of overexpressed LAMP2 with endogenous LAMP2A was quantified. N-number = 17 cells from 3 independent cultures. **(C)** LAMP2-tRFP immunoprecipitates with GFP-Hsc70 in heterologous Co-IP experiments conducted with HEK293T cells expressing the respective constructs. **(D)** The binding between His-SUMO-LAMP2-404-415 and GFP-Hsc70 was decreased by incubation of TAT-LAMP2-404-415 in PD experiments in the indicated ratios. **(E)** The interaction between the cytoplasmic sequence of LAMP2 and the chaperone Hsc70 was heavily reduced by incubation of TAT-LAMP2-404-415 but not the TAT-Scrambled peptide.

3.4.2 TDP-43 localizes to LAMP2-containing lysosomes and is released upon NMDAR activation

TDP-43 is an aggregation-prone protein implicated in neurodegenerative diseases, such as ALS and FTLD, and, interestingly, targeted by CMA (Ormeño et al., 2020). Together with its proven presence in dendrites of neurons, TDP-43 reflects a potential candidate recognized by the CMA machinery (Chu et al., 2019). The potential connection of TDP-43 to the observed fusion of LAMP2-containing lysosomes was next aimed to be examined.

First, TDP-43 tagged with tandem dimer Tomato (tdTomato) was expressed in neurons together with LAMP2-GFP. Confocal imaging revealed that TDP-43 could be visualized in dendrites of neurons and the signal localized frequently in direct proximity to the LAMP2 signal (Figure 25A). Therefore, the colocalization was quantified, and additionally, the opposing signal, plotted together as proximity (Figure 25B). Almost 70 % of TDP-43-tdTomato was either overlapping (~34 %) or opposing (~35 %) with LAMP2-GFP, whereas ~52 % of LAMP2-GFP was associated with TDP-43-tdTomato (~22 % overlap/~30 % opposing).

As the next step, live-cell imaging experiments were carried out with TDP-43-tdTomato and LAMP2-BFP transfected cells. To visualize active CatD, the cells were incubated prior to the experiment with BODIPY-pepstatin A. In images obtained by the merge of first frames, an overlap of signal could be visualized (Figure 25C). Kymographs of dendritic stretches additionally revealed co-trafficking events of TDP-43-tdTomato together with LAMP2-BFP and BODIPY-pepstatin A (Figure 25D). The quantification of data obtained by live-cell imaging experiments revealed an overlap of trajectories in ~55 % of total TDP-43 traces with either LAMP2, BODIPY-pepstatin A, or both (Figure 25E). Thereby, ~13 % of TDP-43 trafficked together with only LAMP2 or BODIPY-pepstatin A. The majority (~29 %) of the co-trajectories could be observed as double-positive, hence the presence of TDP-43 in LAMP2-positive catabolically active lysosomes.
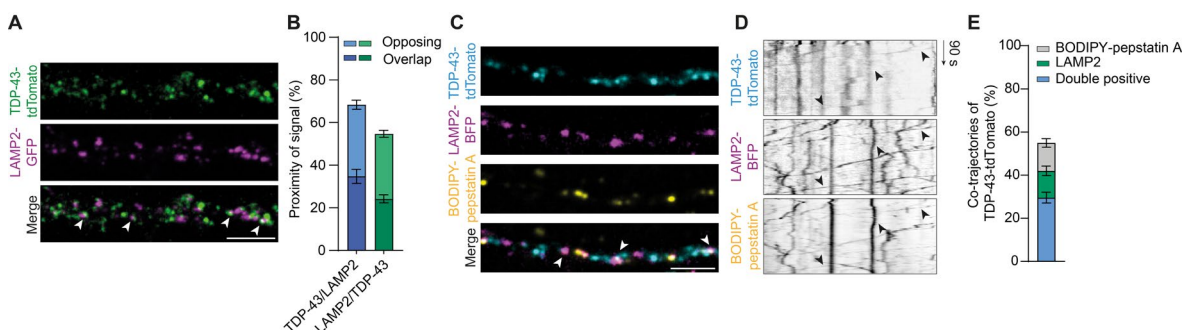
Figure 25: Dendritic TDP-43 is associated with LAMP2, as well as with active CatD. (A) Representative confocal images from dendrites of hippocampal neurons transfected with TDP-43-tdTomato (green) and LAMP2-GFP (magenta). White arrows indicate overlapping and opposing signal. Scale bar 5 µm. **(B)** The degree of overlapping as well as opposing signal was quantified for TDP-43-tdTomato with LAMP2-GFP (TDP-43/LAMP2) and reversed (LAMP2/TDP-43). N-numbers = 35 cells from 7 independent cultures. **(C)** Representative images from merged frames of live-cell

imaging experiments of TDP-43-tdTomato (cyan) and LAMP2-BFP (magenta) transfected hippocampal rat neurons incubated with BODIPY-pepstatin A (yellow). Overlapping signal of the three markers (TDP-43/LAMP2/BODIPY-pepstatin A) is indicated by white arrows. **(D)** Kymographs of dendrites generated from live-cell imaging reflect the movement of TDP-43-tdTomato, LAMP2-BFP and BODIPY-pepstatin A. Black arrows show co-trajectories. **(E)** Quantified co-trafficking of TDP-43-tdTomato with LAMP2-BFP and/or BODIPY-pepstatin A. A high portion of TDP-43-tdTomato shows co-trajectories with LAMP2 and labeled CatD by BODIPY-pepstatin A. N-number = 20 cells from 7 independent cultures.

Since the data indicated the presence of TDP-43 in vesicles containing the LAMP2 isoform used in this thesis, the next question arising was if the stopping and subsequent fusion of LAMP2-positive lysosomes includes release of cargo, namely TDP-43. To this end, primary cultures of cortical neurons were prepared and infected at DIV7 with AAV9 viruses encoding for GFP or GFP-TDP-43. Firstly, the efficiency of infection was assessed after 7 days of expression by fixation of the cortical neurons and subsequent MAP2 immunostaining, labeling neurons (Figure 26A). The quantification revealed a highly infected culture (~69 %; Figure 26B).

After the efficiency of transduction was verified, the release of the GFP-tagged proteins was aimed to be measured by utilizing a GFP-targeting enzyme-linked immunosorbent assay (ELISA). To this end, cortical cultures were infected with AAV_GFP or AAV_GFP-TDP-43 and, after 7-9 days of expression, the cell viability was verified prior to each experiment by incubation with PI. Then, coverslips with neurons were silenced by pre-incubation of TTX, following incubation in Tyrode's buffer containing NMDA or TTX only (control). The medium collected and further used for ELISA experiments.

As expected, no increase of GFP concentration could be measured in the AAV_GFP infected group upon NMDA application compared to the GFP-expressing control group (Figure 26C). On the other hand, the activation of NMDARs by stimulation with NMDA led to a significant increase in the measurements, with almost doubled GFP concentrations, in the medium of AAV_GFP-TDP-43 infected neurons.

Collectively, the results indicate that TDP-43 is present in LAMP2-positive, acidified, lysosomes and that TDP-43 is released from neurons in an NMDAR-dependent manner.
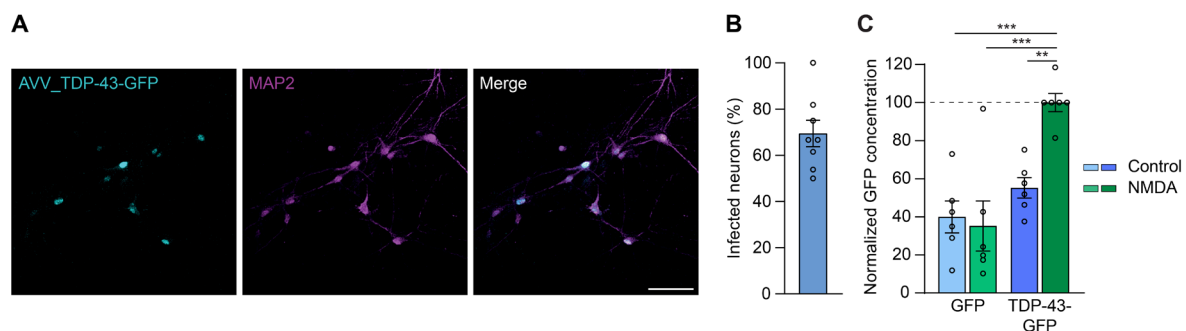
Figure 26: Infected cortical cultures show release of TDP-43 upon NMDAR activation. (A) AAV_TDP-43-GFP (cyan) infected cultured cortical neurons (DIV14) stained against MAP2 (magenta). Scale bar 50 μm. **(B)** A high portion of cells is infected by application of AAV_TDP-43-

GFP as seen in the quantified efficiency of infection of the cortex culture. **(C)** ELISA was used to determine the GFP concentration in the medium without and with NMDA stimulation (20 µM for 15 min) in TTX-silenced cortical neurons infected with AAV_GFP or AAV_TDP-43-GFP. The GFP concentration was normalized to the calculated concentration for NMDA-stimulated TDP-43-GFP group. N-number = 6 replicates from 5 independent cultures. Two-way ANOVA with Tukey posthoc test.

4. Discussion

The lysosome is the digestive endpoint of several catabolic pathways and its proper function is essential for maintaining proteostasis. The knowledge about its role and abundance in the dendritic compartment is limited, however, the existence of mature lysosomes in dendrites was recently shown. Intriguingly, their motility was demonstrated to be regulated by neuronal activation and lysosomal exocytosis in an activity-dependent manner was described (Goo et al., 2017; Padamsey et al., 2017). The results presented in this thesis provide evidence for a highly heterogeneous pool of dendritic lysosomes and demonstrate a connection between the NMDAR subunit GluN2B with LAMP2-positive, acidified, lysosomes. Namely, stopping, as well as fusion, of these lysosomes was observed upon activation of NMDARs. Interestingly, an interaction between the cytoplasmic tail of LAMP2 and the SH3-GK domain of the GluN2B-binding scaffold protein SAP102, but not GluN2B, was further revealed. Moreover, the data provide evidence for a CMA-mediated sequestering of the aggregation-prone protein TDP-43 to LAMP2-containing lysosomes and its subsequent activity-dependent release. These findings shed new light on dendritic lysosomes, their function, as well as the link to neuronal activity, suggesting a potential novel and protective mechanism of activity-dependent protein disposal that leads to fusion-dependent spine remodeling, hence neuronal plasticity.

4.1 Heterogeneity of lysosomal populations in dendrites

The presence of lysosomes in neurons was long thought to be restricted to the cell body, the main catabolic compartment within the cell. Over time, organelles of the autophagic and endolysosomal pathway were observed in axons, with lesser acidic organelles found in distal parts gradually increasing in their acidification during trafficking towards the soma. Only more recently, lysosomes were shown in dendrites as well (Goo et al., 2017; Padamsey et al., 2017). However, the molecular composition of dendritic lysosomes remains unknown.

This study demonstrates the presence of multiple lysosomal proteins that display different distributions in dendrites of cultured hippocampal neurons, emphasizing the heterogeneous population of dendritic lysosomes. The colocalization analysis revealed a rather modest overlap between endogenous LAMP1 and LAMP2, the two most abundantly found lysosomal membrane proteins, estimated to make up for more than 50 % of lysosomal membrane content (Eskelinen, 2006). Findings from live-cell imaging experiments further revealed that LAMP1 vesicles tagged with mKate displayed a less mobile trafficking profile compared to LAMP2. Together, this provided evidence that LAMP1 and LAMP2 are present in different organelles, proposing distinct functions. The data interestingly revealed an unchanged colocalization in regard to the distance to the soma, challenging the most prevalent view of lysosomal presence primarily in proximal

parts of the neuronal cell body (Cheng et al., 2018; Gowrishankar et al., 2015; Maday et al., 2012; Yap et al., 2018).

In contrast to the most prevailing model of gradual decrease of acidified organelles in distance to the cell body, the findings of Padamsey et al. (2017) and Goo et al. (2017) provide evidence that degradative lysosomes are found even in distal parts of dendrites. In line with this, the labeling of active CatD and subsequent analysis of co-trajectories with lysosomal membrane proteins in dendrites demonstrated a catabolic pool of both LAMP1 and LAMP2. Since axons and dendrites are known to be neuronal compartments with specific characteristics, the distribution of degradative organelles could resemble one dissimilarity with dendrites potentially containing more acidified organelles in connection to different catabolic local processes. Nonetheless, one has to note that also in axons few studies reported the existence of acidified lysosomes (Farfel-Becker et al., 2019; Farías et al., 2017; Roney et al., 2021).

The lysosomal membrane proteins LAMP1 and LAMP2 are the most commonly found proteins in the membrane. Although there is evidence that the two proteins are connected to different functions, they are interchangeably used in various studies to label lysosomes (Grochowska et al., 2022). The dynamic membrane exchange within the endolysosomal and autophagic pathway leads to a heterogeneous distribution of membrane proteins within the lysosomal pool, hence the usage of a single marker for lysosomal labeling can introduce misleading results. This became apparent in other studies conducted by Yap et al. (2018) and Cheng et al. (2018), which investigated endolysosomal organelles in neuronal compartments. Yap et al. (2018) and Cheng et al. (2018) both showed that LAMP1 is not exclusively found on lysosomes but is present on different organelles along the endolysosomal pathway. In the study conducted by Cheng et al. (2018), immunostaining of LAMP1 and lysosomal hydrolases revealed ~52 % of colocalization with CatB and ~48% with CatD in dendrites. In this thesis, co-trafficking of LAMP1 with labeled CatD could be observed in around 60 % of the cases, whereas LAMP2 showed a slightly higher overlap with CatD, presenting moderately different results. One has to note, however, that the study of Cheng et al. (2018) was performed in young cortical and dorsal root ganglion neurons (DIV3-7), therefore possibly reflecting different distributions of organelles and their degradative capability. Also, their published data showed that LAMP1 which is negative for CatD colocalized more with Rab7, a LE marker. Further, in context of the fusion of lysosomes with the plasma membrane, a difference between the two lysosomal membrane proteins became apparent. Interestingly, the data revealed exocytosis of lysosomes only for LAMP2-, in contrast to LAMP1-, containing vesicles, collectively indicating a potential higher localization of LAMP1 to LEs that lack the required machinery for fusion. Another study showed that in axons, LAMP1 and CatB/D displayed

co-trafficking with TGN proteins, leading to the model of pre-degradative organelles receiving lysosomal material by TGN-derived transport carriers (Lie et al., 2021). This highlights the diverse organelles that are potentially containing LAMP1 apart from acidified, mature, lysosomes. One could speculate that LAMP1 thereby rather serves as a transport-facilitating protein for different cellular material, whereas LAMP2 is implicated in degradation pathways. In line with this, it is known that LAMP2, namely its isoform LAMP2A, is the required receptor for the process of CMA that mediates the translocation of cytoplasmic cargo to the lysosomal lumen for subsequent degradation (Kaushik and Cuervo, 2018). The data presented in this study show a higher fraction of acidified lysosomes containing LAMP2, potentially reflecting a distinct CMA-competent pool, whereas LAMP1 is known to not interact with the CMA machinery and therefore is not implicated in this degradation pathway (Uytterhoeven et al., 2015).

Apart from LAMP1 as a frequently used lysosomal marker, multiple studies made use of LysoTracker to label acidified vesicles, hence concluding that these are acidified lysosomes. LysoTracker is a fluorescent probe that accumulates in acidic vesicles, however, despite its popularity, LysoTracker was shown to be a rather unreliable marker due to its known characteristic to photoconvert from red to a green fluorescent probe (Freundt et al., 2007). Taken together, one has to be cautious in interpreting results obtained by different lysosomal markers and it is suggested to use multiple markers, including the labeling of active hydrolases such as CatB or CatD, to ensure a more specific detection of mature, acidified lysosomes (Grochowska et al., 2022).

4.2 LAMP2-containing lysosomes are controlled by NMDAR-activity and interact with the scaffold SAP102

Previous studies demonstrated the regulated trafficking of dendritic LAMP1-containing lysosomes by activation of AMPARs and NMDARs, as well as the activity-dependent fusion of LAMP2-positive lysosomes (Goo et al., 2017; Padamsey et al., 2017). NMDARs that contain the subunit GluN2B display a high-affinity binding with CaMKII, an interaction that is required for LTP, hence synaptic plasticity. Therefore, it was of particular interest to study the link of this specific pool of NMDARs to lysosomal function.

Interestingly, the obtained results from live-cell imaging experiments suggested an interplay between the GluN2B-containing NMDARs and mature, LAMP2-positive lysosomes due to a transient dwelling of LAMP2-positive, as well as acidified, vesicles at the SEP-tagged GluN2B subunit in dendrites of hippocampal neurons. The inhibition of the NMDARs was accompanied by decreased visit time of LAMP2 at GluN2B, suggesting that basal activity of GluN2B-containing NMDARs provides first cues for lysosomes to stall in their proximity. The high activation of NMDARs by bath application of NMDA, in contrast, heavily reduced the mobility of LAMP2-containing lysosomes and resulted in

stopping of LAMP2- and CatB-positive vesicles in the proximity of GluN2B. Collectively, this indicated an interaction between GluN2B-containing NMDARs and LAMP2-positive, acidified lysosomes, where GluN2B could act as a stopping hub for surveilling lysosomes that are primed to detect and react to receptor activity.

Further supporting evidence was provided by the detection of activity-dependent fusion of LAMP2-containing lysosomes in the proximity of GluN2B at the plasma membrane and, indeed, conducted KO of GluN2B by a CRISPR/Cas9 approach, resulted in an impaired fusion of pHuji-LAMP2. During live-cell imaging experiments revealing LAMP2-mKate vesicles visiting SEP-GluN2Bs, a localization of LAMP2 in direct proximity of SEP-GluN2B was observed and, therefore, the analysis was conducted with consideration of overlapping, as well as directly opposing, signal. These observations suggested an indirect interaction between GluN2B and LAMP2 including other potential binding partners, possibly by the unique C-terminal sequence of GluN2B. In line with this, the interaction between LAMP2 and GluN2B could not be verified by biochemical assays. The GluN2B-anchoring MAGUK protein SAP102, however, displayed increased colocalization with LAMP2 in fixed hippocampal neurons upon NMDA stimulation. Additionally, a co-recruitment could be observed for proteins expressing the cytoplasmic C-terminal amino acid sequence of LAMP2 and the SH3-GK domain of SAP102 in conducted assays in HEK293T cells. Further, an interaction between the two proteins could be detected in PD experiments. Although the binding of LAMP2 and SAP102 has been thereby demonstrated, the functional link of this interaction has not been revealed directly. As a future perspective, an CRISPR/Cas9-mediated KO of SAP102 could be utilized for functional read-outs, such as live-cell imaging, to verify the necessity of the binding for the stopping, as well as fusion, of LAMP2-containing lysosomes.

Having in mind that SAP102 anchors the GluN2B subunit, the results from the conducted live-cell imaging experiments raised some questions. The data revealed a difference in the stopping time of LAMP2-mKate at the GluN2B subunit upon inhibition of NMDAR activity, whereas the portion of positive SEP-GluN2B remained unchanged, although it should be decreased as well in the proposed scenario. Conducted immunostainings of surface-labeled GluN2B together with SAP102 revealed a high overlap (~70 %) of SAP102 with GluN2B at the plasma membrane, but interestingly the pool of surface GluN2B colocalized with SAP102 to only ~55 %. Taken together, this could indicate that not all GluN2B-containing NMDARs at the plasma membrane are indeed anchored by SAP102, being unable to present the necessary platform for LAMP2 docking and stalling. This is additionally supported by the colocalization analysis in fixed neurons that demonstrated higher colocalization of LAMP2 together with surface GluN2B (~60 %) compared to SAP102 (~35 %).

The underlying binding mechanism of LAMP2 to SAP102 after activation of NMDARs by NMDA thereby remains elusive. Interestingly, it was demonstrated that the MAGUK protein SAP97 interacts with CaM in a Ca^{2+}-dependent manner, consequently leading to a conformational change of the SH3-GK domain of SAP97 which enables the association with other binding partners at the plasma membrane (Paarmann et al., 2002). Although this mechanism has only been described for SAP97, the interaction between SAP102 and CaM upon the presence of Ca^{2+} has been described (Masuko et al., 1999). Hence, the exposure of a binding interface by changes in the intramolecular interaction within the SH3-GK module upon the binding of Ca^{2+}/CaM is likely. One could therefore speculate that the conformational status of the SH3-GK domain of SAP102 transiently changes in the basal state between open and closed conformation, the strong activation of NMDARs, however, results in Ca^{2+} influx and initiation of the binding of Ca^{2+}/CaM (Figure 27A). Consequently, an interaction interface is revealed, providing a platform for physical interaction with the cytoplasmic amino acid sequence of the lysosomal LAMP2 (Figure 27B).
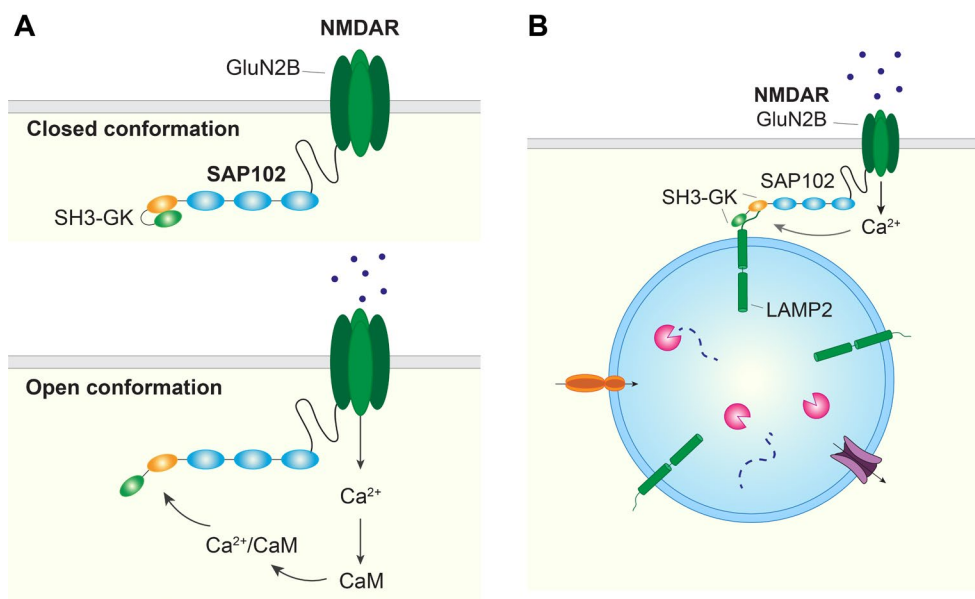
Figure 27: LAMP2-positive lysosomes interact with the SH3-GK module of SAP102 in its open conformation status. (A) The SH3- (orange) GK (green) domain of the GluN2B-anchoring SAP102 is predominantly in closed conformation under basal conditions. Upon Ca^{2+} influx, Ca^{2+} binds to calmodulin (CaM) and Ca^{2+}/CaM can interact with SAP102, resulting in an open conformation of the SH3-GK module. **(B)** The activation of NMDARs containing the subunit GluN2B leads to influx of Ca^{2+}, therefore potentially resulting in a conformational change in the SH3-GK domain of SAP102. This would allow for the binding of SAP102 with the C-terminal sequence of LAMP2, subsequently docking catabolically active lysosomes in close proximity to the plasma membrane.

4.3 Exocytosis of LAMP2-positive lysosomes is mediated by neuronal activity

Intriguing evidence was provided in a study from Padamsey et al. (2017), describing activity-dependent exocytosis of LAMP2-containing lysosomes in neurons and consequent induction of dendritic spine growth. The experiments conducted in this study revealed an activity-dependent fusion of SEP-LAMP2 that was reduced upon NMDAR inhibition, corroborating the previous findings of Padamsey et al. (2017). Strikingly, in line with the report of Padamsey et al. (2017), the fusion, as well as the stopping, upon neuronal activation was observed for LAMP2-, but not LAMP1-, containing vesicles.

The exocytosis of lysosomes was described in different cell types and serves various functions. Secretory lysosomes, for instance, are a specialized form of organelles present in distinct cell types that contain molecules destined for secretion to perform a specific function (Blott and Griffiths, 2002). These organelles are described to play an essential role in the immune system by the release of molecules, such as histamine by basophils or MHC-antigen complexes by macrophages, as well as dendritic cells or B cells, however, their presence has not been shown in neurons (Blott and Griffiths, 2002; Grochowska et al., 2022).

In axons of granule cells, the activity-dependent lysosomal fusion with the plasma membrane leads to the secretion of Cerebellin 1 (Cbln1), a synaptic organizer, which potentially modifies synapses (Ibata et al., 2019). This release was shown to be accompanied by exocytosis of CatB, possibly inducing long-lasting structural changes by digestion of ECM proteins. CatB thereby acts on MMP-9 for the activation, a protease shown to play an important role in dendritic spine growth and LTP (Michaluk et al., 2011; Wang et al., 2008). Also, the study of Padamsey et al. (2017) suggests that the lysosomal disposal of content and therefore release of CatB is the underlying mechanism of long-lasting dendritic spine remodeling. Taken this into account, the observed fusion of LAMP2-positive lysosomes could be accompanied by CatB release, thus driving modifications in spine sizes by MMP-9 activity, hence promoting synaptic plasticity. Interestingly, in the context of LSDs, where lysosomal cargo accumulation due to impaired lysosomal degradation is one major hallmark, it has been proposed that the release of the lysosomal content by exocytosis could serve as an alternative disposal mechanism to remove accumulated cargo meant to be degraded (Marques and Saftig, 2019). In line with this, another study observed a process of secretory autophagy in HEK293T cells that mediates the release of extracellular vesicles and particles (EVPs) during endolysosomal inhibition, also proposed to serve as an alternative pathway for the disposal of material to maintain proteostasis (Solvik et al., 2022).

Bearing this in mind, the observed fusion could reflect an alternative, non-canonical function of lysosomes to keep the proteome in balance and in parallel promote synaptic changes. Hence, it is unlikely, that the observed fusion of LAMP2-positive lysosomes is reflecting the exocytosis of secretory content, hence fusion of secretory lysosomes, due to its underlying function of degradation-targeted substrate disposal.

In the context of the described process of secretory autophagy, the exocytosis of vesicles was shown to be mediated by Rab27a, one Rab protein that was also demonstrated to be involved in various secretory pathways connected to immune responses (Prashar et al., 2017; Solvik et al., 2022). It has been suggested that Rab proteins facilitate the docking of vesicles, thereby allowing the binding between the required SNARE proteins, hence reflecting one interesting candidate for the unknown machinery involved in the fusion of LAMP2-containing lysosomes (Chen and Scheller, 2001). Different studies have demonstrated that the Ca^{2+}-sensor SytVII regulates Ca^{2+}-dependent exocytosis of lysosomes in non-neuronal cells and one study suggested the involvement of the v-SNARE VAMP7 and the t-SNARE SNAP23 underlying this process (Czibener et al., 2006; Martinez et al., 2000; Rao et al., 2004). In neurons, SytVII is implicated in neurotransmitter release, as well as facilitation, and was indeed shown to be localized on active lysosomes in axons (Huson and Regehr, 2020; Vevea et al., 2021). Also, in neurons, SNAP23 facilitates the fusion of vesicles in complex with SytVII (Weber et al., 2014). In line with this, it is tempting to speculate that the complex of SNAP23 and SytVII, potentially including VAMP7, is involved in the exocytosis of LAMP2-containing lysosomes, providing the indispensable fusion machinery.

Another interesting aspect is that the generation of PI(4)P at endosomes was shown to enable fusion with the plasma membrane as part of the recycling pathway, however, PI(4)P can be additionally found on LEs/lysosomes (Hammond et al., 2014; Ketel et al., 2016). One could therefore speculate that the presence of PI(4)P on LAMP2-containing lysosomes enables the fusion, hence disposal of lysosomal content. PI4KIIIα, a type III phosphatidylinositol 4-kinase that generates PI(4)P, was shown to localize in a Ca^{2+}-dependent manner to the plasma membrane of dendrites and is regulated by neuronal activity (Guo et al., 2022). The activation of NMDARs in cultured mouse hippocampal neurons by application of glutamate leads to an increase of PI(4)P at the plasma membrane and was proposed to provide a necessary cue for AMPAR-insertion by exocytosis. Hence, another possibility would be that the exocytosis of LAMP2-positive lysosomes is driven by PI(4)P conversion or that LAMP2-positive, PI(4)P-containing, lysosomes provide the necessary delivery of PI(4)P to the plasma membrane to promote synaptic plasticity. This is supported by findings that in pancreatic β cells the exocytosis of

insulin granules requires PI4K activity (Olsen et al., 2003). PI(4)P could also serve as the required precursor for conversion to PI(4,5)P$_2$ which mediates synaptic vesicle exocytosis in neurons and was shown to accumulate at fusion sites of specialized secretory organelles of endothelial cells (Nguyen et al., 2020; Südhof, 2013).

In addition, further investigations could be performed regarding the synaptic or extrasynaptic localization of lysosomal fusion sites within the dendrites, as well as the role of shaft synapses within this process. The obtained results in this thesis demonstrate that LAMP2 is associated with GluN2B in spine synapses, shaft synapses, as well as extrasynaptically located GluN2B. The abundance of the GluN2B subunit at extrasynaptic sites, as well as shaft synapses, could indicate that the stalling and fusion of LAMP2-positive lysosomes are localized rather to the dendritic shaft or shaft synapses. In line with this, it was hypothesized that shaft synapses are able to control organelle movement, such as lysosomal trafficking, more strongly due to the lack of spatial compartmentalization compared to spine synapses (van Bommel et al., 2019; Sabatini et al., 2002). Further, it has been demonstrated that F-actin patches adjacent to shaft synapses regulate lysosome positioning (van Bommel et al., 2019).

The obtained data in this thesis did not reveal changes in the colocalization of GluN2B with LAMP2 upon 4AP/bic stimulation, considered a synaptic activation protocol, however, the application of NMDA, thereby activating all NMDARs, increased the colocalization between SAP102 and LAMP2. This would support the idea of the involvement of not shaft synapses but extrasynaptically located GluN2B-containing NMDARs in the process of lysosomal fusion. Interestingly, the ECM is a regulator for surface dynamics of NMDARs, in particular of the extrasynaptically localized receptors, that can be remodeled by MMP-9 activity (Michaluk et al., 2011; Petit-Pedrol and Groc, 2021). Hence, the release of lysosomal CatB after exocytosis and the potential activation of MMP-9 by this enzyme could influence the lateral mobility of NMDARs due to ECM digestion, controlling receptor contents and therefore modulating synaptic strength. Since the activation of NMDARs is required for the subsequent fusion of LAMP2-containing lysosomes, one question arising is the source of the necessary activating molecules. In the case of the spine, as well as shaft, synapses, the fusion of vesicles at the connected presynaptic site is the main source of neurotransmitters, however, extrasynaptic NMDARs lack the presynaptic site. Hence glutamate spillover upon high neuronal stimulation, as well as glutamate release by adjacent glia, could be the driving force of fusion events in this scenario.

In contrast to this model, the findings of Goo et al. (2017) show the entering of lysosomes into the dendritic spine in an activity-dependent manner. However, one has to note that this study was conducted with LAMP1 as a lysosomal marker protein, likely reflecting

another pool of endolysosomal organelles. Synaptic NMDARs have been shown to be involved in synapse-to-nucleus signaling, where activation of synaptic NMDARs resulted in nuclear import of phosphorylated extracellular signal-regulated kinase (pERK) that promotes gene expression and in consequence enhanced synaptic strength. On the other hand, extrasynaptic activation of NMDARs leads to inactivation by dephosphorylation of the transcription factor CREB, eventually resulting in cell death (Karpova et al., 2013). Indeed, this was shown to be dependent on the presence of the GluN2B subunit, highlighting distinct pathways connected to this subunit and its localization (Melgarejo da Rosa et al., 2016). This would support a model of lysosomal fusion connected to the activation of synaptic NMDARs, promoting further synaptic plasticity. Collectively, the evidence still suggests that the involvement of extrasynaptic GluN2B-containing NMDARs is more likely. Nevertheless, further investigations have to be conducted to unravel this conundrum.

4.4   LAMP2-containing lysosomes are associated with CMA machinery

The presence of lysosomes in dendrites raises the question of the catabolic pathways connected to these organelles. The observations of this study emphasize the distinct role of LAMP2-containing lysosomes, thereby an interplay with the degradative CMA process seemed likely. CMA is a prominent autophagic pathway that targets a wide range of cytoplasmic proteins. Although it has been well studied, the spatial occurrence of this process within the neuronal cell has not been widely discussed. CMA is implicated in numerous neurodegenerative diseases with target proteins such as Tau or α-synuclein. Most of the studied proteins targeted by CMA are localized to axons and the presynaptic site of the synapse, however, dendritic CMA processes have not been excluded and various CMA target proteins can be found in the dendrites, such as TDP-43 (Andres-Alonso et al., 2021; Chu et al., 2019; Uytterhoeven et al., 2015).

Apart from CMA, other autophagic pathways have been studied in the synaptic context. The process of macroautophagy has been described in the presynaptic site to degrade synaptic vesicles and control the axonal ER (Hernandez et al., 2012; Kuijpers et al., 2021; Lüningschrör et al., 2017). The involvement of macroautophagy in postsynaptic processes, however, is not well described, although it was suggested to be implicated in the degradation of AMPARs and is necessary for spine pruning (Shehata et al., 2012; Tang et al., 2014). Recently, it has been proposed that macroautophagy in dendrites is involved in the degradation of postsynaptic proteins and is essential for LTD (Kallergi et al., 2022).

One report described synaptic microautophagy in the fly model organism *Drosophila melanogaster* as a local quality control pathway for the regulation of neurotransmitter

release (Uytterhoeven et al., 2015). Since LAMP2A is expressed only in mammals and birds, *Drosophila* has been considered to lack CMA processes and utilizes microautophagy as an alternative pathway (Cuervo and Dice, 1996; Uytterhoeven et al., 2015). In this process, Hsc70-4, the ortholog of mammalian Hsc70, deforms membranes and enables turnover of synaptic proteins through endosomal microautophagy, hence rejuvenating the pool of proteins and potentially allowing higher presynaptic efficacy. Interestingly, the expression of human LAMP2A in the fly brain was accompanied by an upregulation of KFERQ motif-dependent degradation pathways, potentially reflecting increased CMA processes (Issa et al., 2018). Collectively, these reports highlight the presence, as well as the importance, of local degradation processes. The data presented in this thesis complementary shows the presence of LAMP2A in dendrites of hippocampal neurons, as well as the interaction between LAMP2 and Hsc70, therefore reflecting CMA machinery. The specificity of the observed stalling and fusion for LAMP2, but not LAMP1, further provided a link between CMA and exocytic lysosomes in dendrites, possibly representing the underlying mechanism of cargo sequestering. In line with this, the *Drosophila* chaperone Hsc70-4 does not show an interaction with LAMP1 in Co-IP experiments, emphasizing the LAMP2-specificity of the indispensable Hsc70 binding to lysosomal proteins during CMA (Uytterhoeven et al., 2015).

The most prevailing approach for the investigation of CMA is the induction of prolonged nutritional deprivation. Responses to growth factors and starvation are mediated by mTOR complexes, especially studied in non-neuronal cells, and, interestingly, the mTORC2 complex has been shown to localize to a sub-group of lysosomes (Jia and Bonifacino, 2019). One study demonstrated that the action of CMA-active lysosomes is inhibited by the binding of mTORC2 at the lysosomal surface and that the inhibition of mTORC2 by Torin1 activates CMA in fibroblasts (Arias et al., 2015). Although mTORC2 is less studied compared to mTORC1, its abundance in neurons is clear and involvement in synaptic plasticity has been revealed (Graber et al., 2013). With this in mind, one could consider, as a future perspective, the usage of mTORC2 inhibitors to upregulate CMA and to monitor the effect on the lysosomal release of CMA substrates and its potential connection to synaptic plasticity. Another study provided evidence for the involvement of phosphatidylinositol 3-kinase (PI3K) in the activation of mTORC2 signaling cascades, a kinase that mediates phosphorylation of $PI(4,5)P_2$ to generate $PI(3,4,5)P_3$. Upon selective inhibition of class III PI3K *in vivo*, CMA was observed to be activated in liver lysosomes of mice, potentially serving as another candidate for the upregulation of CMA (Endicott et al., 2020).

Apart from the nature of local degradation processes in dendrites, the dendritic substrates targeted by this process were of interest. The obtained results from fixed and live-cell imaging experiments conducted in this study revealed that the CMA substrate TDP-43 is abundantly found in lysosomes positive for LAMP2, as well as active CatD. TDP-43 is a prone-to-aggregate protein and there has been various research on the release of TDP-43 as part of an intercellular transmission of TDP-43 aggregates by exosomes in *in vitro* systems, even at synaptic terminals (Feiler et al., 2015; Nonaka et al., 2013). The seeding of aggregated TDP-43 is thereby reported to lead to toxic effects in recipient cells. With this in mind, the observed lysosomal uptake of TDP-43 could serve as a mechanism to prevent high aggregation and consequent exosome-mediated spreading of the protein. It has been shown that CMA degrades only soluble proteins, thus the targeting of TDP-43 by CMA prior to its aggregation could reflect a protective mechanism, resulting in the release of a non-aggregated and non-toxic form of TDP-43 by lysosomal exocytosis (Salvador et al., 2000). Strikingly, the application of NMDA resulted in an increased release of GFP-tagged TDP-43 detected by ELISA, supporting this scenario and providing a link to the described exocytic LAMP2-positive lysosomes studied in this thesis. One has to note, that the published results of seeding TDP-43 have been controversial since other studies could not detect any propagation of TDP-43, possibly due to the usage of different variants and constructs expressing TDP-43 (Jo et al., 2020). Nonetheless, the toxic effect of aggregated TDP-43 has been well established, thereby the disposal of the protein by LAMP2-containing lysosomes would serve as a required protective mechanism to maintain cell viability, accompanied by the promotion of plasticity (Figure 28). Similarly, pathogenic α-Synuclein has been recently shown to be exocytosed by lysosomes, however, LAMP1 was used as the label for lysosomes, and the underlying degradation pathway was suggested to be linked to macroautophagy that targets aggregates ("aggrephagy"; Xie et al., 2021). Therefore, this could reflect another way of cargo disposal mediated by an interplay of LAMP1 and macroautophagy, possibly targeting the aggregated, insoluble substrates that cannot be recognized by the CMA machinery. Nonetheless, more and more studies observe a mechanism of release of harmful proteins to the extracellular milieu as an alternative pathway for classic degradation.
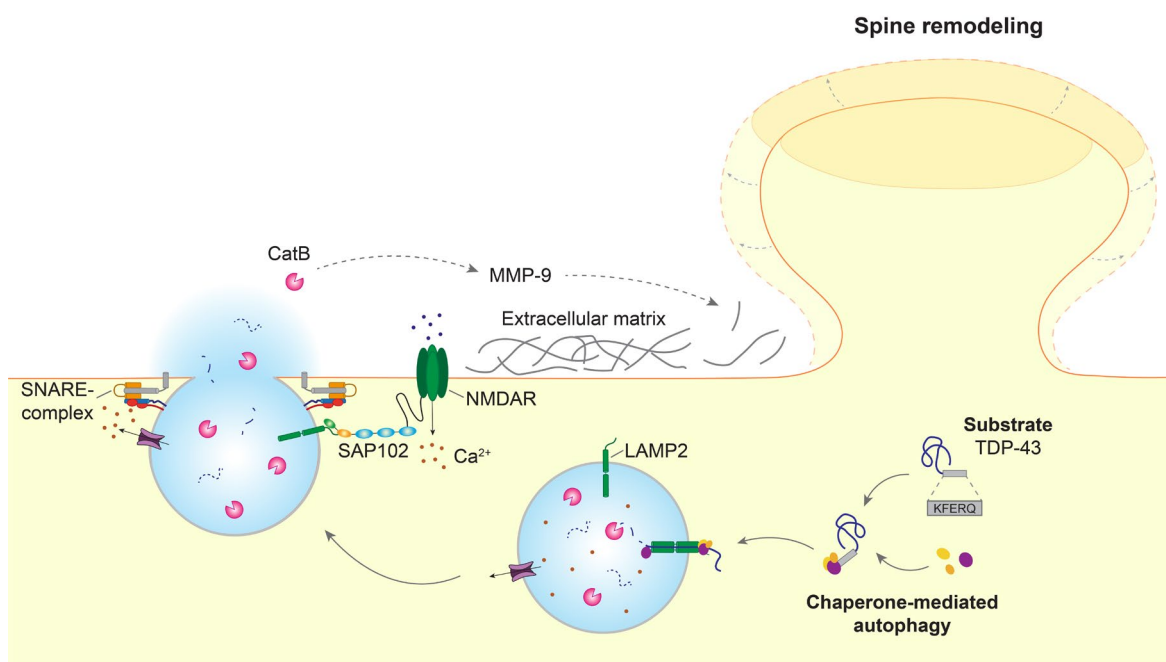
Figure 28: Proposed model of CMA-mediated cargo recruitment for activity-dependent exocytosis of LAMP2-positive lysosomes. Chaperone-mediated autophagy (CMA) targets an intracellular substrate with a KFERQ-like motif, here TDP-43. After recognition by chaperones, the complex binds to LAMP2 at the lysosomal surface, resulting in translocation of the target protein. Upon activation of GluN2B-containing NMDARs, binding of LAMP2 to the SH3-GK module of the scaffolding protein SAP102 is enabled. In the suggested case of extrasynaptically localized NMDARs, the activation likely results from glutamate spillover or astrocytic glutamate release. The efflux of lysosomal Ca^{2+} acts as a trigger for the SNARE-complex to facilitate the fusion of the lysosomal vesicle. The released enzyme CatB can subsequently activate matrix-metalloproteinase 9 (MMP-9), which digests extracellular matrix (ECM) components, hence allowing for dendritic spine remodeling and growth.

The LAMP2 isoform LAMP2A, as one of the three splice variants of LAMP2, was shown to be the key receptor involved in CMA, whereas LAMP2B, as well as LAMP2C, have been studied in other contexts (Cuervo and Dice, 2000; Eskelinen et al., 2005). Reduced levels of CMA have been observed upon exchange of the C-terminal sequence of LAMP2A that is required for the binding to the required chaperone protein Hsc70, nevertheless, the involvement of other LAMP2 isoforms, exhibiting different extraluminal amino acid sequences, in the process of CMA has not been entirely excluded (Cuervo and Dice, 1996, 2000). Interestingly, the heterologous Co-IP data obtained in this thesis verified that the LAMP2B isoform binds the chaperone protein Hsc70. This was additionally supported by PD experiments, in which the application of TAT-LAMP2-404-415, as a dominant-negative peptide, resulted in highly decreased binding between the C-terminus of LAMP2 and full-length Hsc70. Moreover, a high association of endogenous LAMP2A, stained by the usage of an isoform-specific antibody, was observed together with the overexpressed LAMP2B. Taken together, this provided evidence for the co-presence of LAMP2B and LAMP2A in the membrane of the same vesicle. Interestingly, one study revealed that

LAMP2B is required for the translocation of peptides into the lysosomal lumen by the lysosomal peptide transporter associated with antigen processing-like (TAPL; Demirel et al., 2012). LAMP2B thereby serves as stabilizing protein of TAPL. Based on this, one could speculate that LAMP2B exhibits the same function in the membrane of fusion-competent LAMP2-positive lysosomes, stabilizing the multimerized LAMP2A during CMA for subsequent cargo translocation to the lysosomal lumen. In this case, LAMP2B itself would not provide the channel needed for substrate translocation but rather serve as a stabilizing component during the CMA process. To enable the binding of CMA-substrates and their translocation, the multimerization of LAMP2A is required, which has been shown to be facilitated by the presence of a dimerization motif ("GXXXG"; Bandyopadhyay et al., 2008). To further verify the CMA-dependency of LAMP2-containing lysosome fusion, mutation of this amino acid sequence could be carried out to monitor the potential abolishment of substrate translocation and therefore the fusion event accompanied by TDP-43 release. This could be conducted for LAMP2A, as well as for LAMP2B, therefore providing a better insight into which isoform is required to dimerize, hence presenting the translocation channel.

To further strengthen the evidence for the involvement of CMA processes in the sequestering of cargo, the disruption of the LAMP2 interaction with the chaperone Hsc70 would be a useful future approach. The usage of an Hsc70 inhibitor during live-cell imaging experiments could reveal the potentially disrupted stalling and fusion of lysosomes upon NMDA application, therefore verifying that the CMA-competent lysosomes are exocytic and bind to GluN2B-containing NMDARs. One inhibitor, VER-155008, is of particular interest since it has been published to selectively inhibit Hsc70 activity (Wen et al., 2014). Additionally, it would be interesting to study if the release of TDP-43, measured by ELISA, is blocked by the inhibition of Hsc70 or the application of TAT-LAMP2-404-415, utilized as a dominant-negative binding peptide.

Taken together, this study revealed the targeting of intracellular substrates by CMA machinery and a novel process of activity-dependent lysosomal fusion accompanied by the release of lysosomal content, hence potentially driving synaptic plasticity in dendrites (Figure 28). However, a more physiological approach would be recommended for the verification of the obtained results in the future and therefore put it in a broader context. One limitation of the study is the overexpression of proteins for most of the conducted experiments and the high expression of proteins can be accompanied by various alterations within the cell, possibly leading to results that are not transferable to physiological conditions. Although the proteins used in this study are commonly overexpressed, one cannot rule out the possibility of misguiding results. More recently,

different methods utilizing the CRISPR/Cas9 system have been developed for tagging endogenous proteins in cultured neurons, organotypic slice cultures, as well as *in vivo* systems (Uemura et al., 2016; Willems et al., 2020). One prevailing concern regarding the CRISPR/Cas9 approach is the occurrence of off-target effects, however, the methods are constantly improved and optimized, thereby displaying a promising option in the future to circumvent protein overexpression.

Also, *ex vivo* models, such as brain slices, or *in vivo* mouse models could help to verify the results of this study. Interestingly, one report conducted *in vivo* experiments with LAMP2A KO mice that exhibited a removal of LAMP2A in excitatory neurons, demonstrating altered neuronal function (Bourdenx et al., 2021). However, the local alterations within the neurons have not been studied and it would be interesting to conduct further experiments to study the fusion of dendritic lysosomes in such a system. The usage of *ex vivo* or in *vivo* systems would also include a broader view of the underlying neuronal connectivity, as well as the involvement of other cell types within the brain, such as glia. In the conducted study by Bourdenx et al. (2021), a novel chemical activator of CMA by upregulation of LAMP2A expression, named CA77.1, was additionally introduced for the usage *in vitro*, as well as *in vivo*, reflecting another appealing candidate for further experiments, such as the enhanced lysosomal fusion and release of CMA-targeted proteins. The release of proteins, such as TDP-43, could be thereby monitored by increased concentration in the cerebrospinal fluid (CSF) of the used system. Unfortunately, most of the prominent approaches in the field, such as purification of lysosomes, mass-spectrometry (MS), as a method for analysis of the proteome, or the analysis of the secretome, are hard to apply. Considering the heterogeneity of lysosomes and their different distributions in the soma, axon, and dendrites, these methods will not be able to distinguish between the different lysosomal pools in the neuronal compartments, hence not revealing the differences in the focus of this study. Nonetheless, it would give a broader view of changes in protein levels and presence under different conditions, such as inhibition of CMA.

All in all, the present study highlights the heterogeneity of dendritic lysosomes and demonstrates the existence of LAMP2-containing lysosomes that are regulated by NMDAR activity in regards to their mobility and fusion. Interestingly, an interaction of the C-terminus of LAMP2 with the SH3-GK module of the GluN2B-anchoring scaffold protein SAP102 could be revealed. These findings provide evidence that SAP102 serves as a docking site to allow for lysosomal exocytosis upon NMDAR activation, consequently leading to the release of lysosomal content to the extracellular space. The demonstrated presence of CMA machinery in dendrites and its association with LAMP2 suggests the

involvement of CMA processes in the loading of potentially harmful cargo, such as TDP-43, to the lumen of LAMP2-positive lysosome. The fusion of lysosomes with the plasma membrane likely results in the release of the CMA substrates together with active hydrolases, for instance CatB, that in turn could allow for activation of MMP-9, hence cleavage of ECM components and consequently facilitate spine growth (Figure 28). It is likely, that the extrasynaptically located and activated GluN2B-containing NMDARs are thereby the involved receptors anchored by SAP102, thus reflecting the docking site and determining the spot of fusion.

This mechanism provides insight into a novel, specialized, local function of lysosomes, therefore expanding the knowledge about these catabolic organelles. This not only alters the traditional view of them being solely somatic degradation hubs but also sheds new light on their connection to synaptic plasticity. Considering the vast distances lysosomes have to cover to deliver degradation-destined cargo from dendrites to the soma, this mechanism seems to be spatially, as well as temporally more efficient, in particular as a fast response to synaptic activity. Further, it reflects a process that couples the disposal of substrates inevitably to spine remodeling, promoting dendritic spine growth. The digestion of ECM components upon lysosomal exocytosis could in addition result in the increased mobility of NMDARs, hence allowing for the lateral diffusion of receptors to modulate synaptic strength. The disruption of this process would thereby lead to an accumulation of material, as well as the collapse of the catabolic system together with a failed facilitation of local synaptic remodeling, weakening the synaptic strength and eventually resulting in potential cell death signaling pathways. This scenario emphasizes the necessity of dendritic lysosomal fusion for neuronal functionality. Still, further investigations are required to resolve different unknown aspects of this process, such as the underlying fusion machinery or, on the broader scale, the connection to intercellular communication with neighboring cells like glia.

References

Agarraberes FA, Terlecky SR, Dice JF. 1997. An Intralysosomal hsp70 Is Required for a Selective Pathway of Lysosomal Protein Degradation. *Journal of Cell Biology* **137**:825–834.

Akazawa C, Shigemoto R, Bessho Y, Nakanishi S, Mizuno N. 1994. Differential expression of five N-methyl-D-aspartate receptor subunit mRNAs in the cerebellum of developing and adult rats. *J Comp Neurol* **347**:150–160.

Aman Y, Schmauck-Medina T, Hansen M, Morimoto RI, Simon AK, Bjedov I, Palikaras K, Simonsen A, Johansen T, Tavernarakis N, Rubinsztein DC, Partridge L, Kroemer G, Labbadia J, Fang EF. 2021. Autophagy in healthy aging and disease. *Nature Aging 2021 1:8* **1**:634–650.

Anding AL, Baehrecke EH. 2017. Cleaning House: Selective Autophagy of Organelles. *Dev Cell* **41**:10.

Andres-Alonso M, Ammar MR, Butnaru I, Gomes GM, Acuña Sanhueza G, Raman R, Yuanxiang PA, Borgmeyer M, Lopez-Rojas J, Raza SA, Brice N, Hausrat TJ, Macharadze T, Diaz-Gonzalez S, Carlton M, Failla AV, Stork O, Schweizer M, Gundelfinger ED, Kneussel M, Spilker C, Karpova A, Kreutz MR. 2019. SIPA1L2 controls trafficking and local signaling of TrkB-containing amphisomes at presynaptic terminals. *Nature Communications 2019 10:1* **10**:1–17.

Andres-Alonso M, Kreutz MR, Karpova A. 2021. Autophagy and the endolysosomal system in presynaptic function. *Cellular and Molecular Life Sciences 2020 78:6* **78**:2621–2639.

Arias E, Koga H, Diaz A, Mocholi E, Patel B, Cuervo AM. 2015. Lysosomal mTORC2/PHLPP1/Akt Regulate Chaperone-Mediated Autophagy. *Mol Cell* **59**:270–284.

Ariosa AR, Klionsky DJ. 2016. Autophagy core machinery: overcoming spatial barriers in neurons. *J Mol Med* **94**:1217–1227.

Asztely F, Erdemli G, Kullmann DM. 1997. Extrasynaptic Glutamate Spillover in the Hippocampus: Dependence on Temperature and the Role of Active Glutamate Uptake. *Neuron* **18**:281–293.

Auzmendi-Iriarte J, Matheu A. 2021. Impact of Chaperone-Mediated Autophagy in Brain Aging: Neurodegenerative Diseases and Glioblastoma. *Front Aging Neurosci* **12**:509.

Ayala YM, Zago P, D'Ambrogio A, Xu YF, Petrucelli L, Buratti E, Baralle FE. 2008. Structural determinants of the cellular localization and shuttling of TDP-43. *J Cell Sci* **121**:3778–3785.

Ballabio A, Bonifacino JS. 2020. Lysosomes as dynamic regulators of cell and organismal homeostasis. *Nature Reviews Molecular Cell Biology 2019 21:2* **21**:101–118.

Bandyopadhyay U, Kaushik S, Varticovski L, Cuervo AM. 2008. The Chaperone-Mediated Autophagy Receptor Organizes in Dynamic Protein Complexes at the Lysosomal Membrane. *Mol Cell Biol* **28**:5747–5763.

Bard F, Malhotra V. 2006. The Formation of TGN-to-Plasma-Membrane Transport Carriers. *Annu Rev Cell Dev Biol* **22**:439–455.

Barria A, Malinow R. 2005. NMDA Receptor Subunit Composition Controls Synaptic Plasticity by Regulating Binding to CaMKII. *Neuron* **48**:289–301.

Bingol B, Schuman EM. 2006. Synaptic protein degradation by the ubiquitin proteasome system. *Curr Opin Neurobiol* **15**:536–541.

Blanz J, Zunke F, Markmann S, Damme M, Braulke T, Saftig P, Schwake M. 2015. Mannose 6-phosphate-independent Lysosomal Sorting of LIMP-2. *Traffic* **16**:1127–1136.

Blott EJ, Griffiths GM. 2002. Secretory lysosomes. *Nat Rev Mol Cell Biol* **3**:122–131.

Bonnet SAD, Akad DS, Samaddar T, Liu Y, Huang X, Dong Y, Schlüter OM. 2013. Synaptic State-Dependent Functional Interplay between Postsynaptic Density-95 and Synapse-Associated Protein 102. *The Journal of Neuroscience* **33**:13398 LP – 13409.

Boonacker E, Elferink S, Bardai A, Wormmeester J, van Noorden CJF. 2003. Rapid assay to detect possible natural substrates of proteases in living cells. *Biotechniques* **35**:766–774.

Borschel WF, Myers JM, Kasperek EM, Smith TP, Graziane NM, Nowak LM, Popescu GK. 2012. Gating reaction mechanism of neuronal NMDA receptors. *J Neurophysiol* **108**:3105–3115.

Bosch M, Hayashi Y. 2012. Structural plasticity of dendritic spines. *Curr Opin Neurobiol* **22**:383–388.

Bourdenx M, Martín-Segura A, Scrivo A, Rodriguez-Navarro JA, Kaushik S, Tasset I, Diaz A, Storm NJ, Xin Q, Juste YR, Stevenson E, Luengo E, Clement CC, Choi SJ, Krogan NJ, Mosharov E v, Santambrogio L, Grueninger F, Collin L, Swaney DL, Sulzer D, Gavathiotis E, Cuervo AM. 2021. Chaperone-mediated autophagy prevents collapse of the neuronal metastable proteome. *Cell* **184**:2696-2714.e25.

Brix K, Dunkhorst A, Mayer K, Jordans S. 2008. Cysteine cathepsins: Cellular roadmap to different functions. *Biochemie* **90**:194–207.

Brix K, Linke M, Tepel C, Herzog V. 2001. Cysteine Proteinases Mediate Extracellular Prohormone Processing in the Thyroid. *Biol Chem* **382**:717–726.

Brudvig JJ, Weimer JM. 2015. X MARCKS the spot: Myristoylated alanine-rich C kinase substrate in neuronal function and disease. *Front Cell Neurosci* **9**:407.

Buratta S, Tancini B, Sagini K, Delo F, Chiaradia E, Urbanelli L, Emiliani C. 2020. Lysosomal Exocytosis, Exosome Release and Secretory Autophagy: The Autophagic- and Endo-Lysosomal Systems Go Extracellular. *Int J Mol Sci* **21**:2576.

Burd C, Cullen PJ. 2014. Retromer: A Master Conductor of Endosome Sorting. *Cold Spring Harb Perspect Biol* **6**:a016774.

Cajigas IJ, Tushev G, Will TJ, Tom Dieck S, Fuerst N, Schuman EM. 2012. The Local Transcriptome in the Synaptic Neuropil Revealed by Deep Sequencing and High-Resolution Imaging. *Neuron* **74**:453–466.

Carroll RC, Beattie EC, von Zastrow M, Malenka RC. 2001. Role of AMPA receptor endocytosis in synaptic plasticity. *Nature Reviews Neuroscience 2001 2:5* **2**:315–324.

Chater TE, Goda Y. 2014. The role of AMPA receptors in postsynaptic mechanisms of synaptic plasticity. *Front Cell Neurosci* **8**:401.

Chen BS, Gray JA, Sanz-Clemente A, Wei Z, Thomas E v., Nicoll RA, Roche KW. 2012. SAP102 mediates synaptic clearance of NMDA receptors. *Cell Rep* **2**:1120.

Chen C-S, Chen W-NU, Zhou M, Arttamangkul S, Haugland RP. 2000. Probing the cathepsin D using a BODIPY FL–pepstatin A: applications in fluorescence polarization and microscopy. *J Biochem Biophys Methods* **42**:137–151.

Chen YA, Scheller RH. 2001. SNARE-mediated membrane fusion. *Nat Rev Mol Cell Biol* **2**:98–106.

Cheng XT, Xie YX, Zhou B, Huang N, Farfel-Becker T, Sheng ZH. 2018. Characterization of LAMP1-labeled nondegradative lysosomal and endocytic compartments in neurons. *Journal of Cell Biology* **217**:3127–3139.

Cheng XT, Zhou B, Lin MY, Cai Q, Sheng ZH. 2015. Axonal autophagosomes recruit dynein for retrograde transport through fusion with late endosomes. *Journal of Cell Biology* **209**:377–386.

Choy RWY, Park M, Temkin P, Herring BE, Marley A, Nicoll RA, von Zastrow M. 2014. Retromer mediates a discrete route of local membrane delivery to dendrites. *Neuron* **82**:55–62.

Christensen KA, Myers JT, Swanson JA. 2002. pH-dependent regulation of lysosomal calcium in macrophages. *J Cell Sci* **115**:599–607.

Chu JF, Majumder P, Chatterjee B, Huang SL, Shen CKJ. 2019. TDP-43 Regulates Coupled Dendritic mRNA Transport-Translation Processes in Co-operation with FMRP and Staufen1. *Cell Rep* **29**:3118-3133.e6.

Citri A, Malenka RC. 2007. Synaptic Plasticity: Multiple Forms, Functions, and Mechanisms. *Neuropsychopharmacology 2008 33:1* **33**:18–41.

Colledge M, Snyder EM, Crozier RA, Soderling JA, Jin Y, Langeberg LK, Lu H, Bear MF, Scott JD. 2003. Ubiquitination regulates PSD-95 degradation and AMPA receptor surface expression. *Neuron* **40**:595–607.

Collingridge GL, Isaac JTR, Yu TW. 2004. Receptor trafficking and synaptic plasticity. *Nature Reviews Neuroscience 2004 5:12* **5**:952–962.

Conde C, Cáceres A. 2009. Microtubule assembly, organization and dynamics in axons and dendrites. *Nature Reviews Neuroscience 2009 10:5* **10**:319–332.

Cuervo AM, Dice JF. 2000. Unique properties of lamp2a compared to other lamp2 isoforms. *J Cell Sci* **113**:4441–4450.

Cuervo AM, Dice JF. 1996. A Receptor for the Selective Uptake and Degradation of Proteins by Lysosomes. *Science (1979)* **273**:501–503.

Cuervo AM, Dice JF, Knecht E. 1997. A Population of Rat Liver Lysosomes Responsible for the Selective Uptake and Degradation of Cytosolic Proteins. *Journal of Biological Chemistry* **272**:5606–5615.

Cuervo AM, Knecht E, Terlecky SR, Dice JF. 1995. Activation of a selective pathway of lysosomal proteolysis in rat liver by prolonged starvation. *American Journal of Physiology* **269**.

Czibener C, Sherer NM, Becker SM, Pypaert M, Hui E, Chapman ER, Mothes W, Andrews NW. 2006. Ca2+ and synaptotagmin VII-dependent delivery of lysosomal membrane to nascent phagosomes. *Journal of Cell Biology* **174**:997–1007.

Dalla Costa I, Buchanan CN, Zdradzinski MD, Sahoo PK, Smith TP, Thames E, Kar AN, Twiss JL. 2021. The functional organization of axonal mRNA transport and translation. *Nat Rev Neurosci* **22**:77–91.

de Duve C, Pressman BC, Gianetto R, Wattiaux R, Appelmans F. 1955. Tissue fractionation studies. 6. Intracellular distribution patterns of enzymes in rat-liver tissue. *Biochemical Journal* **60**:604–617.

Demirel Ö, Jan I, Wolters D, Blanz J, Saftig P, Tampé R, Abele R. 2012. The lysosomal polypeptide transporter TAPL is stabilized by interaction with LAMP-1 and LAMP-2. *J Cell Sci* **125**:4230–4240.

Dieterich DC, Hodas JJL, Gouzer G, Shadrin IY, Ngo JT, Triller A, Tirrell DA, Schuman EM. 2010. In situ visualization and dynamics of newly synthesized proteins in rat hippocampal neurons. *Nature Neuroscience 2010 13:7* **13**:897–905.

Dittmer F, Ulbrich EJ, Hafner A, Schmahl W, Meister T, Pohlmann R, von Figura K. 1999. Alternative mechanisms for trafficking of lysosomal enzymes in mannose 6-phosphate receptor-deficient mice are cell type-specific. *J Cell Sci* **112**:1591–1597.

Dolphin AC, Lee A. 2020. Presynaptic calcium channels: specialized control of synaptic neurotransmitter release. *Nature Reviews Neuroscience 2020 21:4* **21**:213–229.

Donato A, Kagias K, Zhang Y, Hilliard MA. 2019. Neuronal sub-compartmentalization: a strategy to optimize neuronal function. *Biol Rev Camb Philos Soc* **94**:1023.

Dong XP, Shen D, Wang X, Dawson T, Li X, Zhang Q, Cheng X, Zhang Y, Weisman LS, Delling M, Xu H. 2010. PI(3,5)P2 controls membrane trafficking by direct activation of mucolipin Ca2+ release channels in the endolysosome. *Nature Communications 2010 1:1* **1**:1–11.

Dou Y, Wu HJ, Li HQ, Qin S, Wang YE, Li J, Lou HF, Chen Z, Li XM, Luo QM, Duan S. 2012. Microglial migration mediated by ATP-induced ATP release from lysosomes. *Cell Research 2012 22:6* **22**:1022–1033.

Elias GM, Elias LAB, Apostolides PF, Kriegstein AR, Nicoll RA. 2008. Differential trafficking of AMPA and NMDA receptors by SAP102 and PSD-95 underlies synapse development. *Proc Natl Acad Sci U S A* **105**:20953–20958.

Endicott SJ, Ziemba ZJ, Beckmann LJ, Boynton Jr. DN, Miller RA. 2020. Inhibition of class I PI3K enhances chaperone-mediated autophagy. *Journal of Cell Biology* **219**:e202001031.

Endo Y, Furuta A, Nishino I. 2015. Danon disease: a phenotypic expression of LAMP-2 deficiency. *Acta Neuropathol* **129**:391–398.

Eskelinen EL. 2006. Roles of LAMP-1 and LAMP-2 in lysosome biogenesis and autophagy. *Mol Aspects Med* **27**:495–502.

Eskelinen EL, Cuervo AM, Taylor MRG, Nishino I, Blum JS, Dice JF, Sandoval I v., Lippincott-Schwartz J, August JT, Saftig P. 2005. Unifying Nomenclature for the Isoforms of the Lysosomal Membrane Protein LAMP-2. *Traffic* **6**:1058–1061.

Eskelinen EL, Schmidt CK, Neu S, Willenborg M, Fuertes G, Salvador N, Tanaka Y, Lüllmann-Rauch R, Hartmann D, Heeren J, von Figura K, Knecht E, Saftig P. 2004. Disturbed Cholesterol Traffic but Normal Proteolytic Function in LAMP-1/LAMP-2 Double-deficient Fibroblasts. *Mol Biol Cell* **15**:3132.

Farfel-Becker T, Roney JC, Cheng XT, Li S, Cuddy SR, Sheng ZH. 2019. Neuronal Soma-Derived Degradative Lysosomes Are Continuously Delivered to Distal Axons to Maintain Local Degradation Capacity. *Cell Rep* **28**:51-64.e4.

Farías GG, Guardia CM, de Pace R, Britt DJ, Bonifacino JS. 2017. BORC/kinesin-1 ensemble drives polarized transport of lysosomes into the axon. *Proc Natl Acad Sci U S A* **114**:E2955–E2964.

Feiler MS, Strobel B, Freischmidt A, Helferich AM, Kappel J, Brewer BM, Li D, Thal DR, Walther P, Ludolph AC, Danzer KM, Weishaupt JH. 2015. TDP-43 is intercellularly transmitted across axon terminals. *Journal of Cell Biology* **211**:897–911.

Fellin T, Pascual O, Gobbo S, Pozzan T, Haydon PG, Carmignoto G. 2004. Neuronal Synchrony Mediated by Astrocytic Glutamate through Activation of Extrasynaptic NMDA Receptors. *Neuron* **43**:729–743.

Fernández-Fernández MR, Gragera M, Ochoa-Ibarrola L, Quintana-Gallardo L, Valpuesta JM. 2017. Hsp70 – a master regulator in protein degradation. *FEBS Lett* **591**:2648–2660.

Filipek PA, de Araujo MEG, Vogel GF, de Smet CH, Eberharter D, Rebsamen M, Rudashevskaya EL, Kremser L, Yordanov T, Tschaikner P, Fürnrohr BG, Lechner S, Dunzendorfer-Matt T, Scheffzek K, Bennett KL, Superti-Furga G, Lindner HH, Stasyk T, Huber LA. 2017. LAM TOR/Ragulator is a negative regulator of Arl8band BORC-dependent late endosomal positioning. *Journal of Cell Biology* **216**:4199–4215.

Fontaine SN, Zheng D, Sabbagh JJ, Martin MD, Chaput D, Darling A, Trotter JH, Stothert AR, Nordhues BA, Lussier A, Baker J, Shelton L, Kahn M, Blair LJ, Stevens SM, Jr,

Dickey CA. 2016. DnaJ/Hsc70 chaperone complexes control the extracellular release of neurodegenerative-associated proteins. *EMBO J* **35**:1537.

Frank RA, Grant SG. 2017. Supramolecular organization of NMDA receptors and the postsynaptic density. *Curr Opin Neurobiol* **45**:139.

Frank RAW, Komiyama NH, Ryan TJ, Zhu F, O'Dell TJ, Grant SGN. 2016. NMDA receptors are selectively partitioned into complexes and supercomplexes during synapse maturation. *Nature Communications 2016 7:1* **7**:1–13.

Freundt EC, Czapiga M, Lenardo MJ. 2007. Photoconversion of Lysotracker Red to a green fluorescent molecule. *Cell Research 2007 17:11* **17**:956–958.

Fujiwara Y, Furuta A, Kikuchi H, Aizawa S, Hatanaka Y, Konya C, Uchida K, Yoshimura A, Tamai Y, Wada K, Kabuta T. 2013a. Discovery of a novel type of autophagy targeting RNA. *Autophagy* **9**:403–409.

Fujiwara Y, Kikuchi H, Aizawa S, Furuta A, Hatanaka Y, Konya C, Uchida K, Wada K, Kabuta T. 2013b. Direct uptake and degradation of DNA by lysosomes. *Autophagy* **9**:1167–1171.

Garrity AG, Wang W, Collier CMD, Levey SA, Gao Q, Xu H. 2016. The endoplasmic reticulum, not the pH gradient, drives calcium refilling of lysosomes. *Elife* **5**.

Glasgow NG, Siegler Retchless B, Johnson JW. 2015. Molecular bases of NMDA receptor subtype-dependent properties. *J Physiol* **593**:83–95.

Goaillard JM, Moubarak E, Tapia M, Tell F. 2020. Diversity of Axonal and Dendritic Contributions to Neuronal Output. *Front Cell Neurosci* **13**:570.

Goo MS, Sancho L, Slepak N, Boassa D, Deerinck TJ, Ellisman MH, Bloodgood BL, Patrick GN. 2017. Activity-dependent trafficking of lysosomes in dendrites and dendritic spines. *Journal of Cell Biology* **216**:2499–2513.

Gough NR, Hatem CL, Fambrough DM. 1995. The family of LAMP-2 proteins arises by alternative splicing from a single gene: characterization of the avian LAMP-2 gene and identification of mammalian homologs of LAMP-2b and LAMP-2c. *DNA Cell Biol* **14**:863–867.

Goulet B, Baruch A, Moon NS, Poirier M, Sansregret LL, Erickson A, Bogyo M, Nepveu A. 2004. A cathepsin L isoform that is devoid of a signal peptide localizes to the nucleus in S phase and processes the CDP/Cux transcription factor. *Mol Cell* **14**:207–219.

Govind AP, Jeyifous O, Russell TA, Yi Z, Weigel A v., Ramaprasad A, Newell L, Ramos W, Valbuena FM, Casler JC, Yan JZ, Glick BS, Swanson GT, Lippincott-Schwartz J, Green WN. 2021. Activity-dependent Golgi satellite formation in dendrites reshapes the neuronal surface glycoproteome. *Elife* **10**:68910.

Gowrishankar S, Yuan P, Wu Y, Schrag M, Paradise S, Grutzendler J, de Camilli P, Ferguson SM. 2015. Massive accumulation of luminal protease-deficient axonal lysosomes at Alzheimer's disease amyloid plaques. *Proc Natl Acad Sci U S A* **112**:E3699–E3708.

Graber TE, McCamphill PK, Sossin WS. 2013. A recollection of mTOR signaling in learning and memory. *Learning & Memory* **20**:518–530.

Gray EG. 1959. Electron Microscopy of Synaptic Contacts on Dendrite Spines of the Cerebral Cortex. *Nature 1959 183:4675* **183**:1592–1593.

Grochowska KM, Andres-Alonso M, Karpova A, Kreutz MR. 2022. The needs of a synapse—How local organelles serve synaptic proteostasis. *EMBO J* **41**:e110057.

Guo Z, Jiang CH, Tong C, Yang Y, Wang Z, Lam SM, Wang D, Li R, Shui G, Shi YS, Liu JJ. 2022. Activity-dependent PI4P synthesis by PI4KIIIα regulates long-term synaptic potentiation. *Cell Rep* **38**:110452.

Hällbrink M, Florén A, Elmquist A, Pooga M, Bartfai T, Langel Ü. 2001. Cargo delivery kinetics of cell-penetrating peptides. *Biochimica et Biophysica Acta (BBA) - Biomembranes* **1515**:101–109.

Hamasaki M, Furuta N, Matsuda A, Nezu A, Yamamoto A, Fujita N, Oomori H, Noda T, Haraguchi T, Hiraoka Y, Amano A, Yoshimori T. 2013. Autophagosomes form at ER–mitochondria contact sites. *Nature 2013 495:7441* **495**:389–393.

Hammond GRV, Machner MP, Balla T. 2014. A novel probe for phosphatidylinositol 4-phosphate reveals multiple pools beyond the Golgi. *Journal of Cell Biology* **205**:113–126.

Hanus C, Ehlers MD. 2008. Secretory Outposts for the Local Processing of Membrane Cargo in Neuronal Dendrites. *Traffic* **9**:1437–1445.

Hanus C, Schuman EM. 2013. Proteostasis in complex dendrites. *Nature Reviews Neuroscience 2013 14:9* **14**:638–648.

Hardingham GE, Bading H. 2010. Synaptic versus extrasynaptic NMDA receptor signalling: implications for neurodegenerative disorders. *Nature Reviews Neuroscience 2010 11:10* **11**:682–696.

Hardingham GE, Fukunaga Y, Bading H. 2002. Extrasynaptic NMDARs oppose synaptic NMDARs by triggering CREB shut-off and cell death pathways. *Nature Neuroscience 2002 5:5* **5**:405–414.

Harris AZ, Pettit DL. 2008. Recruiting extrasynaptic NMDA receptors augments synaptic signaling. *J Neurophysiol* **99**:524–533.

Hayashi Y, Shi SH, Esteban JA, Piccini A, Poncer JC, Malinow R. 2000. Driving AMPA receptors into synapses by LTP and CaMKII: requirement for GluR1 and PDZ domain interaction. *Science* **287**:2262–2267.

Heitman J, Movva NR, Hall MN. 1991. Targets for cell cycle arrest by the immunosuppressant rapamycin in yeast. *Science* **253**:905–909.

Henne WM, Buchkovich NJ, Emr SD. 2011. The ESCRT Pathway. *Dev Cell* **21**:77–91.

Herculano-Houzel S. 2009. The human brain in numbers: A linearly scaled-up primate brain. *Front Hum Neurosci* **3**:31.

Hernandez D, Torres CA, Setlik W, Cebrián C, Mosharov EV, Tang G, Cheng H-C, Kholodilov N, Yarygina O, Burke RE, Gershon M, Sulzer D. 2012. Regulation of Presynaptic Neurotransmission by Macroautophagy. *Neuron* **74**:277–284.

Hill SE, Colón-Ramos DA. 2020. The Journey of the Synaptic Autophagosome: A Cell Biological Perspective. *Neuron* **105**:961–973.

Holt CE, Martin KC, Schuman EM. 2019. Local translation in neurons: visualization and function. *Nature Structural & Molecular Biology 2019 26:7* **26**:557–566.

Homma Y, Hiragi S, Fukuda M. 2021. Rab family of small GTPases: an updated view on their regulation and functions. *FEBS J* **288**:36–55.

Honey K, Rudensky AY. 2003. Lysosomal cysteine proteases regulate antigen presentation. *Nature Reviews Immunology 2003 3:6* **3**:472–482.

Hook V, Yoon M, Mosier C, Ito G, Podvin S, Head BP, Rissman R, O'Donoghue AJ, Hook G. 2020. Cathepsin B in Neurodegeneration of Alzheimer's Disease, Traumatic Brain Injury, and Related Brain Disorders. *Biochim Biophys Acta Proteins Proteom* **1868**:140428.

Horton AC, Ehlers MD. 2003. Dual Modes of Endoplasmic Reticulum-to-Golgi Transport in Dendrites Revealed by Live-Cell Imaging. *Journal of Neuroscience* **23**:6188–6199.

Hosaka Y, Araya J, Fujita Y, Kuwano K. 2021. Role of chaperone-mediated autophagy in the pathophysiology including pulmonary disorders. *Inflamm Regen* **41**:1–10.

Huettner JE, Bean BP. 1988. Block of N-methyl-D-aspartate-activated current by the anticonvulsant MK-801: selective binding to open channels. *Proc Natl Acad Sci U S A* **85**:1307.

Hummel JJA, Hoogenraad CC. 2021. Specific kif1a–adaptor interactions control selective cargo recognition. *Journal of Cell Biology* **220**.

Hunziker W, Geuze HJ. 1996. Intracellular trafficking of lysosomal membrane proteins. *BioEssays* **18**:379–389.

Huson V, Regehr WG. 2020. Diverse roles of Synaptotagmin-7 in regulating vesicle fusion. *Curr Opin Neurobiol* **63**:42–52.

Ibata K, Kono M, Narumi S, Motohashi J, Kakegawa W, Kohda K, Yuzaki M. 2019. Activity-Dependent Secretion of Synaptic Organizer Cbln1 from Lysosomes in Granule Cell Axons. *Neuron* **102**:1184-1198.e10.

Issa A-R, Sun J, Petitgas C, Mesquita A, Dulac A, Robin M, Mollereau B, Jenny A, Chérif-Zahar B, Birman S. 2018. The lysosomal membrane protein LAMP2A promotes autophagic flux and prevents SNCA-induced Parkinson disease-like symptoms in the Drosophila brain. *Autophagy* **14**:1898–1910.

Jang M, Bum Um K, Jang J, Jin Kim H, Cho H, Chung S, Park MK. 2015. Coexistence of glutamatergic spine synapses and shaft synapses in substantia nigra dopamine neurons. *Scientific Reports 2015 5:1* **5**:1–16.

Jia R, Bonifacino JS. 2019. Lysosome Positioning Influences mTORC2 and AKT Signaling. *Mol Cell* **75**:26-38.e3.

Jiang X, Litkowski PE, Taylor AA, Lin Y, Snider BJ, Moulder KL. 2010. A Role for the Ubiquitin–Proteasome System in Activity-Dependent Presynaptic Silencing. *The Journal of Neuroscience* **30**:1798.

Jo M, Lee S, Jeon YM, Kim S, Kwon Y, Kim HJ. 2020. The role of TDP-43 propagation in neurodegenerative diseases: integrating insights from clinical and experimental studies. *Experimental & Molecular Medicine 2020 52:10* **52**:1652–1662.

Johnson DE, Ostrowski P, Jaumouillé V, Grinstein S. 2016. The position of lysosomes within the cell determines their luminal pH. *Journal of Cell Biology* **212**:677–692.

Johnson JW, Ascher P. 1987. Glycine potentiates the NMDA response in cultured mouse brain neurons. *Nature* **325**:529–531.

Jordens I, Fernandez-Borja M, Marsman M, Dusseljee S, Janssen L, Calafat J, Janssen H, Wubbolts R, Neefjes J. 2001. The Rab7 effector protein RILP controls lysosomal transport by inducing the recruitment of dynein-dynactin motors. *Current Biology* **11**:1680–1685.

Kallergi E, Daskalaki A-D, Ioannou E, Kolaxi A, Plataki M, Haberkant P, Stein F, Savitski MM, Sidiropoulou K, Dalezios Y, Nikoletopoulou V. 2020. Long-term synaptic depression triggers local biogenesis of autophagic vesicles in dendrites and requires autophagic degradation. *bioRxiv* 2020.03.12.983965.

Kallergi E, Daskalaki AD, Kolaxi A, Camus C, Ioannou E, Mercaldo V, Haberkant P, Stein F, Sidiropoulou K, Dalezios Y, Savitski MM, Bagni C, Choquet D, Hosy E, Nikoletopoulou V. 2022. Dendritic autophagy degrades postsynaptic proteins and is required for long-term synaptic depression in mice. *Nature Communications 2022 13:1* **13**:1–23.

Karpova A, Mikhaylova M, Bera S, Bär J, Reddy PP, Behnisch T, Rankovic V, Spilker C, Bethge P, Sahin J, Kaushik R, Zuschratter W, Kähne T, Naumann M, Gundelfinger ED, Kreutz MR. 2013. Encoding and transducing the synaptic or extrasynaptic origin of NMDA receptor signals to the nucleus. *Cell* **152**:1119–1133.

Katzmann DJ, Babst M, Emr SD. 2001. Ubiquitin-Dependent Sorting into the Multivesicular Body Pathway Requires the Function of a Conserved Endosomal Protein Sorting Complex, ESCRT-I. *Cell* **106**:145–155.

Kaushik S, Cuervo AM. 2018. The coming of age of chaperone-mediated autophagy. *Nature Reviews Molecular Cell Biology 2018 19:6* **19**:365–381.

Kelly PT, McGuinness TL, Greengard P. 1984. Evidence that the major postsynaptic density protein is a component of a Ca2+/calmodulin-dependent protein kinase. *Proceedings of the National Academy of Sciences* **81**:945–949.

Kennedy MB. 2016. Synaptic Signaling in Learning and Memory. *Cold Spring Harb Perspect Biol* **8**:1–16.

Kennedy MJ, Hanus C. 2019. Architecture and Dynamics of the Neuronal Secretory Network. *Annu Rev Cell Dev Biol* **35**:543–566.

Ketel K, Krauss M, Nicot A-S, Puchkov D, Wieffer M, Müller R, Subramanian D, Schultz C, Laporte J, Haucke V. 2016. A phosphoinositide conversion mechanism for exit from endosomes. *Nature* **529**:408–412.

Khobrekar N v., Quintremil S, Dantas TJ, Vallee RB. 2020. The Dynein Adaptor RILP Controls Neuronal Autophagosome Biogenesis, Transport, and Clearance. *Dev Cell* **53**:141-153.e4.

Kiffin R, Christian C, Knecht E, Cuervo AM. 2004. Activation of chaperone-mediated autophagy during oxidative stress. *Mol Biol Cell* **15**:4829–4840.

Kirschke H, Schmidt I, Wiederanders B. 1986. Cathepsin S. The cysteine proteinase from bovine lymphoid tissue is distinct from cathepsin L. *Biochemical Journal* **240**:455.

Kleckner NW, Dingledine R. 1988. Requirement for Glycine in Activation of NMDA-Receptors Expressed in Xenopus Oocytes. *Science (1979)* **241**:835–837.

Kocaturk NM, Gozuacik D. 2018. Crosstalk Between Mammalian Autophagy and the Ubiquitin-Proteasome System. *Front Cell Dev Biol* **6**.

Koga H, Martinez-Vicente M, Arias E, Kaushik S, Sulzer D, Cuervo AM. 2011. Constitutive Upregulation of Chaperone-Mediated Autophagy in Huntington's Disease. *Journal of Neuroscience* **31**:18492–18505.

Kole MHP, Ilschner SU, Kampa BM, Williams SR, Ruben PC, Stuart GJ. 2008. Action potential generation requires a high sodium channel density in the axon initial segment. *Nature Neuroscience 2008 11:2* **11**:178–186.

Korolchuk VI, Menzies FM, Rubinsztein DC. 2010. Mechanisms of cross-talk between the ubiquitin-proteasome and autophagy-lysosome systems. *FEBS Lett* **584**:1393–1398.

Krijnse-Locker J, Parton RG, Fuller SD, Griffiths G, Dotti CG. 1995. The organization of the endoplasmic reticulum and the intermediate compartment in cultured rat hippocampal neurons. *Mol Biol Cell* **6**:1315–1332.

Kuijpers M, Kochlamazashvili G, Stumpf A, Puchkov D, Swaminathan A, Lucht MT, Krause E, Maritzen T, Schmitz D, Haucke V. 2021. Neuronal Autophagy Regulates Presynaptic Neurotransmission by Controlling the Axonal Endoplasmic Reticulum. *Neuron* **109**:299-313.e9.

Kulkarni VV, Anand A, Herr JB, Miranda C, Vogel MC, Maday S. 2021. Synaptic activity controls autophagic vacuole motility and function in dendrites. *Journal of Cell Biology* **220**.

Lawrence RE, Zoncu R. 2019. The lysosome as a cellular centre for signalling, metabolism and quality control. *Nature Cell Biology 2019 21:2* **21**:133–142.

Lee B, Butcher GQ, Hoyt KR, Impey S, Obrietan K. 2005. Activity-Dependent Neuroprotection and cAMP Response Element-Binding Protein (CREB): Kinase

Coupling, Stimulus Intensity, and Temporal Regulation of CREB Phosphorylation at Serine 133. *Journal of Neuroscience* **25**:1137–1148.

Lee H-K, Takamiya K, Han J-S, Man H, Kim C-H, Rumbaugh G, Yu S, Ding L, He C, Petralia RS, Wenthold RJ, Gallagher M, Huganir RL. 2003. Phosphorylation of the AMPA Receptor GluR1 Subunit Is Required for Synaptic Plasticity and Retention of Spatial Memory. *Cell* **112**:631–643.

Leonard AS, Lim IA, Hemsworth DE, Horne MC, Hell JW. 1999. Calcium/calmodulin-dependent protein kinase II is associated with the N-methyl-d-aspartate receptor. *Proceedings of the National Academy of Sciences* **96**:3239–3244.

Lerma J, Zukin RS, Bennett MVL. 1990. Glycine decreases desensitization of N-methyl-D-aspartate (NMDA) receptors expressed in Xenopus oocytes and is required for NMDA responses. *Proc Natl Acad Sci U S A* **87**:2354–2358.

Li S, Raychaudhuri S, Lee SA, Brockmann MM, Wang J, Kusick G, Prater C, Syed S, Falahati H, Ramos R, Bartol TM, Hosy E, Watanabe S. 2021. Asynchronous release sites align with NMDA receptors in mouse hippocampal synapses. *Nature Communications 2021 12:1* **12**:1–13.

Li X, DiFiglia M. 2012. The recycling endosome and its role in neurological disorders. *Prog Neurobiol* **97**:127–141.

Lie PPY, Yang DS, Stavrides P, Goulbourne CN, Zheng P, Mohan PS, Cataldo AM, Nixon RA. 2021. Post-Golgi carriers, not lysosomes, confer lysosomal properties to pre-degradative organelles in normal and dystrophic axons. *Cell Rep* **35**.

Lilienbaum A. 2013. Relationship between the proteasomal system and autophagy. *Int J Biochem Mol Biol* **4**:1.

Ling SC, Polymenidou M, Cleveland DW. 2013. Converging mechanisms in als and FTD: Disrupted RNA and protein homeostasis. *Neuron* **79**:416–438.

Lloyd-Evans E, Waller-Evans H. 2020. Lysosomal Ca2+ Homeostasis and Signaling in Health and Disease. *Cold Spring Harb Perspect Biol* **12**:a035311.

Lü W, Du J, Goehring A, Gouaux E. 2017. Cryo-EM structures of the triheteromeric NMDA receptor and its allosteric modulation. *Science (1979)* **355**.

Lüningschrör P, Binotti B, Dombert B, Heimann P, Perez-Lara A, Slotta C, Thau-Habermann N, R. von Collenberg C, Karl F, Damme M, Horowitz A, Maystadt I, Füchtbauer A, Füchtbauer E-M, Jablonka S, Blum R, Üçeyler N, Petri S, Kaltschmidt B, Jahn R, Kaltschmidt C, Sendtner M. 2017. Plekhg5-regulated autophagy of synaptic vesicles reveals a pathogenic mechanism in motoneuron disease. *Nat Commun* **8**:678.

Luzio JP, Pryor PR, Bright NA. 2007. Lysosomes: fusion and function. *Nature Reviews Molecular Cell Biology 2007 8:8* **8**:622–632.

Maday S, Holzbaur ELF. 2016. Compartment-Specific Regulation of Autophagy in Primary Neurons. *Journal of Neuroscience* **36**:5933–5945.

Maday S, Holzbaur ELF. 2014. Autophagosome biogenesis in primary neurons follows an ordered and spatially regulated pathway. *Dev Cell* **30**:71–85.

Maday S, Wallace KE, Holzbaur ELF. 2012. Autophagosomes initiate distally and mature during transport toward the cell soma in primary neurons. *Journal of Cell Biology* **196**:407–417.

Mak SK, McCormack AL, Manning-Bog AB, Cuervo AM, di Monte DA. 2010. Lysosomal degradation of α-synuclein in vivo. *Journal of Biological Chemistry* **285**:13621–13629.

Mangeol P, Prevo B, Peterman EJG. 2016. KymographClear and KymographDirect: Two tools for the automated quantitative analysis of molecular and cellular dynamics using kymographs. *Mol Biol Cell* **27**:1948–1957.

Marques ARA, Saftig P. 2019. Lysosomal storage disorders – challenges, concepts and avenues for therapy: Beyond rare diseases. *J Cell Sci* **132**.

Martina JA, Chen Y, Gucek M, Puertollano R. 2012. MTORC1 functions as a transcriptional regulator of autophagy by preventing nuclear transport of TFEB. *Autophagy* **8**:903–914.

Martinez I, Chakrabarti S, Hellevik T, Morehead J, Fowler K, Andrews NW. 2000. Synaptotagmin VII Regulates Ca2+-Dependent Exocytosis of Lysosomes in Fibroblasts. *J Cell Biol* **148**:1141.

Masuko N, Makino K, Kuwahara H, Fukunaga K, Sudo T, Araki N, Yamamoto H, Yamada Y, Miyamoto E, Saya H. 1999. Interaction of NE-dlg/SAP102, a neuronal and endocrine tissue-specific membrane-associated guanylate kinase protein, with calmodulin and PSD- 95/SAP90: A possible regulatory role in molecular clustering at synaptic sites. *Journal of Biological Chemistry* **274**:5782–5790.

Mayer ML, Westbrook GL, Guthrie PB. 1984. Voltage-dependent block by Mg2+ of NMDA responses in spinal cord neurones. *Nature 1984 309:5965* **309**:261–263.

McQuate A, Barria A. 2020. Rapid exchange of synaptic and extrasynaptic NMDA receptors in hippocampal CA1 neurons. *J Neurophysiol* **123**:1004–1014.

Mebratu YA, Negasi ZH, Dutta S, Rojas-Quintero J, Tesfaigzi Y. 2020. Adaptation of Proteasomes and Lysosomes to Cellular Environments. *Cells 2020, Vol 9, Page 2221* **9**:2221.

Medina DL, Fraldi A, Bouche V, Annunziata F, Mansueto G, Spampanato C, Puri C, Pignata A, Martina JA, Sardiello M, Palmieri M, Polishchuk R, Puertollano R, Ballabio A. 2011. Transcriptional activation of lysosomal exocytosis promotes cellular clearance. *Dev Cell* **21**:421–430.

Meimaridou E, Gooljar SB, Chapple JP. 2009. From hatching to dispatching: the multiple cellular roles of the Hsp70 molecular chaperone machinery. *J Mol Endocrinol* **42**:1–9.

Melgarejo da Rosa M, Yuanxiang PA, Brambilla R, Kreutz MR, Karpova A. 2016. Synaptic GluN2B/CaMKII-α signaling induces synapto-nuclear transport of ERK and jacob. *Front Mol Neurosci* **9**:66.

Michaluk P, Wawrzyniak M, Alot P, Szczot M, Wyrembek P, Mercik K, Medvedev N, Wilczek E, de Roo M, Zuschratter W, Muller D, Wilczynski GM, Mozrzymas JW, Stewart MG, Kaczmarek L, Wlodarczyk J. 2011. Influence of matrix metalloproteinase MMP-9 on dendritic spine morphology. *J Cell Sci* **124**:3369–3380.

Miesenböck G, de Angelis DA, Rothman JE. 1998. Visualizing secretion and synaptic transmission with pH-sensitive green fluorescent proteins. *Nature 1998 394:6689* **394**:192–195.

Mikhaylova M, Bär J, van Bommel B, Schätzle P, YuanXiang PA, Raman R, Hradsky J, Konietzny A, Loktionov EY, Reddy PP, Lopez-Rojas J, Spilker C, Kobler O, Raza SA, Stork O, Hoogenraad CC, Kreutz MR. 2018. Caldendrin Directly Couples Postsynaptic Calcium Signals to Actin Remodeling in Dendritic Spines. *Neuron* **97**:1110-1125.e14.

Mikhaylova M, Bera S, Kobler O, Frischknecht R, Kreutz MR. 2016. A Dendritic Golgi Satellite between ERGIC and Retromer. *Cell Rep* **14**:189–199.

Mindell JA. 2012. Lysosomal Acidification Mechanisms. *Annu Rev Physiol* **74**:69–86.

Mizushima N, Yamamoto A, Matsui M, Yoshimori T, Ohsumi Y. 2004. In Vivo Analysis of Autophagy in Response to Nutrient Starvation Using Transgenic Mice Expressing a Fluorescent Autophagosome Marker. *Mol Biol Cell* **15**:1101–1111.

Monyer H, Burnashev N, Laurie DJ, Sakmann B, Seeburg PH. 1994. Developmental and regional expression in the rat brain and functional properties of four NMDA receptors. *Neuron* **12**:529–540.

Murata Y, Constantine-Paton M. 2013. Postsynaptic density scaffold SAP102 regulates cortical synapse development through EphB and PAK signaling pathway. *The Journal of neuroscience* **33**:5040–5052.

Napolitano G, Esposito A, Choi H, Matarese M, Benedetti V, di Malta C, Monfregola J, Medina DL, Lippincott-Schwartz J, Ballabio A. 2018. mTOR-dependent phosphorylation controls TFEB nuclear export. *Nature Communications 2018 9:1* **9**:1–10.

Neiss WF. 1984. A coat of glycoconjugates on the inner surface of the lysosomal membrane in the rat kidney. *Histochemistry 1984 80:6* **80**:603–608.

Nguyen TTN, Koerdt SN, Gerke V. 2020. Plasma membrane phosphatidylinositol (4,5)-bisphosphate promotes Weibel–Palade body exocytosis. *Life Sci Alliance* **3**.

Nonaka T, Masuda-Suzukake M, Arai T, Hasegawa Y, Akatsu H, Obi T, Yoshida M, Murayama S, Mann DMA, Akiyama H, Hasegawa M. 2013. Prion-like Properties of Pathological TDP-43 Aggregates from Diseased Brains. *Cell Rep* **4**:124–134.

Nowak L, Bregestovski P, Ascher P, Herbet A, Prochiantz A. 1984. Magnesium gates glutamate-activated channels in mouse central neurones. *Nature* **307**:462–465.

Olsen HL, Høy M, Zhang W, Bertorello AM, Bokvist K, Capito K, Efanov AM, Meister B, Thams P, Yang SN, Rorsman P, Berggren PO, Gromada J. 2003. Phosphatidylinositol 4-kinase serves as a metabolic sensor and regulates priming of secretory granules in pancreatic β cells. *Proc Natl Acad Sci U S A* **100**:5187–5192.

Ormeño F, Hormazabal J, Moreno J, Riquelme F, Rios J, Criollo A, Albornoz A, Alfaro IE, Budini M. 2020. Chaperone Mediated Autophagy Degrades TDP-43 Protein and Is Affected by TDP-43 Aggregation. *Front Mol Neurosci* **13**:19.

Paarmann I, Spangenberg O, Lavie A, Konrad M. 2002. Formation of Complexes between Ca2+·Calmodulin and the Synapse-associated Protein SAP97 Requires the SH3 Domain-Guanylate Kinase Domain-connecting HOOK Region. *Journal of Biological Chemistry* **277**:40832–40838.

Padamsey Z, McGuinness L, Bardo SJ, Reinhart M, Tong R, Hedegaard A, Hart ML, Emptage NJ. 2017. Activity-Dependent Exocytosis of Lysosomes Regulates the Structural Plasticity of Dendritic Spines. *Neuron* **93**:132.

Palmieri M, Impey S, Kang H, di Ronza A, Pelz C, Sardiello M, Ballabio A. 2011. Characterization of the CLEAR network reveals an integrated control of cellular clearance pathways. *Hum Mol Genet* **20**:3852–3866.

Paoletti P, Bellone C, Zhou Q. 2013. NMDA receptor subunit diversity: impact on receptor properties, synaptic plasticity and disease. *Nature Reviews Neuroscience 2013 14:6* **14**:383–400.

Parenti G, Medina DL, Ballabio A. 2021. The rapidly evolving view of lysosomal storage diseases. *EMBO Mol Med* **13**:e12836.

Patel S, Homaei A, El-Seedi HR, Akhtar N. 2018. Cathepsins: Proteases that are vital for survival but can also be fatal. *Biomedicine & Pharmacotherapy* **105**:526.

Pérez L, McLetchie S, Gardiner GJ, Deffit SN, Zhou D, Blum JS. 2016. LAMP-2C Inhibits MHC Class II Presentation of Cytoplasmic Antigens by Disrupting Chaperone-Mediated Autophagy. *The Journal of Immunology* **196**:2457–2465.

Petit-Pedrol M, Groc L. 2021. Regulation of membrane NMDA receptors by dynamics and protein interactions. *Journal of Cell Biology* **220**.

Petralia RS. 2012. Distribution of extrasynaptic NMDA receptors on neurons. *The Scientific World Journal* **2012**.

Pierce JP, Mayer T, McCarthy JB. 2001. Evidence for a satellite secretory pathway in neuronal dendritic spines. *Current Biology* **11**:351–355.

Platt FM, d'Azzo A, Davidson BL, Neufeld EF, Tifft CJ. 2018. Lysosomal storage diseases. *Nature Reviews Disease Primers 2018 4:1* **4**:1–25.

Platt RJ, Chen S, Zhou Y, Yim MJ, Swiech L, Kempton HR, Dahlman JE, Parnas O, Eisenhaure TM, Jovanovic M, Graham DB, Jhunjhunwala S, Heidenreich M, Xavier RJ, Langer R, Anderson DG, Hacohen N, Regev A, Feng G, Sharp PA, Zhang F. 2014. CRISPR-Cas9 Knockin Mice for Genome Editing and Cancer Modeling. *Cell* **159**:440–455.

Prashar A, Schnettger L, Bernard EM, Gutierrez MG. 2017. Rab GTPases in immunity and inflammation. *Front Cell Infect Microbiol* **7**:435.

Pu J, Guardia CM, Keren-Kaplan T, Bonifacino JS. 2016. Mechanisms and functions of lysosome positioning. *J Cell Sci* **129**:4329–4339.

Pu J, Keren-Kaplan T, Bonifacino JS. 2017. A Ragulator-BORC interaction controls lysosome positioning in response to amino acid availability. *Journal of Cell Biology* **216**:4183–4197.

Pu J, Schindler C, Jia R, Jarnik M, Backlund P, Bonifacino JS. 2015. BORC, a Multisubunit Complex that Regulates Lysosome Positioning. *Dev Cell* **33**:176–188.

Raiborg C, Wenzel EM, Pedersen NM, Olsvik H, Schink KO, Schultz SW, Vietri M, Nisi V, Bucci C, Brech A, Johansen T, Stenmark H. 2015. Repeated ER–endosome contacts promote endosome translocation and neurite outgrowth. *Nature 2015 520:7546* **520**:234–238.

Rangaraju V, tom Dieck S, Schuman EM. 2017. Local translation in neuronal compartments: how local is local? *EMBO Rep* **18**:693–711.

Rao SK, Huynh C, Proux-Gillardeaux V, Galli T, Andrews NW. 2004. Identification of SNAREs Involved in Synaptotagmin VII-regulated Lysosomal Exocytosis *. *Journal of Biological Chemistry* **279**:20471–20479.

Ratti A, Buratti E. 2016. Physiological functions and pathobiology of TDP-43 and FUS/TLS proteins. *J Neurochem* **138**:95–111.

Reczek D, Schwake M, Schröder J, Hughes H, Blanz J, Jin X, Brondyk W, van Patten S, Edmunds T, Saftig P. 2007. LIMP-2 Is a Receptor for Lysosomal Mannose-6-Phosphate-Independent Targeting of β-Glucocerebrosidase. *Cell* **131**:770–783.

Reddy A, Caler E v., Andrews NW. 2001. Plasma membrane repair is mediated by Ca(2+)-regulated exocytosis of lysosomes. *Cell* **106**:157–169.

Reilly JE, Hanson HH, Phillips GR. 2011. Persistence of excitatory shaft synapses adjacent to newly emerged dendritic protrusions. *Mol Cell Neurosci* **48**:129.

Reiser J, Adair B, Reinheckel T. 2010. Specialized roles for cysteine cathepsins in health and disease. *J Clin Invest* **120**:3421–3431.

Repnik U, Česen MH, Turk B. 2013. The Endolysosomal System in Cell Death and Survival. *Cold Spring Harb Perspect Biol* **5**:a008755.

Roney JC, Cheng XT, Sheng ZH. 2022. Neuronal endolysosomal transport and lysosomal functionality in maintaining axonostasis. *Journal of Cell Biology* **221**.

Roney JC, Li S, Farfel-Becker T, Huang N, Sun T, Xie Y, Cheng X-T, Lin M-Y, Platt FM, Sheng Z-H. 2021. Lipid-mediated motor-adaptor sequestration impairs axonal lysosome delivery leading to autophagic stress and dystrophy in Niemann-Pick type C. *Dev Cell* **56**:1452-1468.e8.

Rosa-Ferreira C, Munro S. 2011. Arl8 and SKIP Act Together to Link Lysosomes to Kinesin-1. *Dev Cell* **21**:1171–1178.

Rusakov DA, Kullmann DM. 1998. Extrasynaptic Glutamate Diffusion in the Hippocampus: Ultrastructural Constraints, Uptake, and Receptor Activation. *Journal of Neuroscience* **18**:3158–3170.

Ryu SW, Stewart R, Chase Pectol D, Ender NA, Wimalarathne O, Lee JH, Zanini CP, Harvey A, Huibregtse JM, Mueller P, Paull TT. 2020. Proteome-wide identification of HSP70/HSC70 chaperone clients in human cells. *PLoS Biol* **18**:e3000606.

Sabatini BL, Oertner TG, Svoboda K. 2002. The Life Cycle of Ca2+ Ions in Dendritic Spines. *Neuron* **33**:439–452.

Saftig P, Hunziker E, Everts V, Jones S, Boyde A, Wehmeyer O, Suter A, Figura K von. 2002. Functions of Cathepsin K in Bone Resorption 293–303.

Saftig P, Klumperman J. 2009. Lysosome biogenesis and lysosomal membrane proteins: Trafficking meets function. *Nat Rev Mol Cell Biol* **10**:623–635.

Sahu R, Kaushik S, Clement CC, Cannizzo ES, Scharf B, Follenzi A, Potolicchio I, Nieves E, Cuervo AM, Santambrogio L. 2011. Microautophagy of Cytosolic Proteins by Late Endosomes. *Dev Cell* **20**:131–139.

Salvador N, Aguado C, Horst M, Knecht E. 2000. Import of a Cytosolic Protein into Lysosomes by Chaperone-mediated Autophagy Depends on Its Folding State *. *Journal of Biological Chemistry* **275**:27447–27456.

Samie MA, Xu H. 2014. Lysosomal exocytosis and lipid storage disorders. *J Lipid Res* **55**:995–1009.

Sancak Y, Bar-Peled L, Zoncu R, Markhard AL, Nada S, Sabatini DM. 2010. Ragulator-Rag Complex Targets mTORC1 to the Lysosomal Surface and Is Necessary for Its Activation by Amino Acids. *Cell* **141**:290–303.

Sans N, Petralia RS, Wang YX, Blahos J, Hell JW, Wenthold RJ. 2000. A Developmental Change in NMDA Receptor-Associated Proteins at Hippocampal Synapses. *Journal of Neuroscience* **20**:1260–1271.

Sapolsky AI, Howell DS, Woessner JF. 1974. Neutral Proteases and Cathepsin D in Human Articular Cartilage. *J Clin Invest* **53**:1044–1053.

Sardiello M, Palmieri M, Ronza A di, Medina DL, Valenza M, Gennarino VA, di Malta C, Donaudy F, Embrione V, Polishchuk RS, Banfi S, Parenti G, Cattaneo E, Ballabio A. 2009. A gene network regulating lysosomal biogenesis and function. *Science (1979)* **325**:473–477.

Schell MJ, Molliver ME, Snyder SH. 1995. D-serine, an endogenous synaptic modulator: localization to astrocytes and glutamate-stimulated release. *Proc Natl Acad Sci U S A* **92**:3948–3952.

Schindelin J, Arganda-Carreras I, Frise E, Kaynig V, Longair M, Pietzsch T, Preibisch S, Rueden C, Saalfeld S, Schmid B, Tinevez JY, White DJ, Hartenstein V, Eliceiri K, Tomancak P, Cardona A. 2012. Fiji: An open-source platform for biological-image analysis. *Nat Methods* **9**:676–682.

Schrader M, Pellegrini L. 2017. The making of a mammalian peroxisome, version 2.0: mitochondria get into the mix. *Cell Death Differ* **24**:1148–1152.

Schwarz DS, Blower MD. 2016. The endoplasmic reticulum: structure, function and response to cellular signaling. *Cellular and Molecular Life Sciences* **73**:79.

Schwenk F, Baron U, Rajewsky K. 1995. A cre-transgenic mouse strain for the ubiquitous deletion of loxP-flanked gene segments including deletion in germ cells. *Nucleic Acids Res* **23**:5080–5081.

Seki T, Katsuki H. 2022. Mammalian microautophagy: mechanism and roles in disease. *Autophagy in Health and Disease* 385–397.

Settembre C, Zoncu R, Medina DL, Vetrini F, Erdin Serkan, Erdin SerpilUckac, Huynh T, Ferron M, Karsenty G, Vellard MC, Facchinetti V, Sabatini DM, Ballabio A. 2012. A lysosome-to-nucleus signalling mechanism senses and regulates the lysosome via mTOR and TFEB. *EMBO J* **31**:1095–1108.

Shehata M, Matsumura H, Okubo-Suzuki R, Ohkawa N, Inokuchi K. 2012. Neuronal Stimulation Induces Autophagy in Hippocampal Neurons That Is Involved in AMPA Receptor Degradation after Chemical Long-Term Depression. *Journal of Neuroscience* **32**:10413–10422.

Shen W, Ganetzky B. 2009. Autophagy promotes synapse development in Drosophila. *Journal of Cell Biology* **187**:71–79.

Shen Y, Rosendale M, Campbell RE, Perrais D. 2014. pHuji, a pH-sensitive red fluorescent protein for imaging of exo- and endocytosis. *Journal of Cell Biology* **207**:419–432.

Sheng M, Cummings J, Roldan LA, Jan YN, Jan LY. 1994. Changing subunit composition of heteromeric NMDA receptors during development of rat cortex. *Nature 1994 368:6467* **368**:144–147.

Solvik TA, Nguyen TA, Tony Lin Y-H, Marsh T, Huang EJ, Wiita AP, Debnath J, Leidal AM. 2022. Secretory autophagy maintains proteostasis upon lysosome inhibition. *Journal of Cell Biology* **221**.

Spruston N. 2008. Pyramidal neurons: dendritic structure and synaptic integration. *Nature Reviews Neuroscience 2008 9:3* **9**:206–221.

Südhof TC. 2013. Neurotransmitter Release: The Last Millisecond in the Life of a Synaptic Vesicle. *Neuron* **80**:675–690.

Sumi T, Harada K. 2020. Mechanism underlying hippocampal long-term potentiation and depression based on competition between endocytosis and exocytosis of AMPA receptors. *Scientific Reports 2020 10:1* **10**:1–14.

Sun J, Liu Y, Hao X, Lin W, Su W, Chiang E, Baudry M, Bi X. 2022. LAMTOR1 inhibition of TRPML1-dependent lysosomal calcium release regulates dendritic lysosome trafficking and hippocampal neuronal function. *EMBO J* e108119.

Tai HC, Schuman EM. 2008. Ubiquitin, the proteasome and protein degradation in neuronal function and dysfunction. *Nature Reviews Neuroscience 2008 9:11* **9**:826–838.

Takei N, Inamura N, Kawamura M, Namba H, Hara K, Yonezawa K, Nawa H. 2004. Brain-Derived Neurotrophic Factor Induces Mammalian Target of Rapamycin-Dependent Local Activation of Translation Machinery and Protein Synthesis in Neuronal Dendrites. *Journal of Neuroscience* **24**:9760–9769.

Tanaka Y, Guhde G, Suter A, Eskelinen EL, Hartmann D, Lüllmann-Rauch R, Janssen PML, Blanz J, von Figura K, Saftig P. 2000. Accumulation of autophagic vacuoles and cardiomyopathy in LAMP-2-deficient mice. *Nature 2000 406:6798* **406**:902–906.

Tang G, Gudsnuk K, Kuo S-H, Cotrina ML, Rosoklija G, Sosunov A, Sonders MS, Kanter E, Castagna C, Yamamoto A, Yue Z, Arancio O, Peterson BS, Champagne F, Dwork AJ, Goldman J, Sulzer D. 2014. Loss of mTOR-Dependent Macroautophagy Causes Autistic-like Synaptic Pruning Deficits. *Neuron* **83**:1131–1143.

Tom Dieck S, Sanmartí-Vila L, Langnaese K, Richter K, Kindler S, Soyke A, Wex H, Smalla KH, Kämpf U, Fränzer JT, Stumm M, Garner CC, Gundelfinger ED. 1998. Bassoon, a Novel Zinc-finger CAG/Glutamine-repeat Protein Selectively Localized at the Active Zone of Presynaptic Nerve Terminals. *Journal of Cell Biology* **142**:499–509.

Tran A, Silver J. 2021. Cathepsins in neuronal plasticity. *Neural Regen Res* **16**:26–35.

Turk V, Stoka V, Vasiljeva O, Renko M, Sun T, Turk B, Turk D. 2012. Cysteine cathepsins: From structure, function and regulation to new frontiers. *Biochimica et Biophysica Acta (BBA) - Proteins and Proteomics* **1824**:68–88.

Turk V, Turk B, Gunčar G, Turk D, Kos J. 2002. Lysosomal cathepsins: structure, role in antigen processing and presentation, and cancer. *Adv Enzyme Regul* **42**:285–303.

Uemura T, Mori T, Kurihara T, Kawase S, Koike R, Satoga M, Cao X, Li X, Yanagawa T, Sakurai T, Shindo T, Tabuchi K. 2016. Fluorescent protein tagging of endogenous protein in brain neurons using CRISPR/Cas9-mediated knock-in and in utero electroporation techniques. *Sci Rep* **6**:35861.

Uytterhoeven V, Lauwers E, Maes I, Miskiewicz K, Melo MN, Swerts J, Kuenen S, Wittocx R, Corthout N, Marrink SJ, Munck S, Verstreken P. 2015. Hsc70-4 Deforms Membranes to Promote Synaptic Protein Turnover by Endosomal Microautophagy. *Neuron* **88**:735–748.

van Bommel B, Konietzny A, Kobler O, Bär J, Mikhaylova M. 2019. F-actin patches associated with glutamatergic synapses control positioning of dendritic lysosomes. *EMBO J* **38**:e101183.

van den Broeck L, Kleinberger G, Chapuis J, Gistelinck M, Amouyel P, van Broeckhoven C, Lambert JC, Callaerts P, Dermaut B. 2015. Functional complementation in Drosophila to predict the pathogenicity of TARDBP variants: evidence for a loss-of-function mechanism. *Neurobiol Aging* **36**:1121–1129.

Vevea JD, Kusick GF, Courtney KC, Chen E, Watanabe S, Chapman ER. 2021. Synaptotagmin 7 is targeted to the axonal plasma membrane through g-secretase processing to promote synaptic vesicle docking in mouse hippocampal neurons. *Elife* **10**.

Vidak E, Javoršek U, Vizovišek M, Turk B. 2019. Cysteine Cathepsins and Their Extracellular Roles: Shaping the Microenvironment. *Cells 2019, Vol 8, Page 264* **8**:264.

Vieira M, Yong XLH, Roche KW, Anggono V. 2020. Regulation of NMDA glutamate receptor functions by the GluN2 subunits. *J Neurochem* **154**:121–143.

Voges D, Zwickl P, Baumeister W. 2003. The 26S Proteasome: A Molecular Machine Designed for Controlled Proteolysis. *Annu Rev Cell Dev Biol* **68**:1015–1068.

Wandinger-Ness A, Zerial M. 2014. Rab Proteins and the Compartmentalization of the Endosomal System. *Cold Spring Harb Perspect Biol* **6**:a022616.

Wang X bin, Bozdagi O, Nikitczuk JS, Zu WZ, Zhou Q, Huntley GW. 2008. Extracellular proteolysis by matrix metalloproteinase-9 drives dendritic spine enlargement and long-term potentiation coordinately. *Proc Natl Acad Sci U S A* **105**:19520–19525.

Wang T, Martin S, Papadopulos A, Harper CB, Mavlyutov TA, Niranjan D, Glass NR, Cooper-White JJ, Sibarita JB, Choquet D, Davletov B, Meunier FA. 2015. Control of Autophagosome Axonal Retrograde Flux by Presynaptic Activity Unveiled Using Botulinum Neurotoxin Type A. *Journal of Neuroscience* **35**:6179–6194.

Wang W, Zhang X, Gao Q, Lawas M, Yu L, Cheng X, Gu M, Sahoo N, Li X, Li P, Ireland S, Meredith A, Xu H. 2017. A voltage-dependent K+ channel in the lysosome is required for refilling lysosomal Ca2+ stores. *Journal of Cell Biology* **216**:1715–1730.

Wang W, Zhang X, Gao Q, Xu H. 2014. TRPML1: An Ion Channel in the Lysosome. *Handb Exp Pharmacol* **222**:631–645.

Watts RJ, Hoopfer ED, Luo L. 2003. Axon Pruning during Drosophila Metamorphosis: Evidence for Local Degeneration and Requirement of the Ubiquitin-Proteasome System. *Neuron* **38**:871–885.

Weber JP, Toft-Bertelsen TL, Mohrmann R, Delgado-Martinez I, Sørensen JB. 2014. Synaptotagmin-7 is an asynchronous calcium sensor for synaptic transmission in neurons expressing SNAP-23. *PLoS One* **9**.

Wen W, Liu W, Shao Y, Chen L. 2014. VER-155008, a small molecule inhibitor of HSP70 with potent anti-cancer activity on lung cancer cell lines. *Exp Biol Med* **239**:638–645.

Willems J, de Jong APH, Scheefhals N, Mertens E, Catsburg LAE, Poorthuis RB, de Winter F, Verhaagen J, Meye FJ, MacGillavry HD. 2020. ORANGE: A CRISPR/Cas9-based genome editing toolbox for epitope tagging of endogenous proteins in neurons. *PLoS Biol* **18**:e3000665-.

Williams K. 1993. Ifenprodil discriminates subtypes of the N-methyl-D-aspartate receptor: selectivity and mechanisms at recombinant heteromeric receptors. *Mol Pharmacol* **44**.

Winckler B, Faundez V, Maday S, Cai Q, Almeida CG, Zhang H. 2018. The Endolysosomal System and Proteostasis: From Development to Degeneration. *Journal of Neuroscience* **38**:9364–9374.

Won S, Levy JM, Nicoll RA, Roche KW. 2017. MAGUKs: multifaceted synaptic organizers. *Curr Opin Neurobiol* **43**:94.

Wu GY, Deisseroth K, Tsien RW. 2001. Activity-dependent CREB phosphorylation: Convergence of a fast, sensitive calmodulin kinase pathway and a slow, less sensitive mitogen-activated protein kinase pathway. *Proc Natl Acad Sci U S A* **98**:2808.

Xie YX, Naseri NN, Fels J, Kharel P, Na Y, Burré J, Sharma M. 2021. Lysosomal Exocytosis Releases Pathogenic α-Synuclein Species from Neurons. *bioRxiv*.

Yadati T, Houben T, Bitorina A, Shiri-Sverdlov R. 2020. The Ins and Outs of Cathepsins: Physiological Function and Role in Disease Management. *Cells*.

Yang Q, She H, Gearing M, Colla E, Lee M, Shacka JJ, Mao Z. 2009. Regulation of neuronal survival factor MEF2D by chaperone-mediated autophagy. *Science* **323**:124–127.

Yap CC, Digilio L, McMahon LP, Garcia ADR, Winckler B. 2018. Degradation of dendritic cargos requires Rab7-dependent transport to somatic lysosomes. *Journal of Cell Biology* **217**:3141–3159.

Yi JJ, Ehlers MD. 2007. Emerging Roles for Ubiquitin and Protein Degradation in Neuronal Function. *Pharmacol Rev* **59**:14–39.

Zhang C, Cuervo AM. 2008. Restoration of chaperone-mediated autophagy in aging liver improves cellular maintenance and hepatic function. *Nature Medicine 2008 14:9* **14**:959–965.

Zhang X, Wang Y. 2016. Glycosylation quality control by the Golgi structure. *J Mol Biol* **428**:3183.

Zheng CY, Petralia RS, Wang YX, Kachar B, Wenthold RJ. 2010. SAP102 Is a Highly Mobile MAGUK in Spines. *Journal of Neuroscience* **30**:4757–4766.

Zheng C-Y, Wang Y-X, Kachar B, Petralia RS. 2011. Differential localization of SAP102 and PSD-95 is revealed in hippocampal spines using super-resolution light microscopy. *Commun Integr Biol* **4**:104–105.

Zhong J, Zhang T, Bloch LM. 2006. Dendritic mRNAs encode diversified functionalities in hippocampal pyramidal neurons. *BMC Neurosci* **7**:1–12.

Zhou Xianju, Ding Q, Chen Z, Yun H, Wang H. 2013. Involvement of the GluN2A and GluN2B Subunits in Synaptic and Extrasynaptic N-methyl-d-aspartate Receptor Function and Neuronal Excitotoxicity. *J Biol Chem* **288**:24151.

Zhou X., Hollern D, Liao J, Andrechek E, Wang H. 2013. NMDA receptor-mediated excitotoxicity depends on the coactivation of synaptic and extrasynaptic receptors. *Cell Death & Disease 2013 4:3* **4**:e560–e560.

Zhou Y, Danbolt NC. 2014. Glutamate as a neurotransmitter in the healthy brain. *J Neural Transm* **121**:799.

Zhou Y, Takahashi E, Li W, Halt A, Wiltgen B, Ehninger D, Li G-D, Hell JW, Kennedy MB, Silva AJ. 2007. Interactions between the NR2B Receptor and CaMKII Modulate Synaptic Plasticity and Spatial Learning. *Journal of Neuroscience* **27**:13843–13853.

Acknowledgements

I was fortunate enough to meet a variety of great people who supported me, each in their own way, during my PhD studies. Without them, this work would not have been possible.

First of all, I want to thank my supervisor Dr. Michael Kreutz, who gave me the opportunity to participate in this project. I am very grateful for the patience, as well as the inspiring scientific input that I received over the years.

I would also like to thank Prof. Dr. Tim Gilberger for taking the time to be my supervisor from the University of Hamburg.

I am very thankful to my co-supervisor Dr. Katarzyna Grochowska, who mentored me all this time. I appreciate all the energy and time that was invested in me, the help that I received and that I was supported in finding my own way. It was very inspiring to work with you.

I would like to thank the people from the lab and ZMNH that accompanied me over the years. Especially I would like to thank Maru for many nice and nourishing conversations, privately as well as scientifically, and for all the support I received on different levels. I am additionally thankful for Kim, who started this journey with me, Jakob who was a great companion with his great humor and smart ideas, and Sarah who was the best coating and discussion partner, as well as Max for all the help and additionally all the other past and present lab members. I want to thank Dirk, Iris, Ute and Anette for all the pleasant conversations during my time at the ZMNH and for the great support.

Apart from this, I had the pleasure to receive quite some assistance from Dr. Antonia Virgilio and Dr. Bernd Zobiak from the UMIF during my many hours at the microscope. I appreciate the help from the LIN team, especially Dr. Rajeev Raman for his experimental contribution, but also Corinna, Moni, Anna, Sebastian and Ele, as well as Dr. Dawid Glow from the UKE.

I received the biggest support from my family and my friends, and especially Tom. You were by my side during the most challenging time, encouraged and supported me in every way you could.

Eidesstattliche Versicherung

Hiermit versichere ich an Eides statt, die vorliegende Dissertation selbst verfasst und keine anderen als die angegebenen Hilfsmittel benutzt zu haben. Ich versichere, dass das eingereichte gedruckte gebundene Exemplar der Dissertationsschrift und das in elektronischer Form eingereichte Dissertationsexemplar identisch sind.

16.06.2022

Datum, Unterschrift